

# INDUSTRIAL HIGH VOLTAGE

4. CO-ORDINATING
5. MEASURING
6. TESTING.

2413

F.H. KREUGER



578572

# Industrial High Voltage

4. Coordinating
5. Testing
6. Measuring

F.H. Kreuger

Bibliotheek TU Delft



C 0003814968

2413  
281  
6

2 Coordinates  
3 Depth  
4 Temperature

25-25

# Industrial High Voltage

## 4. Coordinating

## 5. Testing

## 6. Measuring

opens with three chapters on insulation coordination made between overvoltages in high-voltage equipment and the specifications which are used for testing high-voltage equipment at overvoltages.

Then three chapters are dedicated to the testing of equipment. Generating and measuring of high voltages are dealt with; statistical analysis and post-mortem analysis of breakdown tests are studied.

The last chapters deal with measuring. At first the measurement of  $\tan \delta$  at high voltage are studied. Then two chapters deal with partial discharges and with the measurement of these discharges.

### Coordinating

Chapter 1	Insulation coordination	1
Chapter 2	Test specifications	11
Chapter 3	Surge arresters	21

### Testing

Chapter 4	Generation of high voltage	35
Chapter 5	Measuring of voltage and current	59
Chapter 6	Breakdown analysis	

### Measuring

Chapter 7	Dielectric loss measurements	
Chapter 8	Partial discharges	
Chapter 9	Discharge measurements	

*Published and distributed by:*

Delft University Press  
Stevinweg 1  
2626 CN Delft  
The Netherlands  
telephone +31 15 783254  
fax +31 15 78 16 61

This book is based on the lectures of Prof.dr.ir. F.H. Kreuger at the Delft University of Technology

Cover design by the author

CIP-GEGEVENS KONINKLIJKE BIBLIOTHEEK, DEN HAAG

Kreuger, F.H.

Industrial high voltage / F.H. Kreuger. – Delft : Delft University Press  
[Vol. II]: 4. Coordinating. 5. Testing. 6. Measuring. – Ill.

Met index, lit. opg.

ISBN 90-6275-562-3 geb.

NUGI 832

Trefw.: elektrotechniek.

Gewijzigde kaart!

© 1992 by F.H. Kreuger

No part of this book may be reproduced in any form by print, photoprint, microfilm or any other means without written permission from Delft University Press

Printed in The Netherlands

# Contents

This book opens with three chapters on **insulation coordination**, where a link is made between overvoltages in high-voltage networks and the specifications which are used for testing high-voltage equipment at overvoltages.

Then three chapters are dedicated to the **testing** of equipment. Generating and measuring of high voltages are dealt with; statistical analysis and post-mortem analysis of breakdown tests are studied.

The last chapters deal with **measuring**. At first the measurement of  $C$  and  $\tan \delta$  at high voltage are studied. Then two chapters deal with partial discharges and with the measurement of these discharges.

## Coordinating

Chapter 1	Insulation coordination	1
Chapter 2	Test specifications	11
Chapter 3	Surge arresters	21

## Testing

Chapter 4	Generation of high voltage	35
Chapter 5	Measuring of voltage and current	59
Chapter 6	Breakdown analysis	79

## Measuring

Chapter 7	Dielectric loss measurements	97
Chapter 8	Partial discharges	117
Chapter 9	Discharge measurements	133

## Some further reading

Index	165
-------	-----

<b>1 Insulation coordination</b>	<b>1</b>
1.1 Overvoltage . . . . .	1
1.2 Lightning impulses . . . . .	2
1.3 Switching impulses . . . . .	3
1.4 A.C. overvoltages . . . . .	7
1.5 Effects of operating voltage . . . . .	8
1.6 D.C. networks . . . . .	10
<b>2 Test specifications</b>	<b>11</b>
2.1 Specifications . . . . .	11
2.2 Standard operating voltages . . . . .	12
2.3 A.C. components . . . . .	13
2.4 D.C. transmission . . . . .	17
<b>3 Surge arresters</b>	<b>21</b>
3.1 General . . . . .	21
3.2 Spark gaps . . . . .	22
3.3 SiC arresters . . . . .	24
3.4 ZnO arresters . . . . .	27
3.5 Location of arresters . . . . .	31
<b>4 Generation of high voltage</b>	<b>35</b>
4.1 A.C. voltage . . . . .	35
4.2 D.C. voltage . . . . .	43
4.3 Impulse voltage . . . . .	48
4.4 Special wave shapes . . . . .	54
<b>5 Measuring of voltage and current</b>	<b>59</b>
5.1 Electrostatic voltmeter . . . . .	59
5.2 Sphere gap . . . . .	60
5.3 Resistive voltage divider . . . . .	63
5.4 Capacitive voltage divider . . . . .	67
5.5 Digital recording . . . . .	69
5.6 Current pulse measurement . . . . .	71
<b>6 Breakdown Analysis</b>	<b>79</b>
6.1 Breakdown tests . . . . .	79
6.2 Weibull Distribution . . . . .	80
6.3 Step-up tests . . . . .	82

# Preface

6.4	Weibull distribution with lower limit . . . . .	83
6.5	Confidence intervals . . . . .	84
6.6	Applications . . . . .	86
6.7	Differential curve . . . . .	89
6.8	Bimodal distribution . . . . .	91
6.9	Interpretation of breakdown tracks . . . . .	91
<b>7</b>	<b>Dielectric loss measurements</b>	<b>97</b>
7.1	Loss angle . . . . .	97
7.2	Physical origin of losses . . . . .	98
7.3	Schering bridge . . . . .	101
7.4	Stray capacitances . . . . .	105
7.5	The dual-balance method . . . . .	106
7.6	Permanently earthed objects . . . . .	108
7.7	Differential transformer bridge . . . . .	110
7.8	Safety precautions . . . . .	113
7.9	Industrial value of $\tan \delta$ . . . . .	114
<b>8</b>	<b>Partial discharges</b>	<b>117</b>
8.1	Types of discharges . . . . .	117
8.2	Appearance (classic description) . . . . .	120
8.3	Appearance (time resolved) . . . . .	123
8.4	Deterioration . . . . .	127
8.5	Non-electrical detection . . . . .	129
<b>9</b>	<b>Discharge measurements</b>	<b>133</b>
9.1	Discharge magnitude . . . . .	133
9.2	Classic detection . . . . .	136
9.3	Implementation of classic detection . . . . .	145
9.4	Time resolved detection . . . . .	151
9.5	Evaluation of discharges . . . . .	155
9.6	Deviating detection techniques . . . . .	157
<b>Annex</b>		<b>161</b>
<b>Some further reading</b>		<b>163</b>
<b>Index</b>		<b>165</b>

8.8	Insulation coordination with power systems	4.8	1
8.8.1	Overvoltage	8.8	1
8.8.2	Lightning impulses	8.8	2
8.8.3	Switching impulses	8.8	3
8.8.4	A.C. overvoltage	8.8	7
8.8.5	Effects of operation on insulation to ground	8.8	8
8.8.6	D.C. networks	8.8	10
8.9	Test specifications	8.9	11
8.9.1	Specification	8.9	11
8.9.2	Standard lightning test	8.9	12
8.9.3	A.C. component	8.9	13
8.9.4	D.C. component	8.9	17
8.9.5	Surge arresters	8.9	21
8.9.6	General	8.9	21
8.9.7	Spark gaps	8.9	22
8.9.8	BIG arresters	8.9	24
8.9.9	ZnO arresters	8.9	27
8.9.10	Location of arresters	8.9	31
8.9.11	Protection against lightning	8.9	31
8.9.12	General protection (overhead lines)	8.8	35
8.9.13	Arresters (overhead lines)	8.8	35
8.9.14	Protection of substations	8.8	43
8.9.15	Non-selective protection	8.8	48
8.9.16	Special protection	8.8	54
8.9.17	Diagnose measurements	8.9	54
8.9.18	Measuring of voltage and currents	1.059	
8.9.19	Electrostatic detection	1.059	
8.9.20	Sphere gap	1.059	
8.9.21	Resistor voltage detector	1.063	
8.9.22	Competitive voltage detector	1.067	
8.9.23	Digital resistive detector	1.069	
8.9.24	Current pulse measurement	71	
8.9.25		Annex	
8.9.26		79	
8.9.27	Breakdown Analysis	80	
8.9.28	Breakdown tests	80	
8.9.29	Weibull Distribution	80	
8.9.30	Step-up tests	82	

# Preface

## Insulation coordination

Friend and foe might agree on the merits of this book. And for the same reason. They might find it short and outspoken, yet they would differ in their opinion on the effect it will have on the reader. Does it provide a firm footing in the matter or merely a glimpse on the subject?

At the end of my career as a high-voltage engineer, I have written this book. I have allowed myself to make my profession as comprehensible as possible: tangible, if that were not too dangerous an expression in high-voltage technique. Although I say to my students "there is some mysticism in high-voltage engineering, keep it so", I do not act on the principle. I have stripped it of mystifications and abstractions that tend to slip in any branch of study, more so in high-voltage technique with its impressive thunderbolts, its mysterious coronas and its invisible discharges. But I am aware that not everybody will appreciate that.

I have been supported in my endeavours by a number of experts, from KEMA in particular, who have critically read many chapters of this book. Moreover, I have had much assistance from Mr. P.H.F. Morshuis of the High-voltage Laboratory of Delft University, who has checked the contents of this book and has directed the desk top publishing. I further thank our secretary, Miss Annette Potting, for typing and assembling these two volumes.

There are three types of overvoltage that affect the design of insulation constructions and determine the requirements for overvoltage

### The author

1. Lightning impulses
2. Switching impulses
3. A.C. overvoltages

Moreover, the demand for uninterrupted service at nominal voltage asks for requirements related to:

- 4. Operating voltage.

These four items will be studied in the following sections.

# Persecution

for this is a very poor place to live in. And I am not sure how long I can stay here. The weather is not good here, and there is no work. The only thing I can do is to go to school or to find a job. But I have no money. Does it follow that I must leave? No, because I have a friend who will help me. He is a good man and he will take care of me. He will give me a place to live in and he will help me get a job. So I will stay here and try my best to make things better. I will work hard and I will study hard. I will also help others and I will always be kind to them. I will never forget the good people I met here. They were very nice and they helped me a lot. I am grateful to them.

Mr. P.H.L. Morris is the High-Holy-Lodge of Duff's University, who was occupying the country house near the city. The house had been occupied by Mr. V.W. Vassal, who had left it recently. Mr. Vassal had sold it to Mr. P.H.L. Morris. Mr. Morris is a very good man and he is a member of the Lodge.

Pettigree, Mr. Pettigree has been granted a loan of £1,000 by the Bank of England, and he is now in a position to buy his home back again. He is very grateful to the Bank for their help.

The author wishes to thank Mr. and Mrs. J.

E. C. H. G.

The author wishes to thank Mr. and Mrs. J. E. C. H. G. for their help in the preparation of this paper.

The author wishes to thank Mr. and Mrs. J.

The author wishes to thank Mr. and Mrs. J. E. C. H. G. for their help in the preparation of this paper.

# Chapter 1

## Insulation coordination

The principal cases are:

High-voltage insulation is costly, but breakdown in insulation is still more costly. It is therefore of great importance to obtain a proper balance between the costs of the insulation and the reliability of the system.

This process of balancing is called *insulation coordination*. It involves the proper choice of the insulation level of the various components in the network: it also involves the proper choice of protection equipment such as spark gaps and surge arresters.

If breakdown is inevitable, it should take place at a preferred location: better in a spark gap than touching a line insulator, and rather in a surge arrester than in a costly power transformer.

The International Electrotechnical Commission, IEC for short, has established a number of standardized insulation levels. Moreover, IEC standards state a series of test requirements, so that manufacturers and users of equipment can make standardized agreements on the characteristics of a network component.

This voltage is maximal if  $R \rightarrow \infty$  and reaches  $U = 2U_0$ .

### 1.1 Overvoltage

There are three types of overvoltage that affect the design of insulation constructions and determine the requirements for overvoltage tests:

1. Lightning impulses
2. Switching impulses
3. A.C. overvoltages.

Moreover, the demand for uninterrupted service at nominal voltage asks for requirements related to:

4. Operating voltage.

These four items will be studied in the following sections.

## 1.2 Lightning impulses

Lightning impulses are caused by:

1. a lightning stroke in the vicinity of a line or a substation. The charge induced on the line by thunderclouds is suddenly released and causes travelling waves of a high voltage level. This cause of a lightning surge is of importance for medium-voltage networks only.
2. a lightning stroke in the tower or in the ground wire of an overhead line. The lightning current passes the impedance  $\omega L + R$  to earth and causes a high voltage at the top of the tower. Flashover along the insulation string, from frame to line, may occur as shown in fig. 1.1.
3. a direct lightning stroke in the line, also shown in fig. 1.1. This stroke is confronted with the characteristic impedance  $Z$ , and the resulting voltage is  $\frac{1}{2} \cdot i \cdot Z$ . At a moderate current of 20 kA and a  $Z$  of about 300  $\Omega$ , the resulting overvoltage amounts to several megavolts.

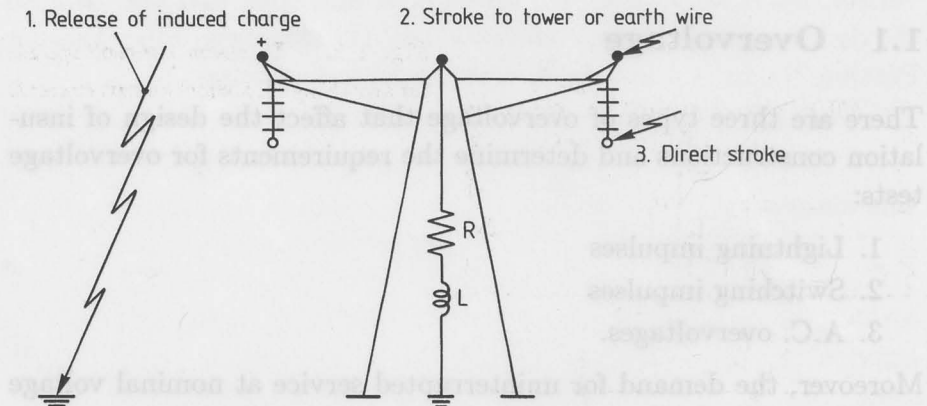


Fig. 1.1. Causes of lightning overvoltages.

In the IEC test specifications, the lightning surge is represented by a standardized impulse with 1.2  $\mu s$  front and 50  $\mu s$  tail, as has been discussed in Volume 1, section 7.3.

### 1.3 Switching impulses

Switching impulses are caused by switching operations in a network. The principal cases are:

#### a. Fault clearing

After switching off a short circuit as shown in fig. 1.2, a transient voltage occurs, which in the most common case is equal to

$$\frac{U}{U_0} = 1 - e^{-\alpha t} (\cos \omega t + \frac{\alpha}{\omega} \sin \omega t)$$

where

$$\alpha = \frac{1}{2RC}$$

and

$$\omega^2 = \frac{1}{LC} - \frac{1}{4C^2R^2}$$

This voltage is maximal if  $R \rightarrow \infty$  and reaches  $\hat{u} = 2U_0$ .

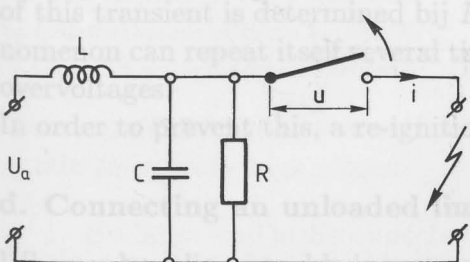
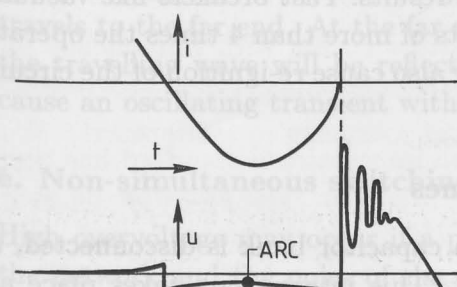
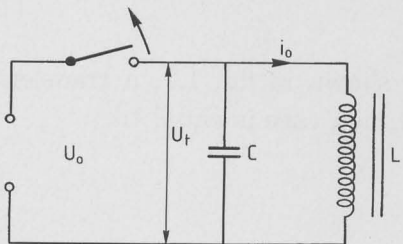


Fig. 1.2. Transient overvoltage after switching off a short circuit current.



### b. Disconnecting unloaded transformers

In contrast to the former case, a small current  $i_0$  is switched off. This current, however, is *inductive* and represents an appreciably large magnetic energy:  $\frac{1}{2}Li_0^2$ , see fig. 1.3.



**Fig. 1.3.** Disconnecting an unloaded transformer.

The current is small and a good circuit breaker can chop this current at any moment. An unsuitable moment occurs if  $i_0 = \text{max}$ . Then the magnetic energy  $1/2L i_0^2$  is transformed into an electrostatic energy in the capacitance  $C$  of the windings:

$$\frac{1}{2}C u^2 = \frac{1}{2}L i_0^2.$$

An oscillating wave is generated with some attenuation and with a frequency

$$\omega = \sqrt{\frac{1}{LC}},$$

and a crest value of

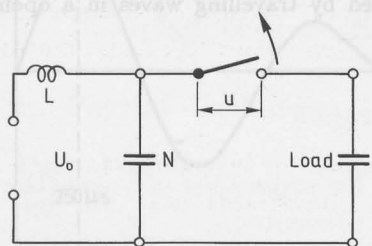
$$\hat{u} = i_0 \sqrt{\frac{L}{C}}.$$

As  $C$  is small, a high overvoltage results. Fast breakers like vacuum switches may cause high transients of more than 4 times the operating voltage. These transients may also cause re-ignition of the circuit breaker.

### c. Disconnecting unloaded lines

If an unloaded line, a cable, or a capacitor bank is disconnected, a *capacitive* current is interrupted. This interruption takes place at

current zero, the capacitor C in fig. 1.4 is then at maximum voltage.



R=Re-Ignition  
E=Extinction

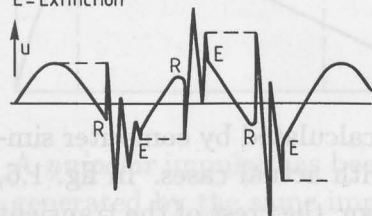


**Fig. 1.4.** Disconnecting an unloaded capacitive component, such as line, cable or capacitor bank.

This voltage persists for a considerable time as the leakage current in the capacitor is small. Meanwhile, the main voltage reverses in half a period, and twice the operating voltage occurs over the contacts of the circuit-breaker. If the circuit breaker re-ignites, a high frequent current starts to flow, which is interrupted after a while, and a transient overvoltage appears. The amplitude and the frequency of this transient is determined bij  $L$  and  $C$  in the network; this phenomenon can repeat itself several times and may lead to considerable overvoltages.

In order to prevent this, a re-ignition-free circuit breaker is required.

#### d. Connecting an unloaded line

Where a long line or cable is energized, a step wave is induced, which travels to the far end. At the far end, and later on at the near end, the travelling wave will be reflected. The repeated reflections will cause an oscillating transient with  $\hat{u}=2U_0$ , as shown in fig. 1.5.

#### e. Non-simultaneous switching

High overvoltage may occur if a power transformer is connected to the network and the poles of the circuit breaker are not simultane-

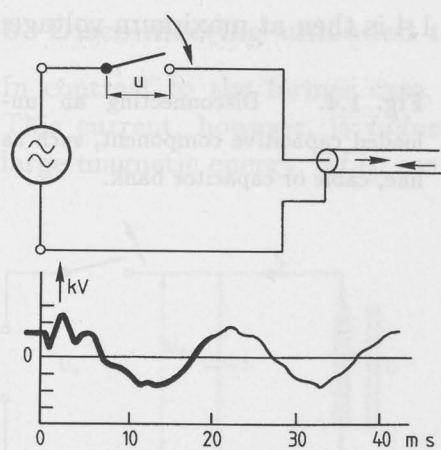


**Fig. 1.5.** Oscillating transient caused by travelling waves in a open line.

ously closed. These overvoltages can be calculated by computer simulation. These calculations agree well with actual cases. In fig. 1.6, an example of such an overvoltage is shown, the crest of the transient is as high as  $4.5 U_0$ .

Many other switching impulses may occur, but the situations above represent the worst cases. They may reach as much as  $5 U_0$ , which is less high than in the case of lightning impulses, but high enough to endanger the insulation.

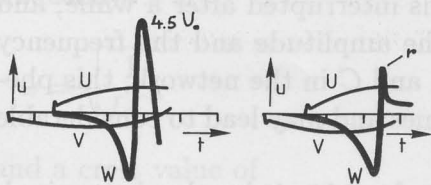


**Fig. 1.6.** Overvoltages occur if the three phases of a transformer  $U$ ,  $V$  and  $W$  are not simultaneously switched on.  
 $r$  = reduction by lightning arrester.

### Testing at switching impulses

In most cases, an oscillating transient occurs with a frequency between some hundreds of Herz to some thousands of Herz. An average value of 1000 Hz may be adopted.

In order to obtain uniformity, an international standard has been devised for testing with switching impulses. The onset of the oscillation is simulated by a front of  $250 \mu s$  as shown in fig. 1.7. The attenuation of the transient is represented by a half value of  $2500 \mu s$ .

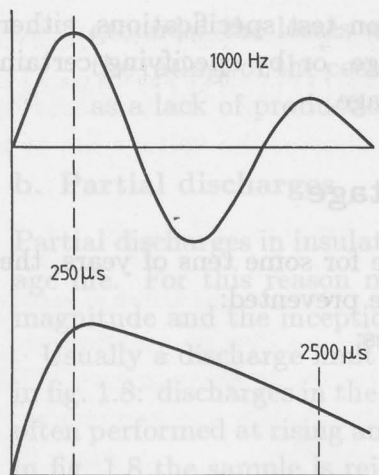


**Fig. 1.7.** Normalized switching impulse representing a 1000 Hz oscillating wave.

Partial discharges in insulation constructions may endanger the voltage withstand capability of some service equipment. For this reason many test specifications set limits to the volume cause of discharge. The discharge current is measured at rising voltage and a voltage of arc initiation is shown. In the example given the shaded area is not accepted. The test is performed at rising voltage at falling voltage. In the example given the shaded area is not accepted because of unwanted discharges at decreasing voltage.

A *unipolar* impulse has been chosen so that a switching surge can be generated by the same impulse generator as a lightning impulse.

It could be asked whether separate testing at switching impulses is needed. H.V. material is in any case tested at lightning impulses up to 9 times  $U_0$ , whereas switching impulses go to about 4.5 times  $U_0$ . It has, however, been found that dielectrics have a lower breakdown strength in the case of switching impulses than in the case of lightning impulses. Many constructions are therefore tested at these moderate switching impulses as well as at high lightning impulses.

## 1.4 A.C. overvoltages

There are three reasons why the 50 or 60 Hz operating voltage can attain temporary high values:

1. If a large load is disconnected, the resistive and reactive voltage drops disappear and an overvoltage occurs until the operating value is restored.
2. The capacitance of an unloaded cable, in combination with a transformer or generator inductance, can increase the voltage.
3. If a ground fault occurs in a network with a non-earthed neutral, the healthy phases will adopt a  $\sqrt{3}$  times higher voltage until the fault is cleared.

These possible events have their effect on test specifications, either by establishing a higher nominal voltage, or by specifying certain tests to be made at phase-to-phase voltage.

### 1.5 Effects of operating voltage

In order to ensure uninterrupted service for some tens of years, the following causes of breakdown should be prevented:

- a. overheating caused by dielectric losses;
- b. partial discharges;
- c. treeing.

#### a. Dielectric losses

The dielectric losses of new equipment are generally so low that they do not endanger the insulation. *especially in recalo*

However, there is some apprehension about the combination of high operating temperature and heating by dielectric losses. This combination might become dangerous in the course of time, as dielectric losses can gradually increase by aging. That is why many test specifications set limits to  $\tan \delta$  at high temperatures (e.g. 90°C), as well as to the stability of  $\tan \delta$  after prolonged tests at increased voltage and heat cycles.

Other reasons for the limitation of  $\tan \delta$  are:

- dielectric losses affect the current-carrying capacity of equipment. In a 400 kV oil-filled cable, for instance, the dielectric losses are responsible for 1/3 of the temperature increase, so that only 2/3 of the admissible temperature rise is available for ohmic losses.
- dielectric losses represent a loss of energy, which may represent an appreciable loss of money.
- dielectric loss measurements are sometimes used as a quality check. A low limit is set to make sure that the manufacturer has control over his manufacturing process. For instance: 33 kV oil-filled insulation is required to have a  $\tan \delta$  smaller or equal to  $35 \cdot 10^{-4}$ . This requirement is not made on operational

grounds: the losses would not affect the breakdown strength, the rating, or the costs of losses. But higher losses are regarded as a lack of production control.

### b. Partial discharges

Partial discharges in insulation constructions may endanger the voltage life. For this reason many test specifications set limits to the magnitude and the inception voltage of discharges.

Usually a discharge limit  $q_0$  and a voltage  $U_t$  are defined as shown in fig. 1.8: discharges in the shaded area are not accepted. The test is often performed at rising and at falling voltage. In the example given in fig. 1.8 the sample is rejected because of unwanted discharges at decreasing voltage.

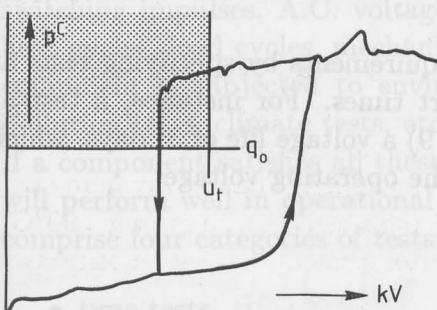


**Fig. 1.8.** Discharge test. Any partial discharge larger than  $q_0$  measured below test voltage  $U_t$  leads to rejection of the object under test, see shaded area.

### c. Treeing

Defects, such as inclusions in the dielectric and protrusions at the electrodes may cause treeing. The same is true for cavities and interstices containing partial discharges. Treeing goes very slowly at low field strengths, it may lead to breakdown after months or years at operating voltage. At an elevated field strength, the rate of growth increases considerably, and breakdown can take place within hours or even minutes. As generally accepted, the voltage life  $L$  varies inversely with the field strength  $E$  to the power  $n$ :

$$L = \frac{c}{E^n}$$

where  $n$  can have values from 9 to 12 and  $c$  is a constant which depends on the size of the defects. On a double logarithmic scale,

this relationship is represented as a straight line, where  $n$  determines the slope of the line and  $c$  the location.

In fig. 1.9 this lifeline is shown for a dielectric with defects of different sizes, the larger the defect the shorter the voltage life at a certain field strength.

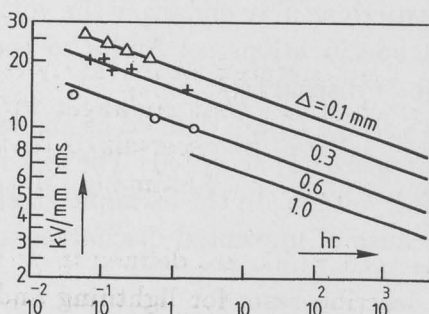


**Fig. 1.9.** Results of endurance tests on a dielectric with cavities of various depths.

This relationship is used in test requirements by specifying tests at elevated voltage for relatively short times. For instance, a test at  $3U_0$  for 24 hours represents (if  $n = 9$ ) a voltage life of  $3^9$  days, which corresponds to about 50 years at the operating voltage.

## 1.6 D.C. networks

Insulation coordination in D.C. links is not all that different from that in A.C. networks. If overhead lines are incorporated in the network, lightning impulses may occur. In both underground and overhead links, switching surges occur.

The effect of the operating voltage, however, is different: measurement of  $\tan \delta$  is superfluous, although it may be used as a check on quality; the same is true for partial discharges.

Test requirements concentrate on endurance tests at overvoltage. The relationship  $L = f(E)$  is not as clear as in the case of A.C. voltage, but overvoltage tests may be based on the same relationship as encountered for A.C. An important test is, therefore, a test carried out at  $2U_0$  for several weeks and which involves load cycles. Sudden polarity reversals, as occur in practice, are incorporated. These polarity reversals are often the most severe part of the test.

# Chapter 2

## Test specifications

### 2.1 Specifications

The study of insulation coordination has generated an inventory of *overvoltages* as well as a survey of mechanisms that endanger the H.V. components at *operating voltage*. It shall be ascertained that the components will withstand these dangers for a lifetime of 30 to 50 years.

10/5/71

July 1971

For this reason, tests have been devised which are defined in *test specifications*. These specifications describe tests for lightning and switching impulses, A.C. voltage and D.C. voltage, combined with heat cycles, load cycles, mechanical loads, etc. In addition, outdoor equipment is subjected to environmental tests such as rain tests, pollution tests, climate tests, etc.

If a component satisfies all these tests, there is a fair chance that it will perform well in operational circumstances. Most specifications comprise four categories of tests:

- type tests *destructive*
- sample tests *destructive*
- routine tests *Non destructive*
- tests after installation *non destructive*

*destructive*

*Type tests* are performed once on a newly designed component, to establish that this design will perform well in service. The type test is not repeated unless essential modifications in the design have been made, such as the use of other materials, an increase in the design stress, a change in the configuration, etc.

*destructive*

*Sample tests* are performed on samples that are chosen at random from a number of components that are to be supplied; one voltage transformer out of 200 transformers, or one sample of 10 m cable out

of 10 km of cable for instance. Sample tests are performed to check whether a batch of products is of the agreed quality. As in the type test, these tests are destructive and the sample is not supplied to a user after the test.

*Non destructive* Routine tests are tests performed on all items to be supplied. They are *non-destructive* tests.

*No destructive* Tests after installation are supplementary to routine tests: in some cases a component is installed on site; for instance, a large power transformer which was too large to be shipped in one piece; or a circuit of an underground power cable. The test is performed to check whether the installed product is fit for use.

Test specifications are based on a standard operating voltage as discussed in section 2.2 below. In subsequent sections, examples of test specifications are discussed: two components for A.C. networks and a cable for D.C. transmission.

In the above cases, only overvoltage tests are discussed. Test specifications contain a multitude of mechanical tests, materials tests, checks on the construction, etc, that are ignored here.

## 2.2 Standard operating voltages

In order to standardize H.V. equipment, and to obtain uniform specifications, the voltage levels of networks have been standardized.

Three definitions play a role:

- $U$  = the line-to-line voltage, determining the name of a network. A "400 kV network" refers to the A.C. voltage between lines.
- $U_m$  = the maximum voltage between lines that may be allowed for an arbitrarily long period.  $U_m$  is usually 5 to 15 % higher than  $U$ .
- $U_0$  = the rated voltage between conductor and earth; thus  $U_0 = \frac{U}{\sqrt{3}}$ . In test specifications,  $U_0$  is the more important value, as test voltages are specified in multiples of  $U_0$ .

Although deviating levels are found, the following list gives a fair picture of the most common operating voltages  $U$  of A.C. systems.

Continental origin	British origin	American origin
10 kV	11 kV	12.5 kV
20 kV	22 kV	23 kV
35 kV	33 kV	35 kV
50 kV	66 kV	69 kV
110 or 150 kV	132 kV	130 kV
220 kV	220 kV	230 kV
400 kV	400 kV	345 kV
800 kV		500 kV
		765 kV

A promising start was made to the standardization of D.C. systems in the choice of 1 x 100 kV in the first undersea installation and some 2 x 200 kV and 2 x 400 kV systems later on. However, this standardization did not persist, all kinds of arbitrary voltage levels have since been installed.

## 2.3 A.C. components

### 220 kV bushing

As an initial example, the voltage tests on a 220 kV bushing are discussed (mechanical, thermal or material tests are ignored), see table 2.1.

The test specification is dominated by the *basic insulation level* (BIL). This is the level of the full-wave *lightning impulse* that in a network must be withstood without any damage or flashover. In the case of 220 kV material, this amounts to 1050 kV.

If there is a surge arrester in the network, the component is protected and a reduced test level can be accepted, one or two steps below BIL. One step below BIL amounts in this case to an impulse level of 900 kV; other types of overvoltages are reduced accordingly.

Reducing the impulse level may be economically advantageous. The list of requirements applies to a bushing at full insulation level: BIL = 1050 kV. This impulse level is high, as is customary for H.V. equipment. The field strength in the dielectric is almost 10 times

Table 2.1: 220 kV bushing

- overvoltage tests -

		REQUIREMENT	AMPLIFICATION OF THE FIELD
TYPE TEST	LIGHTNING IMPULSE no breakdown, flashover allowed no flashover	1210 k $\hat{V}$ 1050 k $\hat{V}$ BIL	9.5 x 8.3 x
	SWITCHING IMPULSE no flashover or breakdown	850 k $\hat{V}$	6.7 x
	A.C. VOLTAGE 1 min. dry 1/2 min. under rain no flashover or breakdown	575 kV 460 kV	4.5 x 3.6 x
ROUTINE TEST	A.C. VOLTAGE 1 min. dry no flashover no breakdown	485 kV	3.8 x
	LOSS MEASUREMENT no increase in $\tan \delta$ up till	147 kV	1.15 x
OPERATING LEVEL	$U_0$ rated voltage line to earth	127 kV	1 x

as high as at operating stress. If, for instance, 8 kV/mm is chosen as the field strength at operating stress, the lightning test demands a dielectric strength of about 80 kV/mm, which is not far from the breakdown strength of such materials. The lightning test is therefore often the determining factor in an insulation design.

Two further comments can be made:

1. It is remarkable that no sample test is specified. This can be attributed to the small number of items that are usually ordered at a time.
2. The A.C. test (1 min. 4.5  $U_0$ ) is rather high and short in comparison with test specifications for other equipment. This could ignite defects that do not endanger the dielectric at a lower voltage; nevertheless, the test does not guarantee a long service life, as is shown in fig. 2.1. A 24-hour test at 3 $U_0$  would have been better, as is shown in the same figure.

### 220 kV power cable

The following example applies to a 220 kV power cable with extruded insulation. All four categories of tests are present: type test, sample test, routine test and after laying test. The overvoltage requirements in these tests are summarized in table 2.2.

**Table 2.2: 220 kV cable with extruded insulation**

- overvoltage tests -			
		TEST REQUIREMENT	AMPLIFICATION OF THE FIELD
TYPE TEST	LIGHTNING IMPULSE 10 <sup>+</sup> and 10 <sup>-</sup> , hot	1050 kV BIL	8.3 ×
	SWITCHING IMPULSE	NONE	
	RAIN TEST AT TERMINALS 1 min. under rain	460 kV	3.6 ×
	ENDURANCE TEST 24 H	380 kV	3 ×
	STABILITY TEST 1000 H and heat cycles	255 kV	2 ×
	SAMPLE TEST 24 H at A.C. VOLTAGE	380 kV	
ROUTINE TEST	A.C. TEST 30 min.	315 kV	2.5 ×
	DISCHARGE TEST discharges < 5 pC	215 kV	1.7 ×
AFTER LAYING TEST	D.C. TEST 15 min.	(880 kV)	
OPERATING LEVEL	U <sub>0</sub> rated voltage-to-earth	127 kV	1 ×

A number of comments can be made. Regarding the destructive *type* and *sample* tests:

1. The field strength that appears in the case of the impulse test is (as in the former case) high, the more so as the dielectric strength of extruded insulation is lowered by reversing the polarity during the test (10 positive, followed by 10 negative impulses) and the test is performed at an operating temperature which offsets the strength by 25 %. Moreover, the cable is tested after severe bending.
2. No switching impulse is required, as it has been found that the lightning impulse test is far more dangerous for this type of dielectric.

3. The voltages at the endurance and at the stability tests have been entered in the life curve shown in fig. 2.1. The life curve has been chosen such that the life of the cable system at  $U_0$  is in the order of 50 years. It appears that the 24-H *endurance* test and the 6-week *stability* test conform well to this life line. These tests are the more demanding as they are combined with bending tests and heat cycles, so that the performance of the semicon screens is checked too.

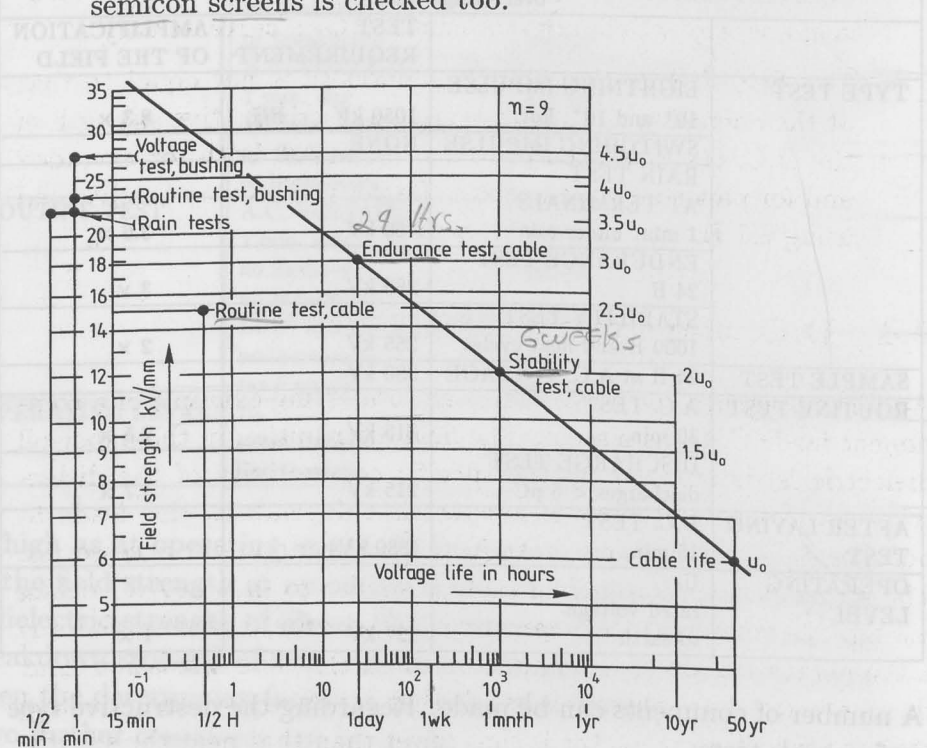


**Fig. 2.1.** Overvoltage tests on a bushing and a power cable presented in a life curve. Destructive tests are located upon the lifeline, non-destructive tests safely below. ( $U_0$  arbitrarily at 6 kV/mm does not affect these conclusions.)

Regarding the *routine* test:

1. The  $\frac{1}{2}$ -H routine test is safely below the life curve, the cable hardly suffers any aging before it is put into use.
2. The discharge test follows the procedure as laid down in fig. 1.8, but is quite severe at  $1.7 U_0$ . Note the difference with the bushing which was tested for discharges by  $\tan \delta$ -measurements, as

is proper for paper insulation; see chapter 9 on discharge detection.

Regarding the *after laying* test:

This test at D.C. is regarded as a compromise. Testing long cable circuits at an A.C. overvoltage demands a reactive power of several MVAs, which cannot be supplied by mobile installations, whereas D.C. asks for small leakage currents only.

The field distribution at D.C., however, is not equal to that at the operating A.C. Moreover, the discriminative strength of the D.C. test has been proved to be small, both for extruded and for paper-insulated cables. Better results may be obtained using 0.1 Hz or other techniques.

## 2.4 D.C. transmission

An oil impregnated cable system is an interesting example of a component for D.C. transmission. The field distribution in the paper-oil dielectric is determined by the specific conductivity of the dielectric. As this conductivity is temperature dependent, this leads to peculiar field distributions, both in the cable and in the accessories. The stress distribution in *cold* cable is similar to that in A.C. cable, see fig. 2.2, curve (a). At *operating temperature*, however, there is a temperature drop from conductor to earth. The insulation near the conductor has consequently a higher conductivity, and the field strength near the conductor is thus lower than that near the sheath, as shown in fig. 2.2, curve (b). D.C. cable systems shall thus be tested under both conditions.

The electrical relaxation time is so long that it may take hours before the field has been settled, which implies that at a reversal of polarity the original field persists in the dielectric and is superimposed by the field of the new polarity. Double field strength results as shown in fig. 2.2, curve c.

Still higher field strengths are produced if polarity reversals coincide with heat cycles.

This mechanism affects the manner of testing, as can be seen from table 2.3 on the test requirements on D.C. cable systems.

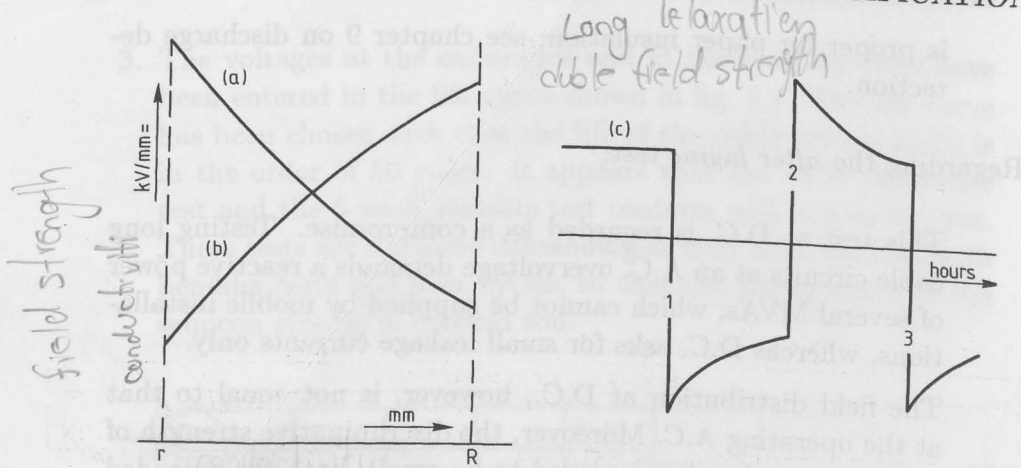


**Fig. 2.2.** Field distribution in D.C. cable

(a) Cold cable, normal distribution.

(b) Cable at full load, the highest field strength occurs at the outer shield.

(c) Field enhancement by polarity reversal, the long relaxation line causes almost double field strength when the system voltage is switched from positive to negative and vice versa.

$r$  = radius conductor

$R$  = outer radius insulation

1,2,3 = first, second and third polarity reversal.

The test specifications in this list concentrate on the *type test*, consisting of:

1. A comparatively mild lightning impulse test.
2. A switching impulse test superimposed on a D.C. voltage of opposite polarity, which complies with the importance of polarity reversals.
3. A stability test of 30 days at  $2U_0$  comparable to the 6-week test at  $2U_0$  for A.C. cables. This test is the more demanding as it is combined with thermal load cycles and as the last 10 cycles are further combined with polarity reversals, corresponding to the field enhancing situations shown in fig. 2.2.

The D.C. *routine test* is mild. The  $\tan \delta$ -test at A.C. is a quality test to check whether the production process is under control.

The *after laying test* is mild and poses no problems in the testing of long lengths.

## Surge arresters

### 3.1 General

Overvoltages in a network can be limited by *surge arresters*, also called *lightning arresters*.

Table 2.3: D.C. cable system for 600 kV

- Example of overvoltage tests -

THE FOLLOWING TYPES OF ARRESTERS ARE IN USE	TEST REQUIREMENT	FIELD AMPLIFICATION
<b>TYPE TEST</b>		
LIGHTNING IMPULSE 10 <sup>+</sup> and 10 <sup>-</sup> impulses at hot cable	1400 kV	2.3 ×
SWITCHING IMPULSE 10 pos. pulses superimposed on $-U_0$ 10 neg. pulses superimposed on $+U_0$	1200 kV	2 × on $\pm U_0$
D.C. STABILITY TEST 10 heat cycles of 24 H 10 heat cycles of 24 II 10 heat cycles combined with polarity reversals	+1200 kV -1200 kV +900 kV to -900 kV	2 × 2 × 1.5 × to -1.5 ×
SAMPLE TEST	none	
<b>ROUTINE TEST</b>		
D.C. TEST 15 min.	-1200 kV	2 ×
A.C. TEST $\tan \delta$ measurement $\tan \delta < 50 \cdot 10^{-4}$ $\Delta \tan \delta < 14 \cdot 10^{-4}$	up to 600 kV <sub>rms</sub>	up to $U_0$ <sub>rms</sub>
<b>AFTER LAYING TEST</b>	D.C. TEST 15 min.	-1080 kV 1.8 ×
<b>OPERATING LEVEL</b>	$U_0$	$\pm 600$ kV $\pm 1 \times$

G.C. TEST		TEST	
NOTATION	EXPLANATION	NOTATION	EXPLANATION
$U_1 = \text{length of } V_1 \text{ at } t_1$	length of $V_1$ at time $t_1$	$U_2 = \text{length of } V_2 \text{ at } t_1$	length of $V_2$ at time $t_1$
$U_3 = \text{length of } V_1 \text{ at } t_2$	length of $V_1$ at time $t_2$	$U_4 = \text{length of } V_2 \text{ at } t_2$	length of $V_2$ at time $t_2$
$V_1 = \text{length of } V_1 \text{ at } t_1$	length of $V_1$ at time $t_1$	$V_2 = \text{length of } V_2 \text{ at } t_1$	length of $V_2$ at time $t_1$
$V_3 = \text{length of } V_1 \text{ at } t_2$	length of $V_1$ at time $t_2$	$V_4 = \text{length of } V_2 \text{ at } t_2$	length of $V_2$ at time $t_2$
$\Delta U_1 = U_2 - U_1$	change in length of $V_1$ from $t_1$ to $t_2$	$\Delta U_2 = U_4 - U_3$	change in length of $V_2$ from $t_1$ to $t_2$
$\Delta V_1 = V_3 - V_1$	change in length of $V_1$ from $t_1$ to $t_2$	$\Delta V_2 = V_4 - V_2$	change in length of $V_2$ from $t_1$ to $t_2$
$\Delta U = U_4 - U_1$	total change in length of $V_1$ between $t_1$ and $t_2$	$\Delta V = V_4 - V_1$	total change in length of $V_2$ between $t_1$ and $t_2$
$\Delta V = V_3 - V_1$	total change in length of $V_1$ between $t_1$ and $t_2$		

is compared with  $\Delta U$ . If they are further compared with each other, the field stations are checked.

The D.G. routine tests each station separately and performs a quality test to check whether the given station is a good one or not.

The after-lap test is used for the testing of short lengths and the before-lap test is used for the testing of long lengths.

# Chapter 3

## Surge arresters

### 3.1 General

Overvoltages in a network can be limited by *surge arresters*, also called *lightning arresters*. A surge arrester presents a momentary path to earth which removes the superfluous charge from the line.

The following types of arresters are in use:

1. Open spark gaps. These are rod gaps, usually bridging open air insulators. Such gaps are simple and inexpensive. Their operation, however, causes a short-circuit in the network as an arc is formed between line and earth.  
*Levq espaciadoras bridge point*
2. An improvement is offered by the SiC arrester. In this arrester, spark gaps are connected in series with non-linear resistors of silicon carbide, which resistors limit the current to earth and prevent a short-circuit.
3. The best performance was obtained after the development of ZnO arresters. This arrester is composed of non-linear resistors of metal oxide, mainly ZnO, without spark gaps.

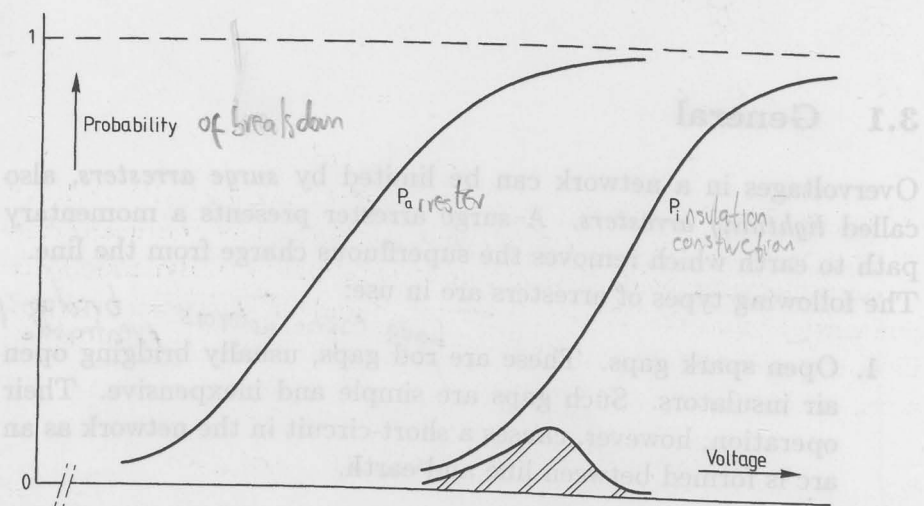
These three types are discussed below. In all cases, the statistical scatter in breakdown voltage is important.

Fig. 3.1 shows the probability  $P$  for breakdown at a voltage  $V$ . Curve  $P_a$  represents the probability of igniting an arrester, curve  $P_i$  that of breakdown in an insulating construction. There remains a probability  $(1 - P_a)$  that the arrester does not react, at the same time there is a probability  $P_i$  that the insulation breaks down at that voltage. This results in a risk of failure of the protected insulation:  $(1 - P_a)P_i$ .

The integral

$$\int (1 - P_a)P_i dv$$

represents the overall *failure risk* which is shown as a shaded area in fig. 3.1.



**Fig. 3.1.** Probability  $P_a$  of an arrester which protects an insulation construction with breakdown probability  $P_i$ . The shaded area represents the failure risk: no ignition of the arrester combined with breakdown of the insulation.

In practice, this risk analysis is difficult to perform. Curve  $P_a$  can be fairly well determined, as a surge arrester restores after each breakdown; curve  $P_i$ , however, is less accessible as each breakdown asks for replacement of the non-restoring sample. Therefore, in actual cases the upper protection limit (e.g. 98 % responses) of the arresters and the lower withstand level of the insulation (e.g. the BIL of that construction) are taken and a safety margin of some 25 % is introduced. This safety margin covers also the effects of ageing, variation in production and other uncertainties.

### 3.2 Spark gaps

Open spark gaps are found in some varieties. The most common one is the rod gap as shown in fig 3.2. This gap usually protects an insulator string, a bushing, a cable terminal, etc.

Sometimes ring-shaped electrodes are used. The arc formed at flashover wanders over the ring and less damage is done to electrodes and insulators.

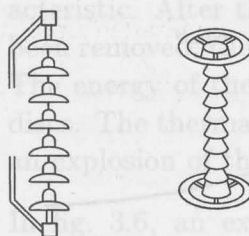


Fig. 3.2. Open spark gaps.

Arcing horns as shown in fig. 3.3 are used at relatively low voltage levels. When an arc is formed, high currents pass the horns and cause a magnetic field. The arc undergoes an electrodynamic force and moves upwards. The arc is stretched and cools. The arc voltage increases and the arc eventually extinguishes. This is a first step to a self-extinguishing arrester.

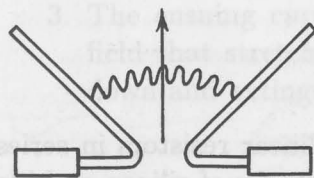


Fig. 3.3. Arcing horn.

Open spark gaps are simple and inexpensive, but the disadvantages are so severe that they are only used as an extra safety measure where other measures have failed. The disadvantages are:

- A short-circuit follows after the gap has been tripped by an overvoltage.
- The scatter in flashover voltages is large, resulting in a large failure risk as shown in fig. 3.1.
- The breakdown to zero voltage takes place in an extremely short time, in the order of  $0.1 \mu\text{s}$ , see fig. 3.4. This steep front may create severe stresses in equipment like transformers.
- The breakdown characteristic is less suitable, as shown in fig. 3.4. If there are steep waves with fronts less than  $1 \mu\text{s}$ , the breakdown voltage increases appreciably. Most insulation constructions have a flat characteristic and are thus not well protected against steep waves.

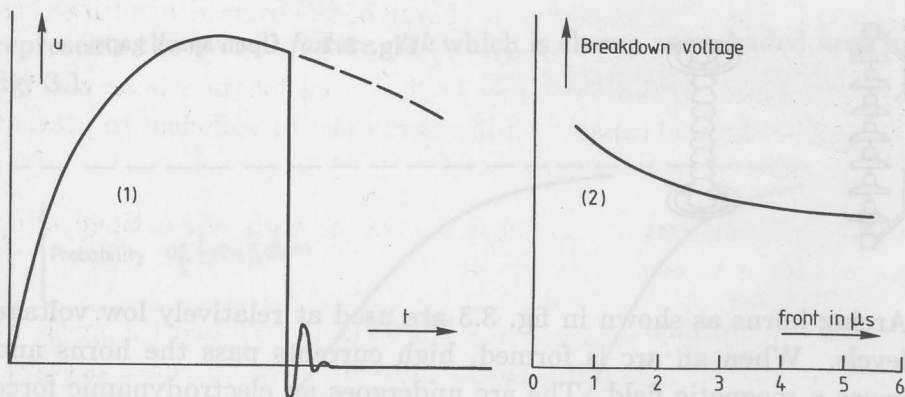


Fig. 3.4. 1) a rod gap creates a steep chopped wave.

2) a rod gap has an unfavourable breakdown characteristic; the protection below a  $1\mu s$  front is poor.

### 3.3 SiC arresters

#### Operation

The SiC surge arrester is composed of non-linear resistors in series with spark gaps. The resistors are made of stacks of silicon carbide discs, which can pass large short-circuit currents of some kilo-amps during a short period of some milliseconds. Each stack of discs is provided with multiple spark gaps. Discs and sparkgaps can be seen in fig. 3.6.

If an overvoltage exceeds the flashover voltage  $U_a$  a current  $i$  flows through the SiC discs, see fig 3.5.

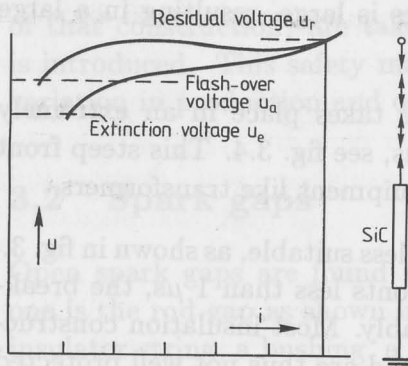


Fig. 3.5. SiC arrester.

The voltage over the discs is restricted by their non-linear char-

acteristic. After the superfluous charge of the overvoltage surge has been removed, the voltage drops to  $U_e$  and the spark gaps extinguish. The energy of the voltage surge is dissipated by the silicon carbide discs. The thermal capacity of the discs must be sufficient to prevent an explosion of the arrester.

In fig. 3.6, an example of an SiC arrester with self-extinguishing spark gaps is shown:

1. At operating voltage, a small current  $i_s$  is caused by the shunt resistors  $s$ . These resistors ensure an even potential distribution when several of these units are placed in series.
2. A voltage surge ignites the spark gaps  $G$  and the current wave passes the SiC discs, where the surge energy is dissipated.
3. The ensuing current  $i_a$  passes the coils, creating a magnetic field that stretches the arcs in the spark gaps. The arcs cool down and extinguish.

### Characteristics

In the following table, some examples are given for the protective characteristics of SiC arresters. Our attention is drawn to the fact that the spark-over voltage at *steep* waves is higher than at *standard* lightning waves, similar to open spark gaps.

Another important characteristic is the *residual* voltage over the arrester during the lightning current wave; arresters are designed for current waves of 5 kA, 10 kA, or 20 kA with a standardized duration of 8/20  $\mu\text{s}$ .

Operating voltage	150 kV	220 kV	400 kV
Spark-over at nominal wave	470 k $\hat{\text{V}}$	500 k $\hat{\text{V}}$	940 k $\hat{\text{V}}$
Spark-over at a steep wave of 1200 kV/ $\mu\text{s}$	540 k $\hat{\text{V}}$	600 k $\hat{\text{V}}$	1010 k $\hat{\text{V}}$
Residual voltage at 10 kA current	440 k $\hat{\text{V}}$	524 k $\hat{\text{V}}$	880 k $\hat{\text{V}}$

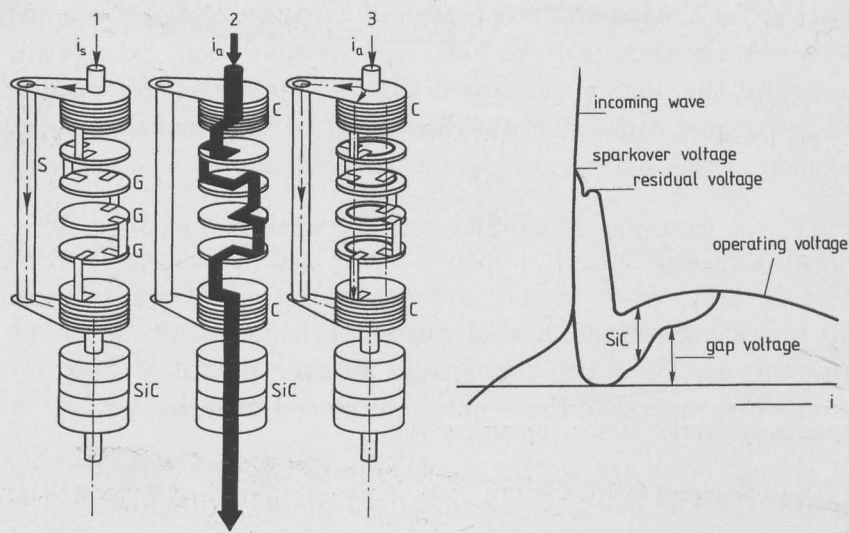


**Fig. 3.6.** SiC surge diverter. An incoming voltage surge trips the spark gaps  $G$  at the spark-over voltage. The current  $i_a$  passes through the non-linear SiC discs and produces there the “residual voltage”. The returning operating voltage is temporarily borne by the SiC disc. In the meantime the spark gaps are extinguished by the magnetic action of the coils  $C$  and the gap voltage increases. The operating voltage re-appears over the spark gaps.

The *protective level* of an arrester is defined as the highest of the following three values:

1. The spark-over voltage at a normal lightning wave;
2. The spark-over voltage at a  $1200 \text{ kV}/\mu\text{s}$  wave, divided by 1.15 (as it is assumed that the solid insulation to be protected is about 1.15 times stronger if there are short time exposures);
3. The residual voltage at the maximum expected current amplitude, chosen here at 10 kA.

The lightning impulse level of the equipment in the network is then chosen at a level which is approximately 25 % higher, as discussed in section 3.1. If this is worked out from the table on page 25, the following lightning withstand levels are obtained, as compared to the basic insulation levels (BILs):

Operating voltage	150 kV	220 kV	400 kV
Basic insulation level, BIL	750 kV	1050 kV	1425 kV
Reduced level	600 kV	680 kV	1200 kV
Reduction by SiC	20 %	35 %	15 %

This is an appreciable decrease in the required insulation level for lightning surges. However, switching surges occur at a lower level and are not always affected by an SiC arrester.

### Comparison with open spark gap

As compared to the open spark gap, several advantages have been gained:

- no short-circuit follows after spark-over.
- the scatter in spark-over voltages is less, which results in a better failure risk level, see fig. 3.1.
- the chopped wave is far less steep than in fig. 3.4.
- the short time breakdown voltage, however, is fairly high as shown in fig. 3.4.

## 3.4 ZnO arresters

The ZnO arrester is composed of discs of metal oxide, usually zinc oxide. The zinc oxide arrester is an important improvement on the SiC arrester, as its non-linear characteristic covers more than 8 decades, see fig. 3.7. This large non-linearity makes it possible to build a surge arrester without spark-gaps: at operating voltages, the leakage current can be limited to some milli-amps, whereas overvoltage impulses can be diverted with current surges of many kilo-amps.

The operation of a metal oxide arrester is simple. Any voltage surge leads immediately (lead times are in the order of 10 ns only) to a current wave which discharges the energy of that wave.

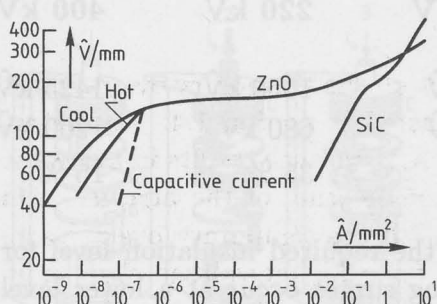


**Fig. 3.7.** The voltage-current characteristic of ZnO arresters is almost flat over many decades. A cool arrester dissipates less leakage current than a hot one after a discharge performance. It can also be seen from this diagram that SiC is quite capable of discharging large currents, but requires a gap in series as the current at the far end of the curve is too large for continuous operation.

### Characteristics

Characteristic for this arrester is the voltage that appears at a switching surge of, for instance, 2 kA and that which appears at a lightning surge of, for instance, 10 kA. These voltages represent the protective levels of the ZnO arrester. The insulation level of the protected equipment is chosen again at a level that is about 25 % higher. In the following table the insulation levels that might be reached with ZnO are compared to the standard insulation level without an arrester.

Operating voltage	150 kV	220 kV	400 kV
Lightning withstand level without arresters, BIL	750 kV	1050 kV	1425 kV
Reduced level	440 kV	660 kV	1030 kV
Reduction by ZnO	40 %	37 %	28 %
Switching withstand level without arrester	550 kV	850 kV	1050 kV
Reduced level	380 kV	570 kV	850 kV
Reduction by ZnO	30 %	32 %	20 %

The reduction of the required insulation level is appreciable so that an attractive decrease in the cost of equipment may be obtained.

### A.C. overvoltage

The reduction, however, is dependent on the temporary overvoltages in the network of the types as discussed in section 1.4. As the arrester is gapless, any increase in the A.C. voltage results in a current through the resistors. To prevent overheating of the arrester, this current may not exceed a safe value. If the temporary overvoltage, TOV for short, is high, an arrester for a higher voltage class must be chosen, which will give an increase in the protection level.

In the extreme example of a network with a non-earthed neutral, the TOV can be as high as  $\sqrt{3}$  times the operating voltage, lasting for many hours. In this case, a ZnO arrester with  $\sqrt{3}$  higher levels must be chosen. If this is applied to the values of the last table, it appears that the reduced levels of that table are increased to about the standard insulation level (BIL). Thus the application of a ZnO arrester would make no sense and an SiC arrester with spark-gaps would here be a better proposition.

### Comparison

If we compare the three methods of protection, the metal oxide arrester scores well:

- *no short-circuit* remains after operating a ZnO arrester.
- *no scatter* in spark-over voltage occurs as there are no spark gaps. The only scatter that remains is due to the scatter in current wave intensity.
- *no steep chopping waves* are formed. In fig. 3.8, the reaction of the three protecting devices is compared. It follows that steep impulses occur in open air gaps and less steep impulses in SiC arresters. The chopping in ZnO arresters is very smooth; this is much appreciated when protecting transformers which are sensitive to steep waves and metal clad switchgear where steep travelling waves with multiple reflections are feared.

The protection against *steep incoming waves* is improved. In fig 3.9, a comparison is made between the insulation level of a power transformer and the protective levels of the three protective devices. The

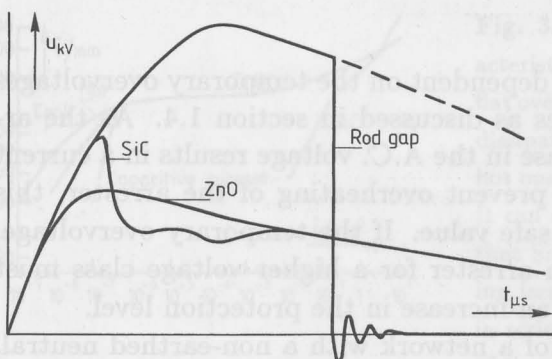


**Fig. 3.8.** Limiting a voltage wave by three types of protecting devices.

range from  $1 \mu s$  to  $8\mu s$  in this figure represents the effect of lightning waves and the range from 100 to  $1000 \mu s$  the effect of switching surges. The upper curve represents the breakdown characteristic of a transformer (as far as such a characteristic can be known because of the high costs of destructive testing).

The second curve is that of a rod-gap; it shows that the rod-gap gives insufficient protection against steep waves: below  $2 \mu s$  front the transformer breaks down at a lower value than the "protective" rod-gap.

The third curve shows the characteristic of an SiC arrester and shows that it protects the transformer well over the full range.

The fourth curve is that of a ZnO arrester. This one is flatter and offers a protective level that is appreciably lower over the full range. The better protection may be used to reduce the failure risk (as indicated in fig. 3.1), to increase the protective range (as will be calculated in section 3.5) so that less arresters are needed in a substation, or to reduce the insulation level so that costs can be saved.

Moreover, *environmental pollution* causes changes in the potential distribution over the porcelain surface. This may lead to unwanted spark-overs of spark gaps in SiC arresters. ZnO-arresters have thus a better resistance to industrial or coastal pollution.

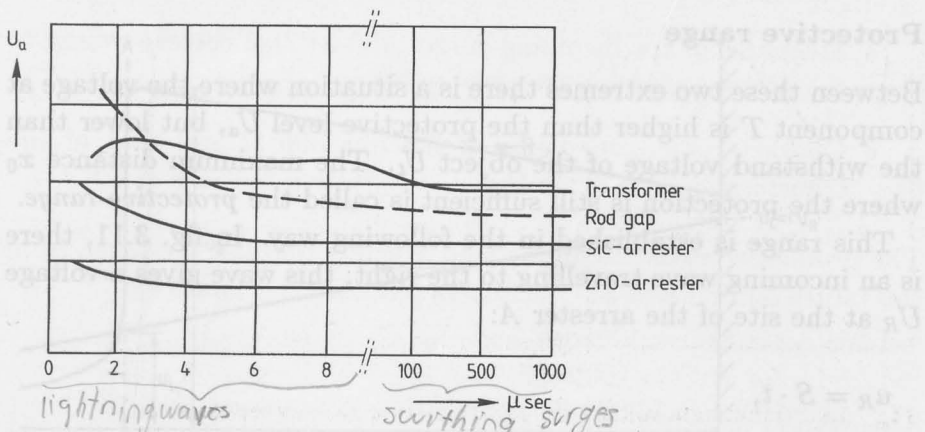


Fig. 3.9. Protecting a transformer by a rod gap, an SiC arrester and a ZnO arrester: breakdown voltage versus breakdown time.

### 3.5 Location of arresters

Surge arresters must be located as near to the equipment to be protected as possible, preferably at the terminals of the equipment.

In fig. 3.10, a lightning arrester *A* is considered at a distance *x* of the protected object, for instance, a transformer *T*. An incoming wave with a steepness of *S* kV/μs comes from the left-hand side.

If *x* is large, in the order of some hundreds of metres, the incoming surge will be limited to the protective level *U<sub>a</sub>* of the arrester. The chopped wave reaches the transformer *T* which has a high surge impedance. The wave is reflected and almost doubles at the terminal of *T*. The voltage arrester is then not quite effective as overvoltages occur at almost twice its protective level: *2U<sub>a</sub>*.

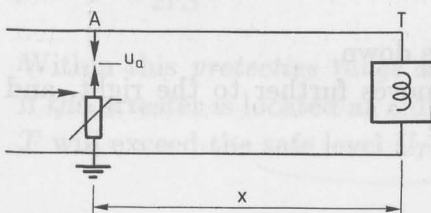


Fig. 3.10. Arrester at a distance *x* to a protected object. If *x* is too large, the overvoltage at the object attains about *2U<sub>a</sub>* and the object is not well protected.

If *x* is small, say a few metres, the wave also reflects but the lightning arrester now reacts at once and the overvoltage cannot grow higher than the protective level *U<sub>a</sub>*.

### Protective range

Between these two extremes there is a situation where the voltage at component  $T$  is higher than the protective level  $U_a$ , but lower than the withstand voltage of the object  $U_t$ . The maximum distance  $x_0$  where the protection is still sufficient is called the *protective range*.

This range is established in the following way. In fig. 3.11, there is an incoming wave travelling to the right, this wave gives a voltage  $U_R$  at the site of the arrester  $A$ :

$$u_R = S \cdot t,$$

where  $S$  is the steepness of the wave in  $\text{kV}/\mu\text{s}$  and  $t$  the time after the wave has reached  $A$ . This wave reflects at  $T$  and comes back at  $A$  with a magnitude  $u_L$ :

$$u_L = r \cdot S(t - 2t_0),$$

where  $r$  is the reflection coefficient at  $T$  and  $t_0$  is the travel time between  $A$  and  $T$ .

These two waves add at  $A$  until the arrester  $A$  breaks down at level  $U_a$ , that is if

$$u_R + u_L = U_a$$

or

$$St_a + rS(t_a - 2t_0) = U_a, \quad (1)$$

where  $t_a$  is the time  $t$  when  $A$  breaks down.

The chopped wave with crest  $St_a$  moves further to the right, and reflects against  $T$  with an amplitude

$$(1 + r)S \cdot t_a.$$

If we allow this voltage to be equal to the withstand voltage  $U_T$  of the transformer  $T$  it follows

$$(1 + r)S \cdot t_a = U_T. \quad (2)$$

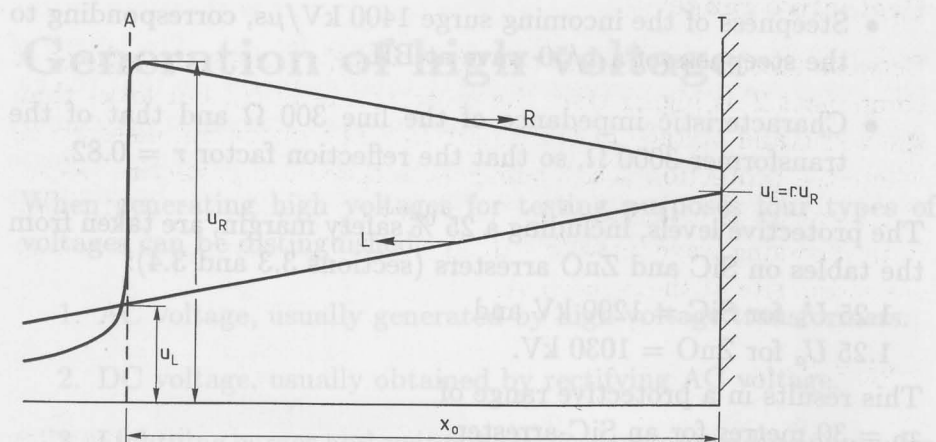


**Fig. 3.11.** Arrester at range  $x$ . The incoming wave  $R$  is reflected and returns as a wave  $L$  to the left. If  $u_R + u_L$  exceed the flash-over voltage  $U_a$  the arrester reacts and a wave with height  $U_R$  reaches the object and causes an overvoltage  $r \cdot U_R$ . From these data the protective range  $x_0$  is calculated.

We now have two equations (1) and (2) from which we can eliminate  $t_a$ . This results in

$$t_0 = \frac{U_T - U_a}{2rS}$$

and as the protective range  $x_0$  is equal to  $vt_0$ , where  $v$  is the propagation velocity:

$$x_0 = \frac{U_T - U_a}{2rS} v.$$

Within this *protective range*  $x_0$  the component  $T$  is just protected; if the arrester is located at a distance larger than  $x_0$ , overvoltages at  $T$  will exceed the safe level  $U_T$ .

### Example

A 400 kV transformer in a substation is chosen as an example and the following characteristics are entered:

- Full withstand level  $U_T = \text{BIL} = 1425 \text{ kV}$ ;

- Steepness of the incoming surge  $1400 \text{ kV}/\mu\text{s}$ , corresponding to the steepness of a  $1/50$  wave at BIL;
- Characteristic impedance of the line  $300 \Omega$  and that of the transformer  $3000 \Omega$ , so that the reflection factor  $r = 0.82$ .

The protective levels, including a 25 % safety margin, are taken from the tables on SiC and ZnO arresters (sections 3.3 and 3.4):

$1.25 U_a$  for SiC = 1200 kV and

$1.25 U_a$  for ZnO = 1030 kV.

This results in a protective range of  $x_0 = 30$  metres for an SiC-arrester, and

$x_0 = 52$  metres for a ZnO arrester,

which is a considerable difference when designing a substation.

### Effect of cables

If underground cables are used for entering a station, the steepness of the incoming wave is substantially decreased. With a cable of 300 to 700 metres, the steepness may decrease from 15 to 30 times. On the other hand, the velocity  $v$  is a factor 1.5 smaller, so that the protective range is 10 to 20 times larger than with open lines.

Moreover, the vulnerable insulation of transformers is less stressed by these slow rising waves, so that the use of underground cables to enter a station is an attractive proposition.

# Chapter 4

## Generation of high voltage

When generating high voltages for testing purposes four types of voltages can be distinguished.

1. AC voltage, usually generated by high voltage transformers.
2. DC voltage, usually obtained by rectifying AC voltage.
3. Lightning surges and switching surges, generated by an impulse generator.
4. Special voltages, such as square waves, for testing lightning arresters or 0.1 Hz for testing cable circuits.

This classification is held to in the present chapter.

### 4.1 A.C. voltage

#### Transformers

Test transformers are characterized by

- high step-up ratios; 500 kV transformers have been built with a primary voltage of 0.5 kV.
- a limited power rating. The current capacity at the high voltage side is usually one to a few amps.
- short-circuit resistance, as breakdown of tested objects may occur frequently.

A short circuit causes the exertion of mechanical forces in the windings, but these are easily withstood at the relatively low currents in question. However, the likelihood of these breakdowns also demands for a good potential distribution over the windings to prevent local

stressing caused by transients. The transformer is therefore wound in layers which are dimensioned as shown in fig. 4.1. The length of the layers is inversely proportional to their diameter, so that the capacitance between layers is kept constant and transients are equally divided over the layers. This results in the typical trapezoidal shape of the H.V.winding, similar to the condenser foils in bushings as discussed in Volume 1, section 11.3.

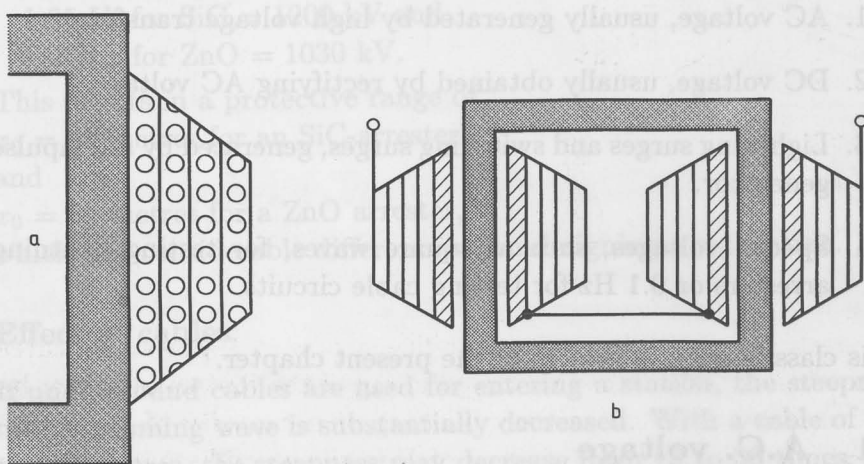


**Fig. 4.1.** a. The layers in an H.V. test transformer are arranged in a trapezoidal shape so that mutual capacitances are made constant and an even potential distribution is obtained at transients during breakdown.

b. Two of these windings in series results in a compact design with the magnetic core at mid-potential.

### Cascade transformers

Although the choice of a secondary voltage is almost unlimited, for practical purposes, transformers are seldom built for voltages higher than 300 to 500 kV. For higher test voltages, several transformers are arranged in *cascade*, as shown in fig. 4.2. The top of the first transformer is connected to the base of the second transformer and so on. The primary windings of the higher transformers have to be energized at a high voltage level. This problem is solved by adding a tertiary winding to the top of the lower transformers. This extra winding is of thick wire and is connected to the primary winding of the following transformer.

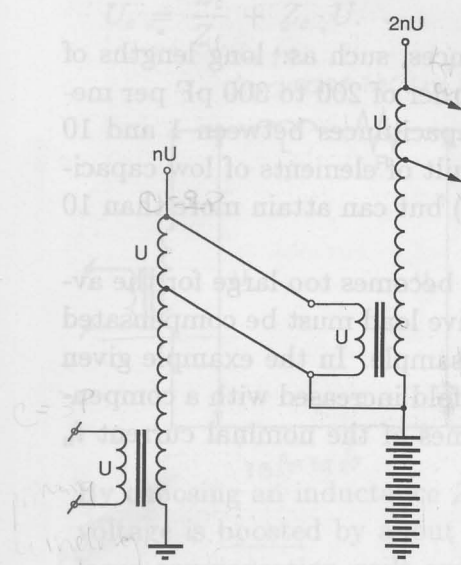


**Fig. 4.2.** Example of a set of cascade transformers. The first transformer has an extra winding that passes the required energy to the second transformer, and so on.

Primary voltage:  $U$

Step-up ratio:  $n$

This tertiary winding must be of sufficient power. A cascade of three stages demands that the primary winding of the first transformer be of a capacity of  $3P$ , a tertiary winding of a capacity of  $2P$  in the first stage and a tertiary winding of  $P$  in the second stage ( $P$  being the power rating of each transformer).

Cascade transformers function well and have some important advantages:

- The single transformers can be used separately, which, in practice in high-voltage laboratories, accounts for perhaps as much as 90 % of the time.
- If required, a three-phase test voltage can be made with the individual transformers of a set of three.

A disadvantage is the high internal impedance of the cascade circuit. The impedances of the individual transformers are not added as would be expected, but they are transformed in a complicated way. For example, in a set of transformers with a 2.5 % short circuit impedance, the cascade connection of two transformers has an 8 % impedance and the cascade of three transformers as much as 23 %.

### Parallel compensation

Some test objects have large capacitances, such as: long lengths of cable which have capacitances in the order of 200 to 300 pF per metre; large power transformers, with capacitances between 1 and 10 nF; and *GIS* substations which are built of elements of low capacitance (in the order of 50 pF per meter) but can attain more than 10 nF in complete substations.

In these cases the capacitive current becomes too large for the average test transformer and the capacitive load must be compensated by an inductance in parallel with the sample. In the example given in fig. 4.3a, the capacitive current is  $n$ -fold increased with a compensating current which may be  $n \pm 1$  times of the nominal current  $i_n$  of the transformer, satisfying

$$|j\omega C U + \frac{U}{j\omega L}| \leq i_n.$$

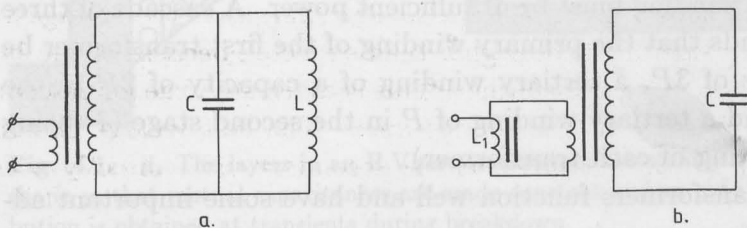


Fig. 4.3. (a) Secondary compensation.

(b) Primary compensation.

In some cases a *primary* compensation is used, as shown in fig. 3.4b. Thus a smaller supply unit can be used as long as the load is purely capacitive. If the maximum allowable current of the supply is  $i_s$  and the transformer ratio is  $N$ , the primary inductance  $L_1$  will satisfy

$$|j\omega C U N + \frac{U}{j\omega L_1 N}| \leq i_s.$$

### Series resonance

Most samples subjected to a high-voltage test are capacitive. The voltage over a capacitive sample can be increased by connecting an inductance in series as shown in fig. 4.4. If the losses in the inductance are neglected, the voltage  $U_c$  over the object is

$$U_c = \frac{Z_c}{Z_L} + Z_c \cdot U.$$

*L to increase the voltage over C*

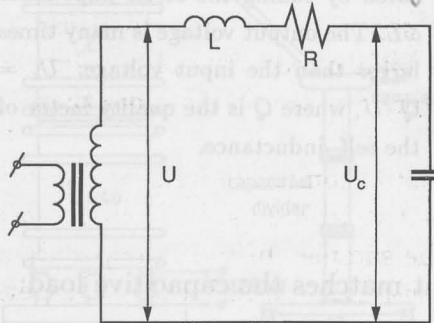


Fig. 4.4. Boosting a transformer by series resonance:  $U_c > U$ .

*most samples objects in HV are capacitive*

By choosing an inductance  $Z_L$  which is not larger than  $\frac{1}{4Z_c}$ , the test voltage is boosted by about 30 %. In industrial laboratories where large compensation coils are available, this is a convenient way to raise the output of the transformers.

The situation shown in fig. 4.4 is also a warning that the voltage at the secondary side might be higher than expected because of the *internal* inductance of a transformer. This is especially true for cascade sets with their large internal inductance. The test voltage should therefore always be measured at the secondary side, directly over the sample.

This applies also to the case of large loss currents such as discharge currents during rain tests or in the presence of heavy corona. In these cases the voltage at the sample may be lower than expected and should be measured *in situ* as well.

### Resonance transformer

If the inductance  $L$  is completely matched to the capacitance  $C$ , high voltage can be generated using an inductance coil only. Such an inductance coil is called a *resonance transformer*, as shown in fig. 4.5 and 4.6. The internal resistance  $R$  (also representing magnetic losses) cannot longer be neglected; the voltage  $U_c$  over the sample is

$$U_c = \frac{1}{j\omega C} \cdot \frac{U}{j\omega L + \frac{1}{j\omega C} + R}.$$

*T*

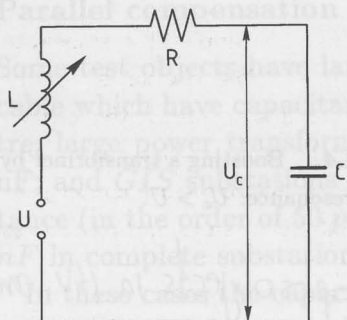


**Fig. 4.5.** Resonance transformer. The load  $\frac{1}{\omega C}$  is completely compensated by tuning the series impedance  $\omega L$ . The output voltage is many times larger than the input voltage:  $U_c = Q \cdot U$ , where  $Q$  is the quality factor of the self-inductance.

The inductance  $L$  is varied so that it matches the capacitive load:

$$j\omega L = \frac{-1}{j\omega C}$$

and

$$\frac{U_c}{U} = \frac{j\omega L}{R},$$

and as  $\frac{\omega L}{R}$  is the quality factor  $Q$  of a coil:

$$|\frac{U_c}{U}| = Q.$$

With modern constructions and materials, quality factors from 40 to 100 can be obtained, so that very high voltages can be reached when feeding with moderate voltages, in the order of 10 to 20 kV. In fig. 4.6 an example is shown of a resonance transformer with a quality factor of  $Q = 40$ . The circuit is supplied by a voltage regulator of 12.5 kV so that a test voltage of 500 kV can be obtained. The current capacity is 30 A, so that large-capacitance samples can be tested. Also small samples, near zero capacitance, can be tested because a voltage divider of about 50 nF is present, which then serves as the load.

The two halves of the resonance transformer can be connected in parallel so that extremely large samples, over 1  $\mu\text{F}$ , can be tested at half the nominal voltage. This is especially of interest when testing long delivery lengths of cable.

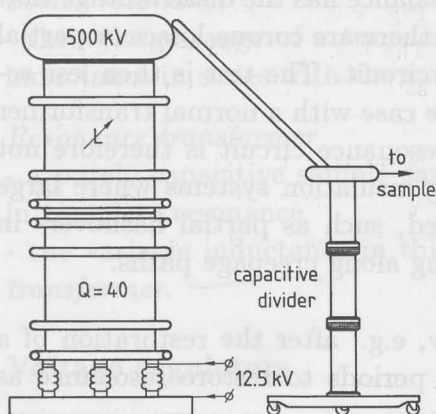


**Fig. 4.6.** Example of a resonance transformer. The reactor is continuously variable to match the capacitance of the sample. At a quality factor  $Q = 40$  this resonance circuit generates 500 kV at an excitation voltage 12.5 kV.

A resonance transformer has several advantages, and one disadvantage:

1. The *wave shape* is purely sinusoidal because high harmonics are not amplified. This improves the accuracy of breakdown tests and is of advantage in Scheringbridge tests.
2. The resonance transformer requires a small power supply. The primary current is the same as the "secondary" current, i.e. the current required by the test object. The supplied power  $P$  is purely ohmic and compared to the capacitive power  $P_c$  in the sample is equal to

$$P = \frac{P_c}{Q}.$$

At a  $Q$  of 40 the required power is only 2.5 % of the (capacitive) power that would be required by a normal transformer circuit. This results in considerable savings in power supply and voltage regulators.

3. *Short-circuit currents* are limited. If a sample breaks down the resonance is broken off, and no heavy currents can arise. The cause of the breakdown is not destroyed and might possibly be traced which is of considerable advantage when doing development work.

4. Simultaneously, this delicate balance has the disadvantage that *fast voltage drops* can occur if there are corona losses or partial breakdowns occur in the test circuit. The test is then less severe than would have been the case with a normal transformer circuit. The use of a series resonance circuit is therefore not permissible for tests involving insulation systems where large pre-discharges can be expected, such as partial flashovers in air, or in systems with tracking along creepage paths.

The recovery of the voltage is slow, e.g. after the restoration of a flashover it takes many oscillation periods to restore resonance as shown in fig. 4.7.

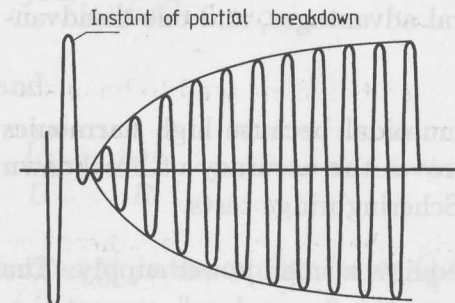


**Fig. 4.7.** If resonance is distorted by a partial breakdown it takes about  $Q$  oscillations before the resonance is completely restored.

### Summary

In summing up, it can be said that the following supply sources for high voltage A.C. are used:

#### *Transformers*

- up to 300 to 500 kV
- in some extreme cases 1 MV may be found as well.

#### *Transformers in cascade*

- usually a set of three
- cascade voltages of 1 MV or more.

#### *Parallel compensation*

- in both the preceding cases, an extra source of capacitive load is found by parallel compensation.

### Series resonance

- the voltage range of a transformer circuit can be extended by an inductance in series with the sample.

### Resonance transformer

- a purely capacitive sample can be tested with the aid of a circuit in complete resonance
- the variable inductance in this circuit is designated as *resonance transformer*.

## Voltage regulators

The primary winding of an H.V. test set-up is supplied with a variable voltage. This variable voltage may be equipped with tapped windings, but these windings give rise to an irregular variation in the voltage.

Sometimes rotating machines are used but these tend to be unstable at heavy capacitive loads. An interesting solution to the above problems is provided by the variable flux transformer as shown in fig. 4.8.

The magnetic circuit comprises a ring-shaped armature, where the magnetic field passes through a circular air gap. In this air gap the magnetic field is evenly divided. The last turn of the secondary winding is guided through this circular field as shown in fig. 4.8. One of the other windings is tapped off by means of a sliding contact. Between this sliding contact and the last winding, a whole number of turns is present, plus  $\alpha$  degrees of the circular field.

When turning the secondary winding around its axis the number of turns can be varied, whereas the flux encompassed by the last turn varies continuously. A continuous voltage regulator is thus provided.

## 4.2 D.C. voltage

### Rectifiers

D.C. voltage is, in the majority of cases, generated by rectifying an A.C. voltage. Rectifying units are based on silicon-diodes of 2 to 3 kV; by the series connection of these diodes and by providing a homogeneous voltage distribution, H.V. diode units can be built for hundreds of kilovolts of blocking potential.

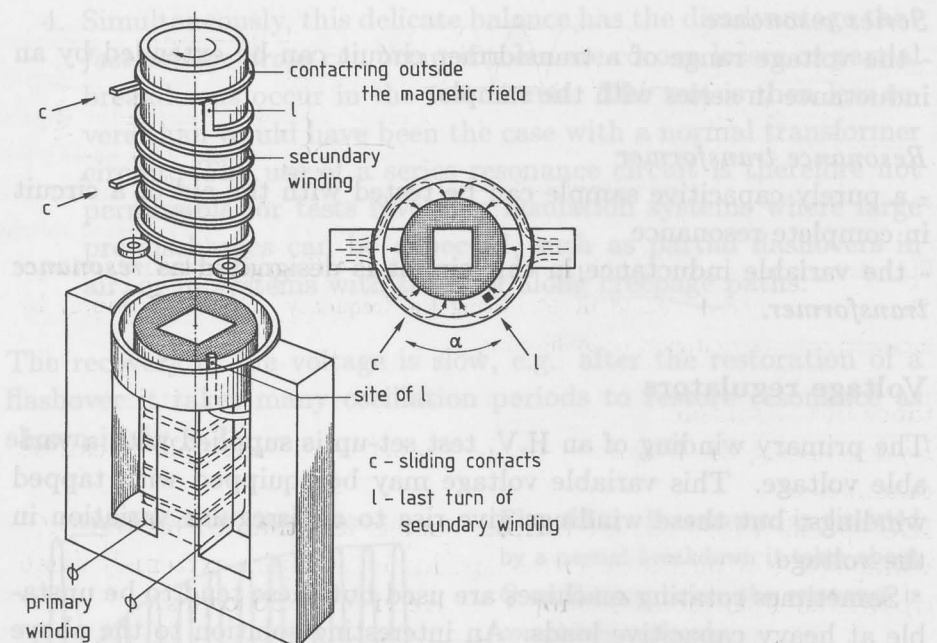


**Fig. 4.8.** Continuous voltage regulator. The last turn  $l$  of the secondary winding is guided through an airgap with a homogeneous magnetic field. The secondary winding can be turned around so that the angle  $\alpha$  between  $l$  and the sliding contacts  $c$  is varied. Thus the secondary winding encompasses a flux that can continuously be varied between  $\alpha=0$  and  $\alpha=360^\circ$ . This enables a continuous variation of the secondary voltage. The lower contact  $c$  follows the spiral so that the number of turns is varied as well.

### Rectifier circuits

For voltages up to about 200 kV, single-phase or bi-phase rectifiers are used, as shown in fig. 4.9. The bi-phase rectifier has the advantage that the magnetic core of the transformer is not saturated with a D.C. current and that the ripple on the D.C. voltage is about halved.

The size of the ripple is calculated as follows:

Between two loading periods  $T$  the leakage current  $i_0$  causes a loss of charge of  $i_0 T$ . This results in a voltage drop

$$v_r = \frac{i_0 T}{C} \quad \text{or} \quad \frac{i_0}{2fC},$$

if  $f$  is the frequency of the A.C. input voltage and  $C$  is the capaci-

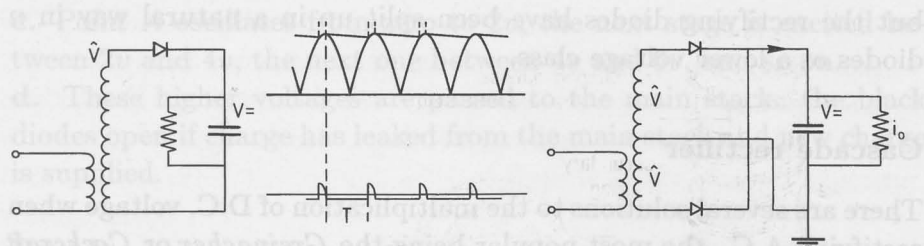


**Fig. 4.9.** Single-phase and bi-phase rectification of A.C. to generate D.C. voltage. The ripple can be decreased by increasing the frequency of the A.C. supply by increasing the capacitance, or by filtering.

tance of the sample.

By increasing the frequency or the capacitance the ripple  $v_r$  can be diminished.

IEC specifications require a ripple that is less than 5% of the D.C. voltage for test purposes. Other applications require extremely small ripples, such as the D.C. supply for electron microscopes.

An interesting variation is the circuit shown in fig. 4.10, which is used in industrial supply units for low energy applications, such as electron microscopes or radar units.

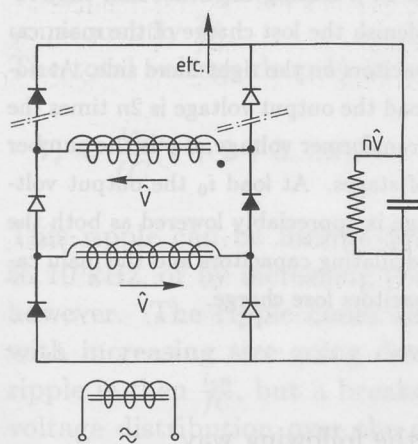


**Fig. 4.10.** An industrial H.V. rectifier. The secondary windings of the transformer are wound in opposite directions. The voltages are added up in a zigzag. At zero load a D.C. voltage of  $n$  times  $\hat{v}$  is obtained.

The secondary windings  $w_1, w_2$  to  $w_n$  are wound in opposite directions so that  $v_1$  is opposite to  $v_2$ ,  $v_2$  to  $v_3$ , etc. In one half of the voltage cycle, the black diodes are opened, in the other half the white ones. The voltages  $v_1$  to  $v_n$  are added and a D.C. voltage  $nv$  is generated. The circuit functions as a bi-phase circuit, as shown in fig. 4.9,

but the rectifying diodes have been split up in a natural way in  $n$  diodes of a lower voltage class.

### Cascade rectifier

There are several solutions to the multiplication of D.C. voltage when rectifying A.C., the most popular being the *Greinacher* or *Cockcroft & Walton* cascade circuit depicted in fig. 4.11.

If the voltage of the input transformer is positive, the *black* diodes are opened and the *main column* on the right-hand side is charged. When the transformer voltage becomes negative, the *white* diodes are opened and the capacitors of the *oscillating column*, on the left-hand side are loaded.

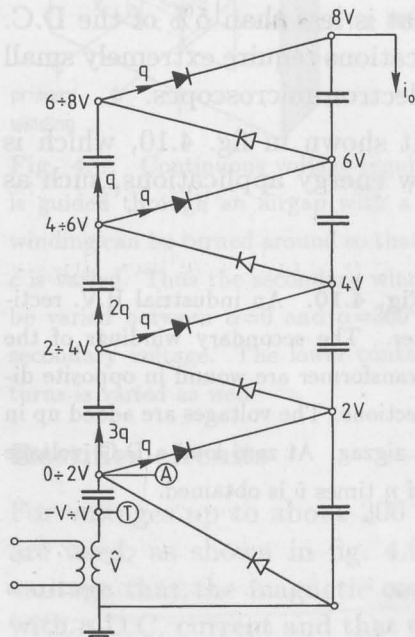


Fig. 4.11. Cascade rectifier according to Greinacher. The column of capacitors on the left-hand side is oscillated by the supplying transformer. During one half of the voltage cycle the oscillating capacitors are charged (up to  $2V$ ). During the other half they replenish the lost charge of the main capacitors on the right-hand side. At no-load the output voltage is  $2n$  times the transformer voltage, if  $n$  is the number of stages. At load  $i_0$  the output voltage is appreciably lowered as both the oscillating capacitors and the main capacitors lose charge.

Voltage multiplication is obtained in the following way:

- In the negative half-period point  $A$  is kept at earth potential as the white diode is open; point  $T$  is at  $-v$ .
- In the following half-period the top of the transformer  $T$  oscillates from  $-v$  to  $+v$ ; as the capacitor is loaded, the potential at  $A$  oscillates from 0 to  $2v$ . At the same time, the black diode opens and this  $2v$ -potential is passed to the first main capacitor on the right.

- c. Point A oscillates from zero to  $2v$ , the next stage is excited between  $2v$  and  $4v$ , the next one between  $4v$  and  $6v$ , and so on.
- d. These higher voltages are passed to the main stack: the black diodes open if charge has leaked from the main stack and new charge is supplied.

### Ripple

During every cycle the last stage on the left-hand side supplies a leakage charge  $q$ , see fig. 4.11. The next stage has to supply the same charge  $q$  to its main capacitor, but also to the oscillating capacitor above:  $2q$  together. The next stage downwards supplies again  $q$  to the smoothing stack, but it also supplies  $2q$  to the capacitor above,  $3q$  altogether; etc.

The upper oscillating stack suffers a voltage drop  $\Delta V$ :

$$\Delta V = \frac{q}{C} = \frac{i_0}{fC},$$

if  $i$  is the leakage current in the sample and  $f$  is the frequency of the A.C. supply.

The next stage supplies a double charge, and its voltage drop is consequently  $\frac{2i_0}{fC}$ .

The total voltage drop  $V_r$  in  $n$  stages is consequently

$$V_r = \frac{i_0}{fC} (1 + 2 + 3 \dots n).$$

This ripple can be limited by increasing the frequency  $f$ , e.g. up to 10 kHz, or by increasing the capacitances  $C$ , which is very costly however. The ripple could also be limited by choosing capacitors with increasing size going downwards:  $C$ ,  $2C$ ,  $3C$ , etc. The total ripple is then  $\frac{i_0 n}{fC}$ , but a breakdown in the sample causes an uneven voltage distribution over the capacitors; the smaller capacitors are then overstressed and tend to break down.

As an example, a cascade generator of 5 equal stages of 100 kV at  $f = 10$  kHz,  $C = 1$  nF and  $i_0 = 1$  mA produces a ripple of  $V_r = 1500$  Volt or 0.3 % of the supplied D.C. voltage.

The voltage drop in the stages is also of consequence in selecting the *number of stages* that can be included in a cascade rectifier. The

voltage drop in the lowest stage increases fast when increasing the number of stages  $n$ , and if this voltage drop becomes larger than  $2v$ , further adding of stages is useless or even detrimental. Depending on the load, frequency and capacitance, the number of stages in practical circuits varies from 3 to 10.

### 4.3 Impulse voltage

Impulse voltages are unipolar and are divided into:

- Lightning pulses to simulate overvoltages caused by lightning strokes.
- Switching pulses to simulate overvoltages caused by switching in networks.

Impulse voltages are characterized by their front time:  $T_f$  in fig. 4.12, and their time to half-value:  $T_h$ .

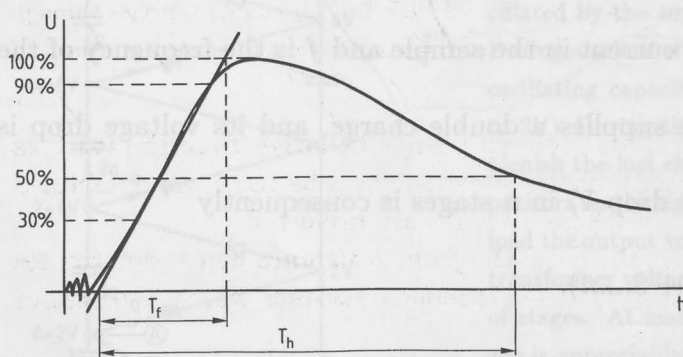


**Fig. 4.12.** A standardized impulse voltage. According to IEC, a lightning impulse has a front of  $1.2 \mu s$  and a tail (to half-value) of  $50 \mu s$ . A switching impulse has a front of  $250 \mu s$  and a tail of  $2500 \mu s$ .

According to IEC specifications, the definition of the front time is  $T_f = 1.67 (T_{90} - T_{30})$ : the measurements are performed between 30 % and 90 % of the crest value. In this way the high frequency transients at the foot and the overshoot at the crest are not taken into account.

*Lightning impulses* are standardized at  $T_f = 1.2 \mu s \pm 30 \%$  and  $T_h = 50 \mu s \pm 20 \%$ .

*Switching impulses* are standardized at  $T_f = 250 \mu s \pm 20 \%$  and  $T_h = 2500 \mu s \pm 60 \%$ .

### Basic circuit

The design of an impulse generator is based on the basic circuit depicted in fig. 4.13. In this circuit,  $C_d$  is the *discharge capacitance* where the energy of the impulse generator is stored and  $C_l$  is the *load capacitance*: the combined capacitance of the sample and the voltage divider.

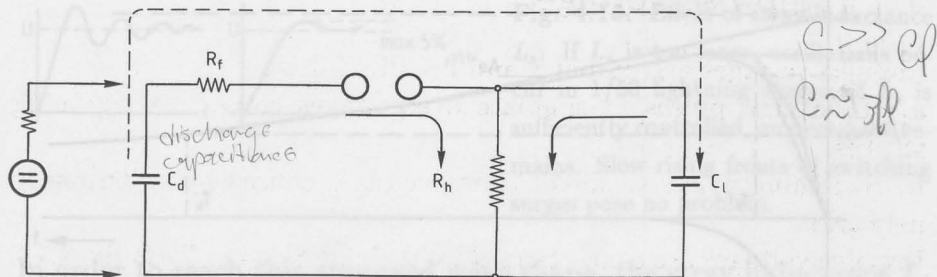


**Fig. 4.13.** Single-stage impulse generator. When the sphere gap is triggered, the charge of the capacitance  $C_d$  is transferred through  $R_f$  to the load  $C_l$ , following the dotted arrow. After this, the combined charge of  $C_d$  and  $C_l$  vanishes through  $R_h$ , following the full arrow. A double exponential wave is generated as shown in fig. 4.14.

The discharge capacitance should always be larger than the load, as otherwise the efficiency of the generator will be too low. A factor 3 may be acceptable, but higher values are preferred.

Further to this circuit,  $R_f$  is the *front resistance* which determines the front time and  $R_h$  is the *discharge resistance* which determines the time to half-value.

The impulse generator functions as follows: the discharge capacitor  $C_d$  is charged by a D.C. source. At a certain moment, the sphere gap breaks down and the capacitance  $C_d$  discharges itself into the load with a time constant

$$\tau_2 = R_f \frac{C_d \cdot C_l}{C_d + C_l}$$

see the dotted line in fig. 4.13.

The voltage at the load increases fast; when this voltage has reached its crest a slower discharge phenomenon sets in, with a time constant

$$\tau_1 = R_h (C_d + C_l),$$

see the full arrow in fig. 4.13. These two charge displacements cause a voltage surge of the shape

$$u = A(e^{-\frac{t}{\tau_1}} - e^{-\frac{t}{\tau_2}}),$$

as shown in fig. 4.14.

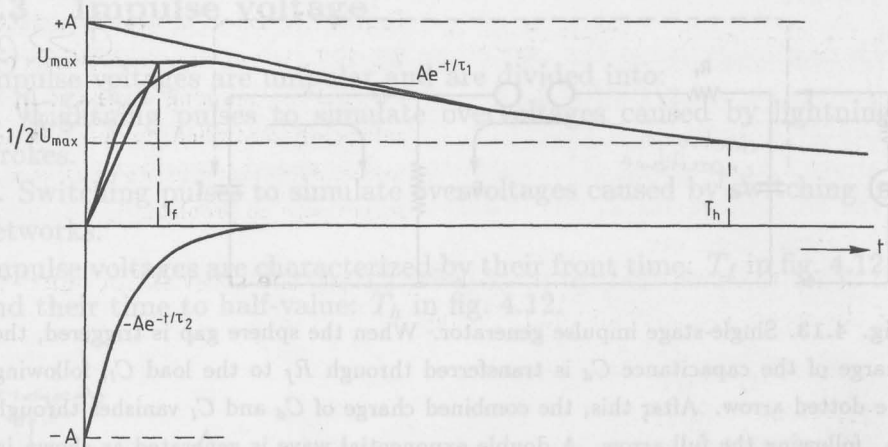


Fig. 4.14. Double exponential curve as generated by impulse generators.

The time constants  $\tau_1$  and  $\tau_2$  bear a certain relationship to the front and half-value times, which have to be computed for every wave shape. For the 1.2/50 wave, the relations are  $T_f = 2.96 \tau_2$  and  $T_h = 0.73 \tau_1$  and front and discharge resistors have to be set accordingly. For the 250/2500 wave  $T_f = 2.4 \tau_2$  and  $T_h = 0.87 \tau_1$ .

The efficiency of the generator is for lightning impulses about

$$\eta = \frac{C_d}{C_d + C_l},$$

and for switching impulses about

$$\eta = \frac{C_d}{C_d + C_l} \cdot \frac{R_h}{R_f + R_h},$$

the efficiency and, consequently, the attainable crest-voltage is thus considerably lower when generating switching impulses.

The inductance of the circuit should be kept low; low-inductance

elements are used and the layout is kept as compact as possible. If too much inductance is present, a waveform as shown in fig. 4.15a occurs; with front times less than  $1 \mu\text{s}$  these oscillations cannot be prevented. At about  $1 \mu\text{s}$  front time the oscillations have vanished but some overshoot still occurs, as shown in fig. 4.15b. IEC standards allow, therefore, an overshoot of up to 5 %.

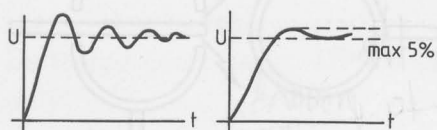


**Fig. 4.15.** Effect of stray inductance  $L_s$ . If  $L_s$  is too large, oscillations occur in 1/50 lightning surges; if  $L_s$  is sufficiently controlled, an overshoot remains. Slow rising fronts of switching surges pose no problem.

In order to reach this approved wave shape, the stray inductance  $L_s$  of the generator circuit shall satisfy:

$$2\sqrt{\frac{L_s}{C_d} + \frac{L_s}{C_l}} \leq R_f.$$

### Multistage generators

A single stage impulse generator according to this basic circuit is used for impulse voltages up to 100 to 200 kV. For higher voltages, the multistage *Marx generator* is used, according to fig. 4.16. With this circuit surprisingly high voltages can be generated by charging the discharge capacitors  $C_d$  *in parallel* and discharging them *in series*. The sphere gaps are diagonally placed between the stages. When the first one is fired, the others follow and a voltage  $n \cdot V$  is generated, where  $n$  is the number of stages and  $V$  the output of one stage. There is no limit to the number of stages as in the case of the Greinacher rectifier, impulse generators up to 10 MV have been built. The wave shape is the same as that of a single stage generator and the same expressions apply for the front and half-value times if  $nR_f$ ,  $nR_h$  and  $\frac{1}{n}C_d$  are inserted.

The *charging resistors*  $R_c$  which are needed for charging the generator are connected in parallel with the discharge resistors  $R_d$  when the generator is fired, they are chosen to be many times larger than  $R_d$  in order not to affect them.  $R_d$  and  $R_f$  in such a generator can

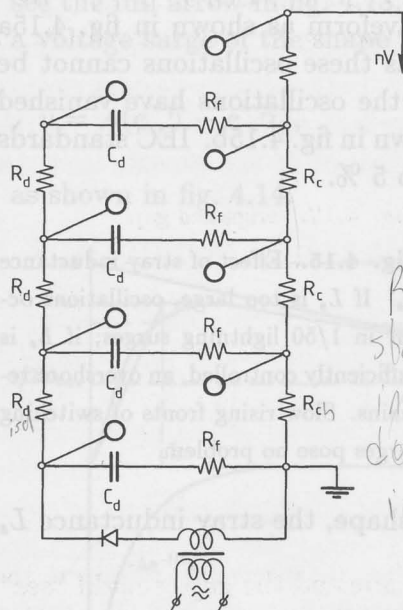


**Fig. 4.16.** Multistage impulse generator. The discharge capacitors  $C_d$  are charged in parallel and are discharged in series when the sphere gaps are fired. The output voltage is multiplied by  $n$ , where  $n$  is the number of stages.

*Rf at the  
stages to prevent  
internal oscillations  
due to the stray  
inductances*

be varied in order to adjust the front and half-value times.

The *first sphere gap* is usually given a slightly smaller gap distance than the other ones: it must be prevented that the higher gaps fire first and that the other stages do not fire, or fire too late.

*Firing the impulse generator* can be accomplished in three ways:

1. By slowly charging the stages until the gaps break down and the generator produces an impulse. Slow charging of the generator starts again, the mechanism repeats itself and the generator produces an impulse every minute or so. The reproducibility of the impulse voltages, however, is unsatisfactory.
2. The first sphere gap is triggered by passing a metal rod ( $E_{cyl} = 2E_{gap}$ ) between the spheres. This yields a good reproducibility, but the instant of firing is still not well defined.
3. In order to determine the exact moment of firing, so that the time sweep of oscilloscopes and other measuring equipment can be tripped, a *triggered sphere gap* according to fig. 4.17 is used. A trigger impulse in the order of 10 kV is used to break down the annular gap. This causes a distortion of the main field,

ultra-violet radiation fills the gap and a source of charged particles occurs at the triggered electrode, so that breakdown of the main gap is initiated.

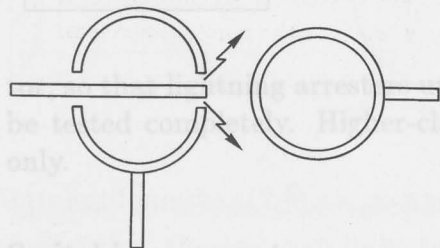


Fig. 4.17. Triggered gap.

Switching current

Current waves of 2000 to 3000  $\mu\text{s}$  are generated in a travelling wave generator according to fig. 4.20.

In all these cases the gaps should be in line and the gaps should "see" each other. Thus the ultra-violet light of the first gap irradiates the others so that breakdown is initiated. If the radiation is blocked, the firing of the generator will be inconsistent and often be incomplete. Internal oscillations are prevented by dividing the front resistors  $R_f$  over the stages. It would have been more practical to concentrate the front resistance  $\Sigma R$  in series with the generator; however, stray inductance would cause oscillations within the stages which would spoil the wave-shape and even cause breakdown of the discharge capacitors.

### Chopped waves

Wave fronts of less than 1  $\mu\text{s}$  are difficult to obtain because of the inductance of the lay-out, nevertheless steep waves with fronts of 0.1  $\mu\text{s}$  or less are needed to test transformers which are sensitive to steep waves. For this reason chopped waves are generated, as shown in fig. 4.18. A rod gap or a triggered multi-gap is placed in parallel with the sample. After a delay-time  $t_0$  the wave is chopped within a time that may be shorter than 0.1  $\mu\text{s}$ .

A rod gap is simple, but it has the disadvantage that the delay time and the steepness are not fully controlled. A triggered gap is more reliable.

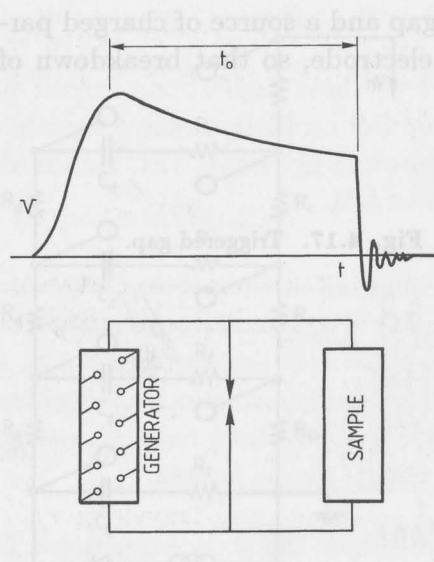


**Fig. 4.18.** Chopped waves are made to simulate the effect of steep fronts. Either a rod gap or a triggered gap chops the wave after  $t_0$  microseconds.

#### 4.4 Special wave shapes

##### Voltage-current generators

For the testing of surge arresters, voltage impulses have to be applied which are followed by current waves of large magnitude. Simulation of lightning is performed with 4/10  $\mu\text{s}$  current waves up to 100 kA and 8/10  $\mu\text{s}$  current waves up to 40 kA, in accordance with the specifications in sections 3.2 and 3.3. For simulating switching surges, tests are performed with 2000 to 3000  $\mu\text{s}$  up to 4 kA.

Further tests are performed, such as stability tests at 115°C, tests with polluted porcelain, tests with repeated current waves, etc.

##### Lightning current

A circuit for generating lightning current is made by connecting all the discharge capacitors  $C_d$  of an impulse generator in parallel, so that a discharge capacitance of several  $\mu\text{F}$  is obtained. The wave front is shaped by an inductance in the order of some tens of  $\mu\text{H}$ , so that no energy is lost in a front resistor. The circuit is attenuated by the resistance of the surge arrester under test, see fig. 4.19.

A 10  $\mu\text{F}$  discharge capacitance can in this way generate a 4/10  $\mu\text{s}$  wave of about 65 A and a 8/20  $\mu\text{s}$  wave of about 40 kA.

The test voltage is limited to the output of one stage of the genera-

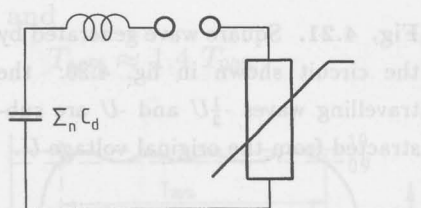


Fig. 4.19. Circuit for generating short waves of high current: 4/10 or 8/20  $\mu$ s.

tor, so that lightning arresters up to about 35 kV phase-to-earth can be tested completely. Higher-class arresters can be tested in parts only.

### Switching current

Current waves of 2000 to 3000  $\mu$ s are generated in a travelling wave generator according to fig. 4.20.

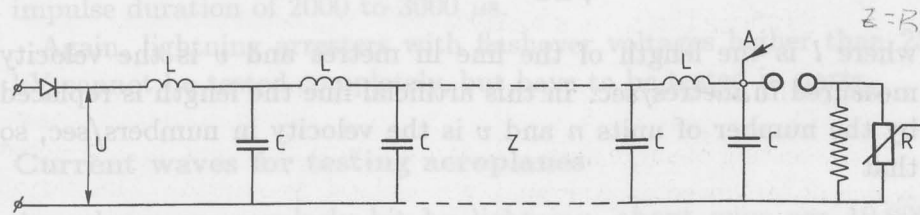
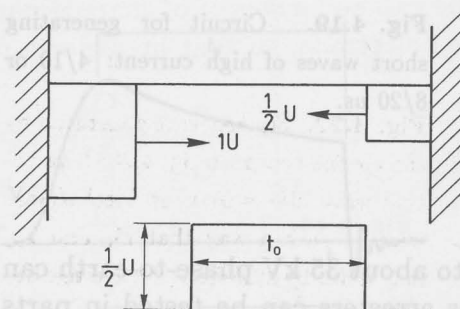


Fig. 4.20. Circuit for generating long waves of fairly high current. The circuit forms an artificial delay line that is charged up to  $U$  kV. After triggering the sphere-gap at  $A$ , a travelling wave  $-\frac{1}{2}U$  goes to the left, reflects and doubles to  $-U$ . The wave is subtracted from the initial  $U$  so that at  $A$  a square wave of twice the delay time results, see also fig. 4.21.

An artificial delay line of 8 to 10 units is charged by a rectifier. When all capacitors are charged, a trigger-impulse is given at  $A$  so that the sphere-gap fires and the delay line feeds into the sample  $R$ . The characteristic impedance  $Z$  of the delay line is chosen to be equal to  $R$ . The voltage  $A$  is then equally divided between  $Z$  and  $R$  and a negative wave  $-\frac{1}{2}U$  moves to the left, see fig. 4.21. This voltage is subtracted from the voltage  $U$  that was present in the line. When this travelling wave meets the other side, the wave is reflected and is doubled. The double wave  $U$  reaches  $A$  and is not reflected again ( $R = Z$ ) so that the voltage at  $A$  becomes  $U - U = 0$  and remains so.



**Fig. 4.21.** Square wave generated by the circuit shown in fig. 4.20: the travelling waves  $\frac{1}{2}U$  and  $-U$  are subtracted from the original voltage  $U$ .

A square wave is generated as shown in fig. 4.21, of amplitude  $\frac{1}{2}U$  and duration  $t_0$ .

In a normal line

$$t_0 = \frac{2l}{v} \quad \text{and} \quad v = \frac{1}{\sqrt{LC}},$$

where  $l$  is the length of the line in metres and  $v$  is the velocity measured in metres/sec. In this artificial line the length is replaced by the number of units  $n$  and  $v$  is the velocity in numbers/sec, so that

$$t_0 = \frac{n}{v} = 2n\sqrt{LC},$$

where  $L$  and  $C$  are the impedances per unit.

$Z$  must be well matched to  $R$  as otherwise a multi-step response is generated. This means that

$$Z = \sqrt{\frac{L}{C}} = R.$$

It follows from these two relations that

$$C = \frac{t_0}{2nR} \quad \text{and} \quad L = CR^2.$$

In spite of the limited number of units (8 to 10), and the non-linearity of the sample, a reasonably square wave is obtained, as shown in fig. 4.22. It appears that

$$T_{90\%} \approx 2(n-1)\sqrt{LC},$$

and

$$T_{10\%} \approx 1.4 T_{90\%}$$

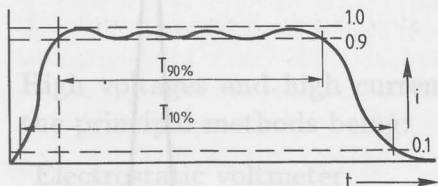


**Fig. 4.22.** Square wave generated by the circuit shown in fig. 4.20. The actual wave differs from an ideal square wave in such a way that  $T_{10}$  and  $T_{90}$  may differ by 20% from the average duration.

In order to obtain this reasonably perfect wave shape, it has been found that the first two inductances should be  $\frac{2}{3}L$  and the last one  $2L$ . In actual generators, the capacitances are adjustable in steps up to about  $50 \mu F$  and the inductances up to about  $5 \text{ mH}$  per unit. Currents up to  $4 \text{ kA}$  can be generated at voltages up to  $25 \text{ kV}$  at an impulse duration of 2000 to 3000  $\mu s$ .

Again, lightning arresters with flashover voltages higher than  $25 \text{ kV}$  cannot be tested completely, but have to be tested in parts.

### Current waves for testing aeroplanes

Aeroplanes are regularly hit by lightning, about once per 10.000 flight hours. The fuselage conducts the lightning current, this current causes no danger in metal planes. However, non-metallic parts such as radar domes may be damaged. The development of non-metallic planes has strengthened the interest in the effect of lightning currents. In order to simulate several current waves in one stroke, special generators have been developed. The current wave in the test object is composed of four phases as shown in fig. 4.23.

The first phase represents the current at the lightning stroke, phase II represents the supply of charge after the stroke. Phase III represents those cases where a longer-period current remains after a stroke, phase IV represents a restrike in the lightning channel which frequently occurs in practice.

Such complicated patterns are not generated by one generator. Several generators are placed in parallel, as shown in fig. 4.24, where the components I to IV generate the current phases I to IV shown in the preceding figure. Voltages up to  $20 \text{ kV}$  can be excited to generate these currents.

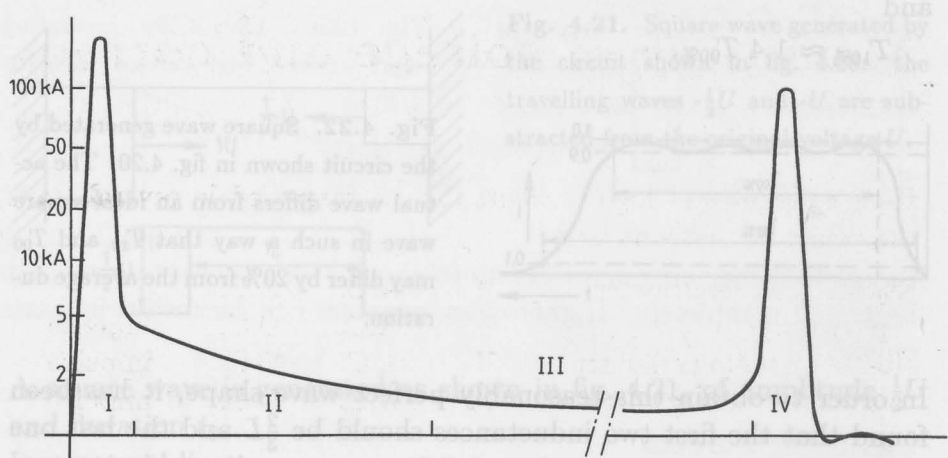


Fig. 4.23. Lightning wave for testing aeroplanes and non-metallic parts of aeroplanes.

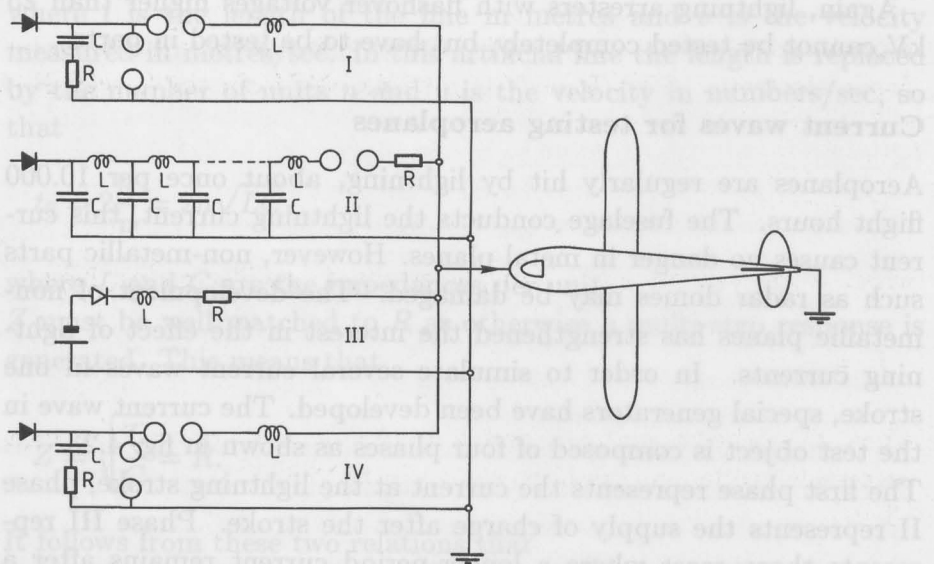


Fig. 4.24. Circuit for generating current waves for testing aeroplanes. It consists of four components that are triggered one by one. Components I and IV are generators for short current waves as shown in fig. 4.19. Component II is a generator for long current waves of a few kA's, as shown in fig. 4.20. Component III generates a current of some hundreds of amps for a few seconds by switching on a conventional battery. Each component is triggered at the right moment by a sphere gap or a thyristor.

# Chapter 5

## Measuring of voltage and current

High voltages and high currents can be measured in several ways, the principal methods being:

Electrostatic voltmeter	U	A.C.	D.C.	
Sphere gaps	U	A.C.	D.C.	impulse
Resistive voltage divider	U	A.C.	D.C.	impulse
Capacitive voltage divider	U	A.C.	D.C.	impulse
Shunt	i	A.C.	D.C.	impulse
Rogowski coil	i	A.C.		impulse

### 5.1 Electrostatic voltmeter

The electrostatic voltmeter makes use of the electrostatic force between electrodes. This force  $F$  can be derived from the energy  $P$  of the electric field between the electrodes:

$$F = \frac{dP}{dx},$$

where  $dx$  represents a small displacement of the electrodes. Now

$$P = \frac{1}{2}CV^2,$$

where  $C$  is the capacitance and  $V$  is the voltage between the measuring electrode and earth, as shown in fig. 5.1.

Then

$$F = \frac{1}{2}V^2 \frac{dC}{dx} = \frac{1}{2}V^2 \frac{d}{dx} \frac{\epsilon S}{d} \quad (\text{where } d \text{ is a variable}),$$

so that

$$F = \frac{1}{2}V^2 \cdot \epsilon \frac{S}{d^2}.$$

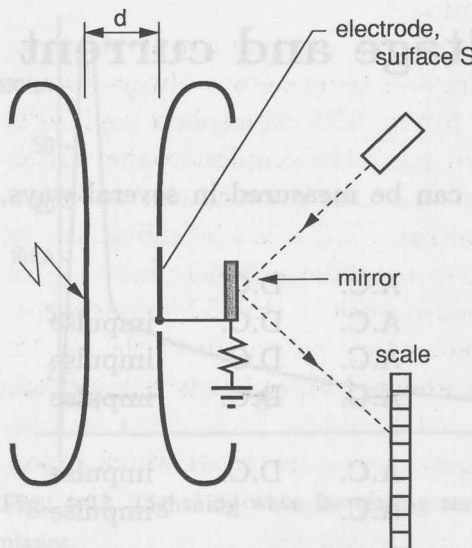


**Fig. 5.1.** Electrostatic voltmeter. The electrostatic force at the measuring electrode causes a small displacement of the mirror. This movement is amplified by a beam of light. The scale is quadratic so that the first quarter of the scale is not very reliable.  
 $S$  = surface of the measuring electrode  
 $d$  = distance between electrodes

As  $\epsilon$ ,  $S$  and  $d$  are fixed quantities which are determined by the design of the instrument, the force  $F$  is proportional to  $V^2$ . The indication at the scale is thus non-linear. Moreover, if an A.C. voltage is measured, the meter indicates the *root-mean-square* value.

Electrostatic voltmeters are available from a few kV full scale to some 500 kV full scale. They have the advantage of a very high input impedance: an insulation resistance of certainly more than  $10^{12}\Omega$  and an input capacitance of the order of magnitude of 10 pF. Hence the electrostatic voltmeter is attractive for tests where the measuring system shall not load the source; for instance a voltage measurement of floating electrodes in high-voltage constructions can well be made with an electrostatic meter.

The basic principle is independent of frequency, so that in practice any voltage from D.C. to 100 MHz can be measured. For obvious reasons the meter cannot be used for measuring lightning or switching surges.

## 5.2 Sphere gap

The most widely known instrument for measuring high voltage is the sphere gap, although its way of functioning makes it more a calibrat-

ing device than a measuring instrument.

Measuring high voltage with the aid of a sphere gap is based on the fact that air of known pressure and temperature always breaks down at the same field strength: for air of 1 atmosphere and  $20^{\circ}\text{C}$  this is about 3 kV/mm. The sphere gap is the simplest configuration where a uniform and predictable field occurs between electrodes.

A high-voltage circuit and its voltage divider can be calibrated by determining the gap distance where breakdown takes place. With the aid of the international IEC tables, such as IEC-52, an inspector can check a test circuit in any laboratory anywhere in the world. The method is not very accurate, about 3 %, but it is reliable and foolproof.

In the IEC specifications, accurate tables are given which represent the correlation between the breakdown strength and the gap distance, as shown in fig. 5.2.

### 5.3 Resistive voltage divider

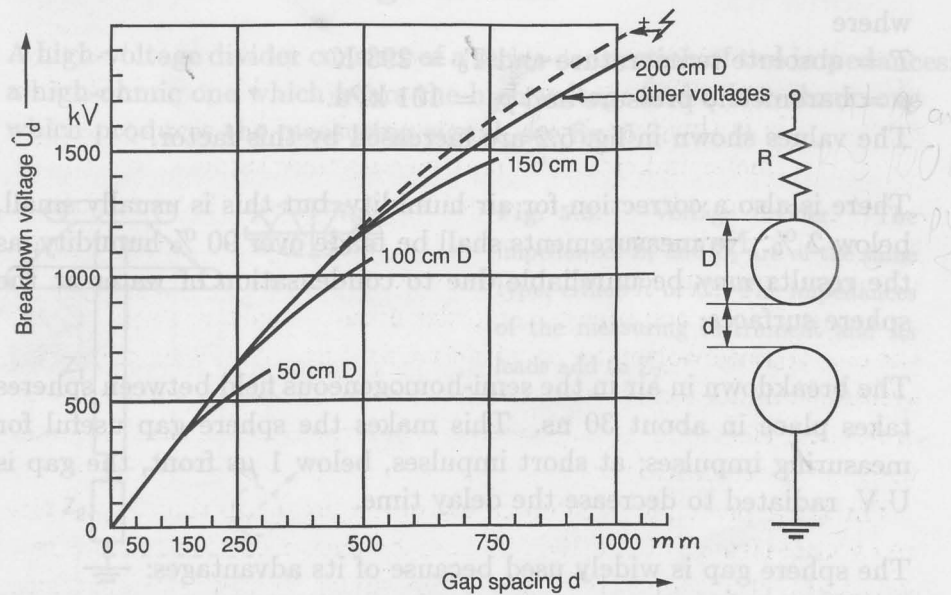


**Fig. 5.2.** The crest voltage  $\hat{U}_d$  at which a sphere gap breaks down as a function of gap spacing. The exact values are well documented in IEC tables. This relationship is used for calibrating D.C., A.C., and impulse voltages. The sphere gap is usually protected by a resistance  $R$  of about  $100 \text{ k}\Omega$  at D.C. and A.C. tests and  $R < 300\Omega$  at impulse tests.

Small corrections are made for air pressure, temperature and humidity.

An accurate field distribution is obtained by satisfying the following

requirements:

- the spheres shall be smooth and free of defects
- no dust shall be present; this applies particularly to D.C. measurements
- the curvature of the surface shall be constant; this can be checked with a spherometer which consists essentially of a tripod with a probe in the centre
- no air currents may be present

A correction  $S$  is made for air density as follows:

$$S = \frac{p T_0}{p_0 T},$$

where

$T$  = absolute temperature and  $T_0 = 293$  K

$p$  = barometric pressure and  $p_0 = 101$  kPa.

The values shown in fig. 5.2 are increased by this factor.

There is also a correction for air humidity, but this is usually small, below 2 %. No measurements shall be made over 90 % humidity, as the results may be unreliable due to condensation of water at the sphere surfaces.

The breakdown in air in the semi-homogeneous field between spheres takes place in about 30 ns. This makes the sphere gap useful for measuring impulses; at short impulses, below 1  $\mu$ s front, the gap is U.V. radiated to decrease the delay time.

The sphere gap is widely used because of its advantages:

- simple device, universally applicable
- measures the crest voltage which usually is decisive in dielectric testing
- measures all types of voltages: D.C., A.C., switching and lightning surges

- large scope: from a few kV's with small spheres of some centimetres diameter to MV's with spheres of some metres diameter

The disadvantages are:

- the accuracy is modest; about 3 % at A.C. and impulses, and about 5 % at D.C.
- does not give a voltage reading but is used to calibrate the readings of a primary voltage source or those of a voltage divider
- time consuming; in order to obtain full accuracy long test series are needed to determine the 50 % breakdown value

### 5.3 Resistive voltage divider

A high-voltage divider consists of a series-connection of two impedances: a high-ohmic one which bears the high voltage and a low-ohmic one which produces the measuring signal, see fig. 5.3.

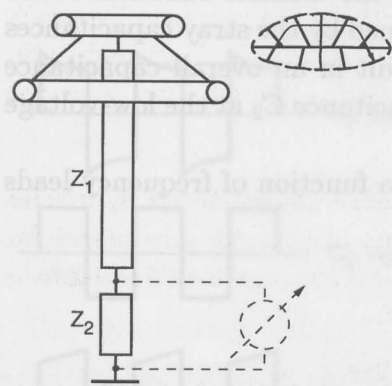


**Fig. 5.3.** Voltage divider. The impedances  $Z_1$  and  $Z_2$  are of the same type, either  $R$  or  $C$ . The impedances of the measuring instrument and its leads add to  $Z_2$ .

In order to prevent corona, which both drains the voltage source and affects the readings, the high-voltage electrode is rounded off by toroids, spheres, or quasi-curved bodies made up of many small plates, as shown in fig. 5.3

In actual cases either *resistors* or *capacitors* are chosen to represent the impedances  $Z_1$  and  $Z_2$ .

### Resistors

The high-voltage arm of the resistive divider is made up of stacks of individual resistors. Wire wound resistors risk having too much self-induction and a strong capacitance; commercially available carbon or metal film resistors are used resulting in a negligible self-induction and a small stray capacitance. The resistors are selected for low temperature and voltage dependency and they are usually aged by heat treatment to obtain a good stability.

The resistors are housed in cylinders of insulating material filled with oil to prevent flashover and corona at the individual resistors. The total length of the cylinders is about 4 metres for every MV, this is required to prevent flashover at lightning and switching surges; dividers for A.C. voltage can be about half as long.

The total resistance of a 1 MV impulse divider may be in the order of 10 to 30 k $\Omega$ . Dividers for higher voltage are usually of the capacitive type.

### Stray capacitances

After constructing a well-designed resistive divider, two types of stray capacitances are left which may affect the transfer function of the divider. The first type of parasite is formed by the stray capacitances over the individual resistors. They result in an overall capacitance  $C_1$  over the high-voltage arm and a capacitance  $C_2$  at the low-voltage side, as shown in fig. 5.4.

Calculation of the transfer function as a function of frequency leads to

$$\frac{v_2}{v_1} = \frac{\frac{R_2}{1+j\omega R_2 C_2}}{\frac{R_1}{1+j\omega R_1 C_1} + \frac{R_2}{1+j\omega R_2 C_2}}$$

If  $R_1 C_1 = R_2 C_2$  the transfer function becomes independent of the frequency:

$$\frac{v_2}{v_1} = \frac{R_2}{R_1 + R_2}$$

The resistive voltage divider can be made frequency-independent by trimming the capacitance  $C_2$ .

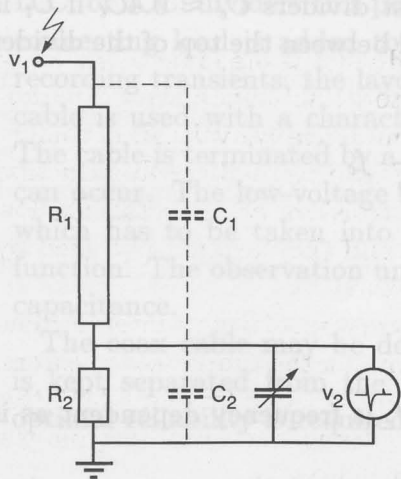


**Fig. 5.4.** Resistive voltage divider. Resistors can be built with negligible self-induction, but parallel stray capacitance cannot be prevented. Their effect can be eliminated by matching  $C_2$  so that  $C_2 = \frac{R_1}{R_2} \cdot C_1$ .

$$C_2 = \frac{R_1}{R_2} C_1.$$

A practical approach is to feed a square wave to the high-voltage side and to adjust the wave shape at the low-voltage side as shown in fig. 5.5. After this adjustment the transfer is true up to very high frequencies and for very steep waves.

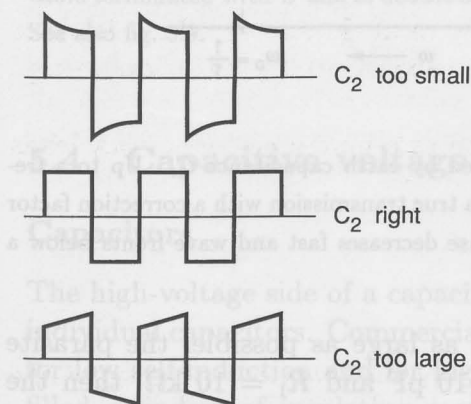


**Fig. 5.5.** Tuning of a resistive divider. The parasite  $C_2$  is trimmed in such a way that the time constant  $C_1 R_1 = C_2 R_2$ . This is obtained by feeding a square wave into the divider.

Another parasite is the stray capacitance from different parts of the divider to earth. The parasites are represented in fig. 5.6 by one earth capacitance at the centre of the high-voltage arm. It has ex-

perimentally been shown that in most dividers  $C_e \approx 0.4C_t$  if  $C_t$  is the total capacitance that is measured between the top of the divider and earth. The transfer function is:

$$\frac{v_{21}}{v_1} = \frac{R_2}{R_1 + R_2} \cdot \frac{1}{1 + j\omega\tau} = \frac{R_2}{R_1 + R_2} \cdot f_c$$

where  $\tau$  is a time constant:

$$\tau = \frac{R_1(R_1 + 2R_2)C_e}{4(R_1 + R_2)}.$$

It follows that the correction factor  $f_c$  is frequency dependent as is graphically shown in fig. 5.6.

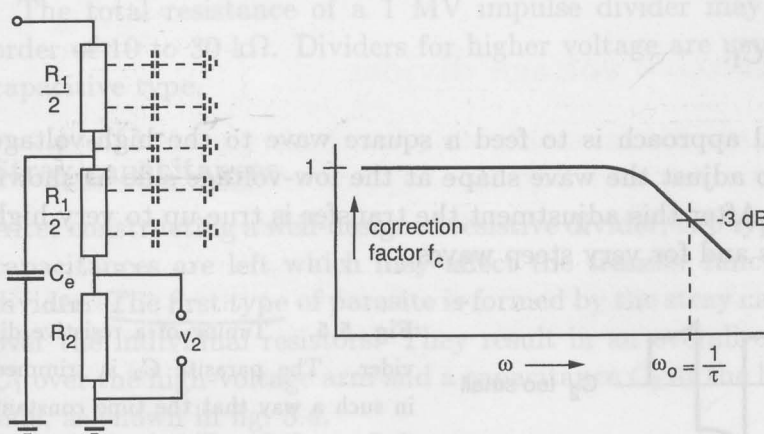


Fig. 5.6. Stray capacitances represented by earth capacitance  $C_e$ . Up to a frequency  $\omega_0 = \frac{1}{\tau}$  the resistive divider gives a true transmission with a correction factor  $f_c$  is 1. Above this frequency the response decreases fast and wave fronts below a length  $\tau$  are not well reproduced.

In order to make the bandwidth as large as possible, the parasite  $C_e$  is kept small. Assume  $C_e = 10 \text{ pF}$  and  $R_1 = 10 \text{ k}\Omega$ , then the bandwidth is about 6 MHz and details longer than about 30 ns can be reproduced.

### Low-voltage arm

For safety reasons, a distance has to be maintained between the divider and the observation equipment as shown in fig. 5.7. For

D.C. or A.C. dividers this poses no problems, the capacitance of the connecting load is added to  $C_2$  and is taken into account. When recording transients, the layout must be carefully designed. A coax cable is used with a characteristic impedance  $Z$ , e.g. 50 or 75  $\Omega$ . The cable is terminated by a resistance  $R = Z$ , so that no reflections can occur. The low-voltage arm is thus loaded with a resistance  $Z$  which has to be taken into account when calculating the transfer function. The observation unit shall have a high-ohmic input of low capacitance.

The coax cable may be double-screened and the measuring loop is kept separated from the high current loop in the laboratory if optimal reliability is required.

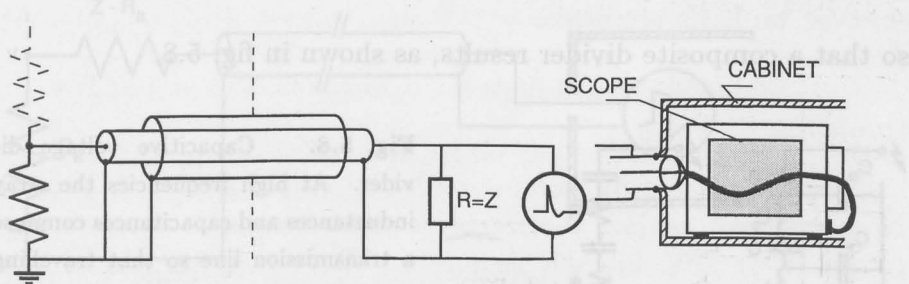


Fig. 5.7. The low-voltage arm of a resistive divider is connected to unit 0 by a coax cable terminated with  $Z$  and is double screened to prevent pick up of disturbances. See also fig. 5.9.

## 5.4 Capacitive voltage divider

### Capacitors

The high-voltage side of a capacitive divider is made up of stacks of individual capacitors. Commercially available capacitors are selected for low self-induction and for high stability. They are housed in oil filled cylinders of insulating material at a length as indicated for resistive dividers.

### Oscillations

Although selected capacitors are used, it cannot be prevented that some stray induction  $L_s$  in the order of a few  $\mu\text{H}$  occurs. Together

with the stray-capacitance to earth  $C_e$ , a transmission line is formed as can be seen from fig. 5.8. (The main capacitors  $C$  do not block this line). The lower side of the line is short-circuited and the upper side can be regarded to be open or at least mismatched. If an impulse enters this line, travelling wave oscillations will occur with very little attenuation, as virtually no losses are present in the capacitors and the stray impedances.

Damping resistors  $R$  are therefore introduced which shall be at least

$$R = 3\sqrt{\frac{L_s}{C_e}},$$

so that a composite divider results, as shown in fig. 5.8.

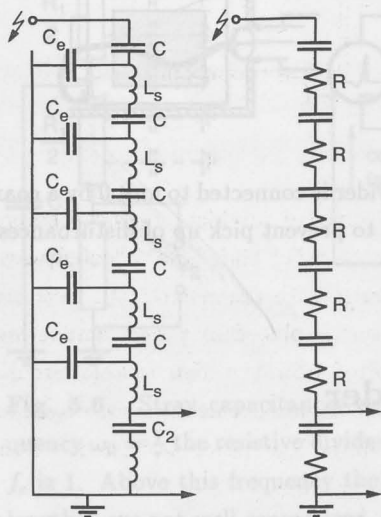


**Fig. 5.8.** Capacitive voltage divider. At high frequencies the stray inductances and capacitances compose a transmission line so that travelling waves may occur which result in oscillations. These oscillations are eliminated by introducing attenuation resistors  $R$ .

This composite divider acts at high frequencies as a resistive divider. The time constant of that divider is about equal to the time constant  $\tau$  as calculated in section 5.3 for resistive dividers.

In an actual example of a 4 MV voltage divider, the upper capacitance is 400 pF, the combined resistance is 260  $\Omega$  and a 70 ns front time can be reached. The divider has a length of 15 metres.

### Low-voltage arm

The low-voltage part of the divider is connected to the observation unit by a coax cable with its characteristic impedance in a way as shown in fig. 5.9. An input resistor is provided which is made equal to the characteristic impedance of the cable minus the attenuation resistance:  $Z - R_a$ . A fast transient voltage arriving at the low-voltage arm is divided over this input resistor and the surge impedance  $Z$ , it enters the cable and is doubled at its open end where it can be recorded. The reflected wave travels back and is eliminated by the series connection of  $Z - R_a$  and  $R_a$  ( $=Z$ ).

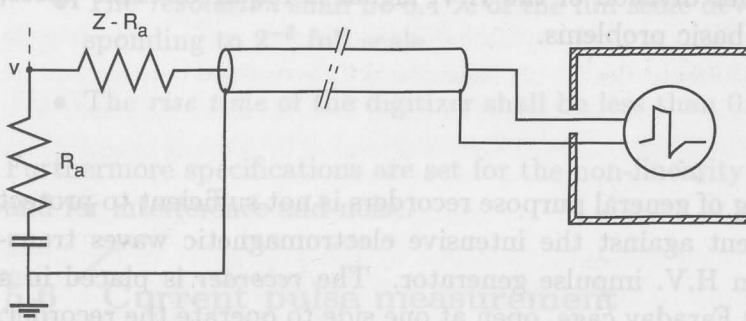


Fig. 5.9. Low-voltage arm of an attenuated capacitive divider. Signal  $v$  enters the coax cable, it is recorded (and it reflects) at the other end. The reflected wave is absorbed by the input resistance  $Z - R_a$  in series with the attenuation resistors  $R_a$ , their sum being  $Z$ . The recording instrument is placed in a well conducting cabinet (e.g. aluminum) with the open end averted from the high-voltage circuit. The coax cable is terminated at the rear end of the cabinet. This measure, together with other precautions, prevents disturbances from the high power test circuit. This is particularly advised if digital recording devices are used.

## 5.5 Digital recording

Digital recording has the advantage over conventional recording by oscilloscopes that the information obtained can be stored and processed better. The use of digital recorders asks for precautions in at least the following three areas:

1. Voltage level of the signal.

2. Shielding against disturbances.
3. Digitalizing the signal.

### Voltage level

Conventional surge test oscilloscopes give direct access to the deflection plates of the cathode-ray tube. The signal can be divided by an adjustable attenuator. The voltage level of the observation unit is quite high, up to about 1 kV. This has the great advantage that the test circuit is fairly insensitive to electromagnetic interference.

Digital recorders and oscilloscopes accept far lower input voltages so that further division of the H.V. signal is required. This poses, however, no basic problems.

### Shielding

The shielding of general purpose recorders is not sufficient to protect the instrument against the intensive electromagnetic waves transmitted by an H.V. impulse generator. The *recorder* is placed in a (incomplete) Faraday cage, open at one side to operate the recorder. At the wall opposite the opening, the signal is received and is passed to the recorder as briefly indicated in fig. 5.7 and 5.9. The recorder is operated at its maximum range.

The *incoming coax line* is double-screened, the outer screen is earthed at both sides. The coax cable is preferably laid in a metallic conduit. Loops are avoided. A further improvement consists of introducing optical transmission by means of glass-fibre cable. Any disturbance caused by potential differences is prevented in this way.

The *main supply* is filtered by inserting an *rf-filter* in the supply line. The recorder is further protected against overvoltages and interference by an isolating transformer with an extremely low capacitance between the windings.

An IEC standard specifies a number of tests to check these precautions, such as current injection in the coax cable shield, a 4 kV transient from the power supply and the application of fast rising electric and magnetic fields of about 0.1 kV/mm and 1 kA/mm. An overall check is made by operating the complete high-voltage and measuring circuit at full test voltage, but without an input signal at

the coax line (line short-circuited or removed).

## Digitizing

A number of requirements are specified by IEC to maintain sufficient accuracy, in the order of 2 % in voltage measurements and about 4 % in time measurement.

- The *sampling rate* shall be more than  $\frac{30}{T}$  if  $T$  is the shortest time-interval to be resolved. The sampling rate shall also be larger than  $8f_m$  if  $f_m$  is the highest frequency to be measured.
- The *resolution* shall be 0.4 % of the full scale deviation, corresponding to  $2^{-8}$  full scale.
- The *rise time* of the digitizer shall be less than 0.03 T.

Furthermore specifications are set for the non-linearity of the scales and for interference and noise.

## 5.6 Current pulse measurement

When performing high-voltage tests, in particular impulse tests, the magnitude of the current(s) in the test object is of interest as well. Two techniques are commonly used: the low-ohmic shunt and the Rogowski coil.

### Low-ohmic shunt

Measuring current with a low-ohmic shunt leads to the very simple circuit of fig. 5.10a. The resistivity is usually in the range of 1 to 100 mΩ. At these low values, the stray capacitances are so low that they are negligible for frequencies up to about 100 MHz. If normal wire wound resistors are used, however, the self-inductance  $L$  becomes too large and an equivalent circuit, as shown in fig. 5.10b, is valid. The shunt can then be used at D.C. or at A.C. of fairly low frequencies only.

In order to obtain a low stray inductance, a coaxial construction is adopted. The voltage drop over the inner cylinder is measured, as shown in fig. 5.11. The bandwidth of this coaxial shunt is not

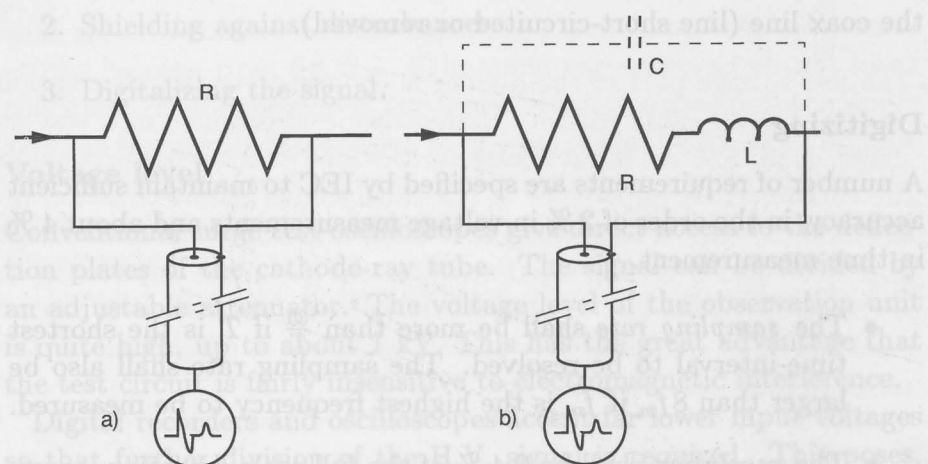


**Fig. 5.10. a.** Measuring current with a low-ohmic resistor:  $v = R \cdot i$ . **b.** Impulse currents and high frequencies can not be measured if conventional constructions are used for the resistor: the inherent self-induction tends to affect the result:  $v = Ri + L \frac{di}{dt}$ . The simple relationship of figure a is restored by choosing coaxial shunts as shown in fig. 5.11.

determined by its self-induction, but by the skin effect in the inner resistive cylinder. The skin depth  $\delta$  in the wall is equal to

$$\delta^2 = \frac{1}{\pi \cdot f \cdot x \mu_0 \mu_r},$$

where  $\delta$  is the depth in the material at which the magnetic field is reduced  $\frac{1}{e}$  times,  $f$  is the frequency,  $\mu_0 = 4\pi \cdot 10^{-7} \frac{Vs}{Am}$  and  $\mu_r$  is the relative magnetic permeability, in most resistive materials  $\mu_r \approx 1$ . By choosing a small wall thickness, the bandwidth can be increased to about 100 MHz, which is more than sufficient for most industrial tests. For special purposes, a bandwidth up to 1000 MHz can be obtained, which corresponds to a time constant of the order of 1 ns. A further restriction is the heat dissipation that can be offered by the shunt. If a current pulse  $i$  occurs during a short time  $t$ , the temperature rise  $T$  is adiabatic and the resistive cylinder  $R$  absorbs an energy

$$\int_0^t i^2 R \cdot dt = G \cdot T \cdot c,$$

where  $G$  is the weight of the inner cylinder, and  $c$  is the specific

The flux density  $B_{rad}$  is proportional to the current  $i$  and the distance between the two cylinders is proportional to the current  $i$ . The flux through the coil:

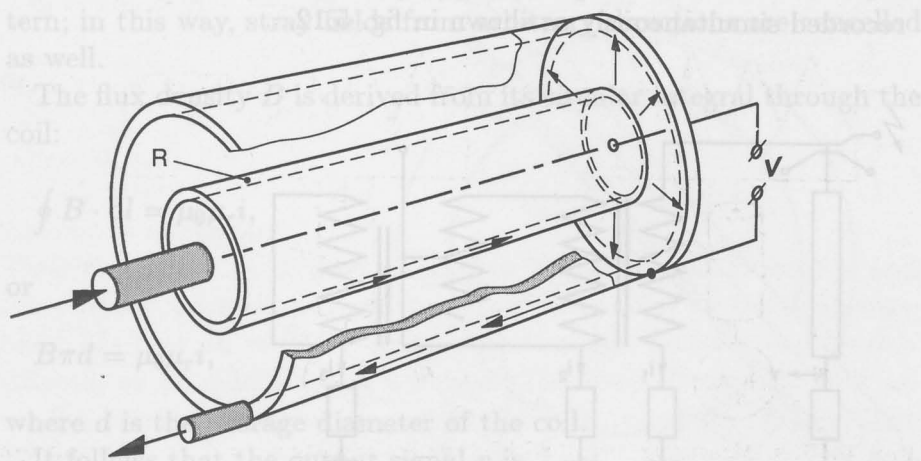


**Fig. 5.11.** Coaxial shunt. The self-inductance is negligible because of the drastic reduction of the magnetic flux. The inner cylinder  $R$  is made of resistive material, with a low temperature coefficient ( $1$  to  $10^{-6}$  per  $^{\circ}\text{C}$ ) to secure linearity. The voltage drop  $v$  is measured across the inner cylinder. It follows that the output signal is proportional to the current  $i$ .

$$\int_0^t i^2 dt = \frac{G \cdot T_m c}{R},$$

where  $T_m$  is the maximum permissible temperature rise.

It follows that the impulse rating is directly proportional to the weight  $G$ , which leads to weighty constructions if large currents have to be measured.

This demand for weight is contrary to the requirement for a small wall thickness to restrict the skin effect. A good compromise, however, can be found and shunts in the multi kA-range can be made which are able to record all required details of current impulses caused by lightning and chopped lightning waves.

### Combined voltage-current test

When impulse testing a power transformer, the H.V. winding is connected to the impulse generator and its voltage divider. The H.V. winding, L.V. winding and tertiary windings are connected to earth

via a shunt. The voltage  $v$  and the current waves  $i_1, i_2$  and  $i_3$  are recorded simultaneously as shown in fig. 5.12.

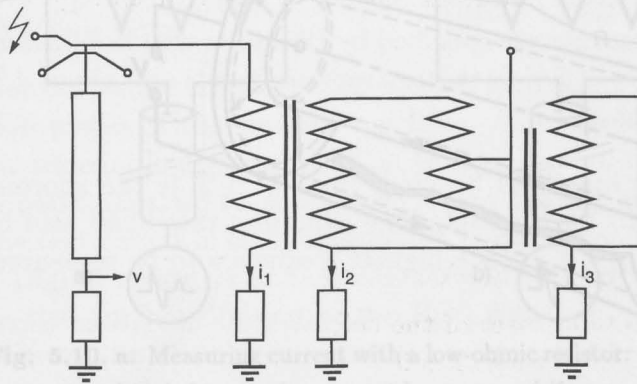


Fig. 5.12. Impulse testing of a power transformer. The non-tested windings are short-circuited, their capacitive currents  $i_2$  and  $i_3$  are measured.

Reference records are made at approximately 60 % of the test voltage (or any voltage sufficiently low not to cause dielectric defects). Then the transformer is tested at full test level, often with 10 positive and 10 negative shots, and is tested with chopped waves if required. Oscillograms are made of all shots and all full-level recordings are required to have the same wave shape as the reference record.

### Rogowski coil

If no metallic contact with the current conductor is wanted a coil as shown in fig. 5.13 is used.

The output voltage  $v$  of the coil is equal to

$$|v| = \frac{d\phi}{dt},$$

the encompassed flux  $\phi$  being equal to

$$\phi = n \cdot A \cdot B,$$

where  $n$  is the number of turns,  $A$  is the surface of one winding and  $B$  is the magnetic flux density. A large number of turns and turns perpendicular to the ring, are supposed. As turns are by necessity

tilted, two winding are usually applied with turns in a crosswise pattern; in this way, stray fields from arbitrary directions are cancelled as well.

The flux density  $B$  is derived from its circular integral through the coil:

$$\oint \mathbf{B} \cdot d\mathbf{l} = \mu_0 \mu_r i,$$

or

$$B\pi d = \mu_0 \mu_r i,$$

where  $d$  is the average diameter of the coil.

It follows that the output signal  $v$  is

$$v = \frac{n\mu_0 \mu_r A}{\pi d} \frac{di}{dt},$$

also written as

$$v = M \frac{di}{dt},$$

so that the output signal of the coil is directly proportional to the time-derivative of the measured current.

Integration of  $\frac{di}{dt}$  is required to obtain a signal that is proportional to  $i$ . This can be realized in two ways:

- with an electronic integrator
- with a passive network

Following the second possibility an interesting passive network can be formed from the self-induction  $L$  of the Rogowski coil itself. This is shown in fig. 5.13a. The output signal  $v_2$  is

$$v_2 = Ri_2,$$

where  $i$  is derived from

$$v = (R + R_s)i_2 + L \frac{di_2}{dt}.$$

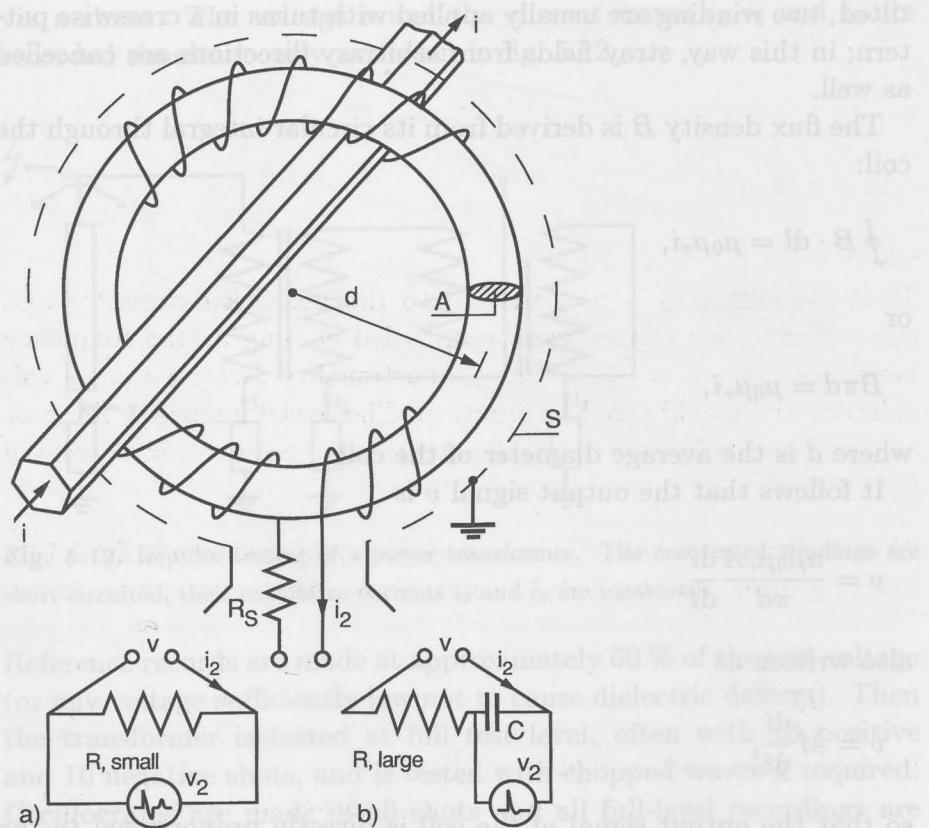


**Fig. 5.13.** Rogowski coil. The coil is placed around a conductor to measure the current  $i$  in the conductor. The coil is screened against electric stray fields by screen  $S$ . The output voltage is equal to  $v = M \frac{di}{dt}$ , where  $M$  is the mutual inductance between coil and conductor. The signal  $v$  can be integrated by electronic means or by a passive circuit. In figure a a passive circuit is formed by the inherent self-inductances of the coil and by  $R + R_s$ . In figure b an  $RC$  network is used. In both cases a linear relationship  $v_2 = c \cdot i$  is achieved.

A low value is chosen for  $R$  so that for frequencies resulting in  $\omega L > R + R_s$  the effect of  $R + R_s$  can be neglected and

$$v = L \frac{di_2}{dt}, \quad \text{or} \quad i_2 = \frac{1}{L} \int v \cdot dt$$

$$v_2 = Ri_2 = R \int \frac{M}{L} \frac{di}{dt} dt$$

or

$$v_2 = c \cdot i,$$

where  $c$  is a constant.

Thus the signal  $v_2$  is proportional to the measured current  $i$  and the current wave shapes can be recorded as long as the frequency band lies over  $\omega_0 = \frac{R+R_s}{L}$ . The proportionality factor  $c$  can be calculated, or be calibrated in practice. The lower frequency limit  $\omega_0$  can be lowered by decreasing  $R$ ; at the cost, however, of decreased sensitivity.

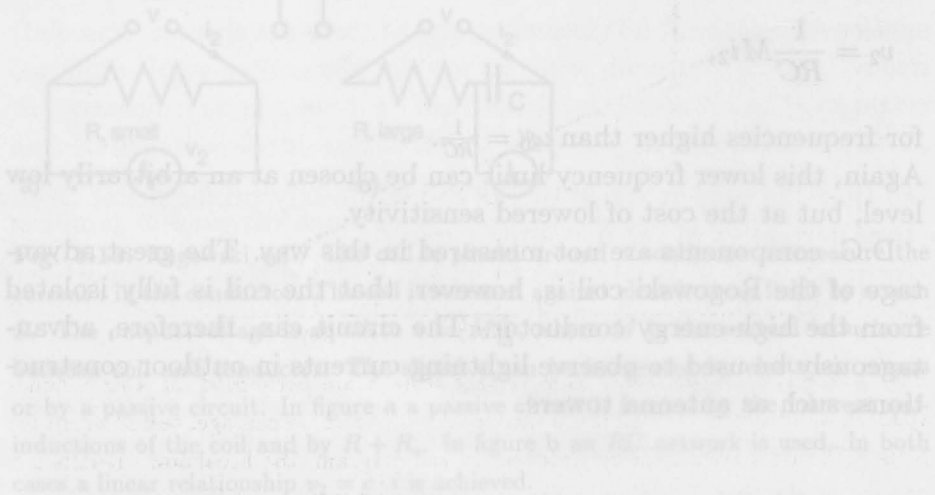
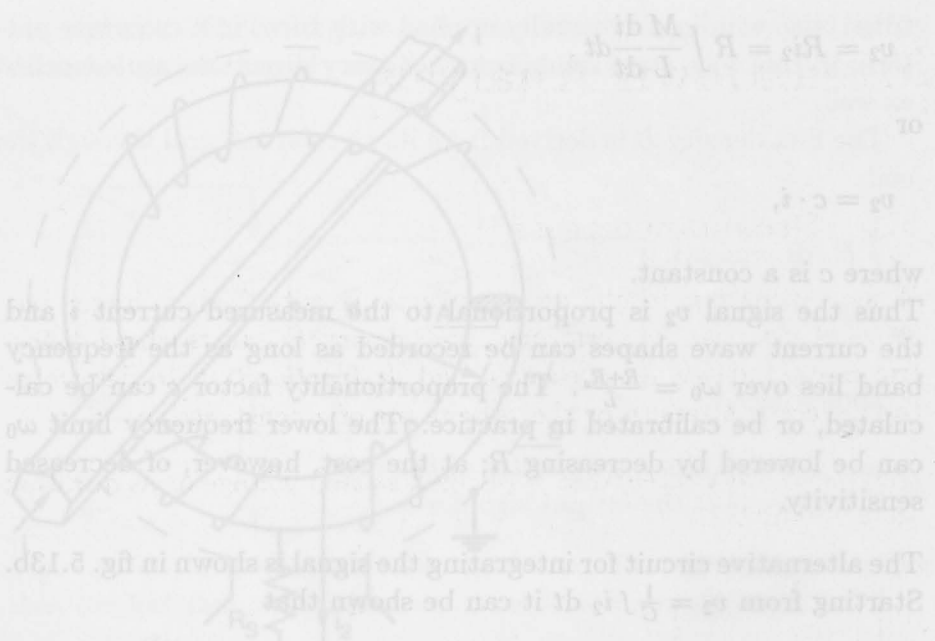
The alternative circuit for integrating the signal is shown in fig. 5.13b. Starting from  $v_2 = \frac{1}{C} \int i_2 dt$  it can be shown that

$$v_2 = \frac{1}{RC} Mi_2,$$

for frequencies higher than  $\omega_0 = \frac{1}{RC}$ .

Again, this lower frequency limit can be chosen at an arbitrarily low level, but at the cost of lowered sensitivity.

D.C. components are not measured in this way. The great advantage of the Rogowski coil is, however, that the coil is fully isolated from the high-energy conductor. The circuit can, therefore, advantageously be used to observe lightning currents in outdoor constructions, such as antenna towers.



A low value is chosen for  $R_2$  so that for frequencies resulting in  $\omega L > R + R_2$  the effect of  $R + R_2$  can be neglected and

$v = L \frac{di_2}{dt}$  or  $i_2 = \frac{1}{L} \int v \cdot dt$

and

# Chapter 6

## Breakdown Analysis

### 6.1 Breakdown tests

When evaluating insulation constructions with high voltage, two types of tests can be performed: *non-destructive tests* where dielectric characteristics are measured and *destructive tests* to determine the dielectric strength or the voltage life of a construction.

Destructive tests are either performed as step voltage or as duration tests, see fig. 6.1.

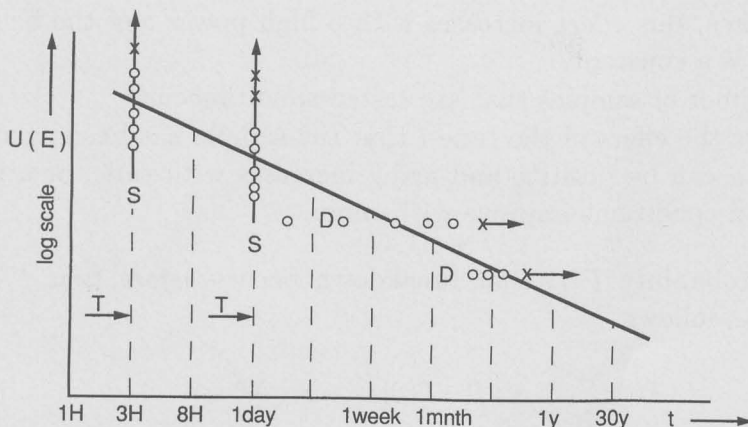


Fig. 6.1. Breakdown tests. Step voltage tests  $S$  are performed for a fixed time-span  $T$ , after which the voltage is increased by a fixed percentage, tested again for a time  $T$ , and so on, until breakdown. In the diagram, the breakdown results are entered at the time  $T$  (although the previous aging would justify somewhat longer times) and at the voltage  $U$  (or the field strength  $E$ ) where breakdown took place. Samples where no breakdown occurred are indicated with an arrow. Duration tests  $D$  are performed at a fixed voltage (or field strength) and the times-to-breakdown are entered at their  $U$  (or  $E$ ) level. The scatter in the results is usually so large that comparison or further processing of results is impossible without statistical tools.

In both cases, a large scatter is encountered in life tests often stretch-

ing over several decades of time. In order to cope with these widely scattering results, a statistical method has been adopted based on statistics that had been developed by the mathematician *Weibull* for aging tests on mechanical structures.

## 6.2 Weibull Distribution

The Weibull distribution of a *duration test* is based on the probability  $\Delta P$  that a sample that is unbroken at time  $t$  will break down before  $t + \Delta t$ . Weibull makes the following assumption for this probability:

$$\Delta P = k E^b p t^a \Delta t.$$

$E^b$  represents the effect of the field strength  $E$ . In accordance with the experience, this effect increases with a high power  $b$  of the field strength;  $k$  is a constant.

$p$  is the number of samples that are tested simultaneously.

$t^a$  represents the effect of the time  $t$  that the sample has been aged. The power  $a$  can be positive and aging increases with time, or  $a$  is negative and conditions improve with time.

Now the probability  $P(t)$  that breakdown occurs *before time  $t$*  is calculated as follows:

$$\begin{array}{lcl} P(t + \Delta t) & = & P(t) + [1 - P(t)] \times \Delta P \\ \text{Breakdown before } t + \Delta t & = & \text{breakdown before } t + \text{no breakdown before } t \times \text{breakdown between } t \text{ and } t + \Delta t \end{array}$$

It follows that

$$\frac{P(t + \Delta t) - P(t)}{1 - P(t)} = \Delta P,$$

which can be read as a differential equation:

$$\frac{dP(t)}{1 - P(t)} = \Delta P = k \cdot E^b p \cdot t^a \Delta t,$$

which can be integrated:

$$-\ln[1 - P(t)] = \frac{k}{a+1} E^b p t^{a+1} + C,$$

replace  $a+1$  by  $m$ , then

$$\ln[1 - P(t)] = -\frac{k}{m} E^b p t^m + C.$$

From the boundary condition  $P(t)=0$  if  $t=0$ , it follows that  $C=0$ . The probability for breakdown before moment  $t$  is thus:

$$P(t) = 1 - \exp[-\frac{k}{m} E^b p t^m].$$

By introducing a time constant  $t_0$ :

$$t_0 = \left( \frac{m}{k} \cdot \frac{1}{E^b} \cdot \frac{1}{p} \right)^{\frac{1}{m}}$$

this expression can be simplified to

$$P(t) = 1 - \exp - \left[ \frac{t}{t_0} \right]^m.$$

This is the classic expression for the Weibull distribution which is found in most literature on the subject. For practical reasons it is usually written in a double-logarithmic shape:

$$\ln\{-\ln[1 - P(t)]\} = m \ln t - m \ln t_0.$$

A vertical scale  $y = \ln\{-\ln[1 - P(t)]\}$  is used for the probability  $P(t)$ . Time  $t$  is projected at the horizontal scale as  $x = \ln t$ . Then a straight line  $y = mx - C_0$  occurs, as shown in fig. 6.2. The slope of this line is given by  $m$ , and its location is given by the time constant  $t_0$  that is found at  $P=63.2\%$ .

An unknown distribution of breakdowns is recorded as follows: if  $p$  samples have been tested, the first breakdown is entered as  $P(t) = \frac{1}{p+1}$  at its time-to-breakdown, the second one as  $\frac{2}{p+1}$  at its particular time-to-breakdown, and so on. ( $p+1$  is used to prevent  $P$  reaching 1). These data are plotted, a straight line is drawn through them, and  $t_0$  and  $m$  are determined. In fig. 6.16, at the

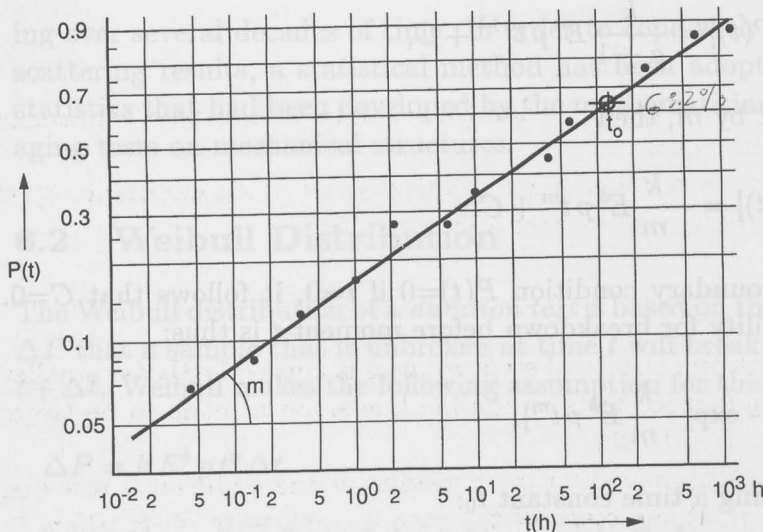


**Fig. 6.2.** Weibull distribution on Weibull probability paper. The probability  $P(t)$  that a sample has broken down before  $t$  is entered at a normalized scale for  $P(t)$ ; the time to breakdown  $t$  is projected at a logarithmic time scale. The statistic population is then represented by a straight line. An indication for the average *life time* is found at the spot where the Weibull curve reaches  $P = 63.2\%$ ; the breakdown time there is equal to  $t_0$ , the *time constant* of the Weibull distribution. An indication of the scatter in the population is given by the slope of the curve which is equal to the *exponent*  $m$  of the Weibull distribution.

end of this chapter, a diagram is presented for this purpose. In this way, an extensive set of scattered results can be represented by two characteristic values,  $t_0$  and  $m$  only; this is the great strength of the use of a distribution like Weibull's.

(The time constant  $t_0$  is, in the literature, also called *scale parameter* and the slope  $m$  is called *shape parameter*).

### 6.3 Step-up tests

The preceding distribution was worked out for endurance tests; the same expression can be used for step-up tests. In that case, the voltage  $u$  (or the field strength  $E$ ) at which breakdown occurs, is entered at the horizontal scale and a Weibull diagram, as shown in fig. 6.3 is recorded, where

$$P(u) = 1 - \exp\left[-\left(\frac{u}{u_0}\right)^b\right],$$

where  $u_0$  is the 63.2 % breakdown strength and slope  $b$  represents the scatter in results.

There exists a relationship with the slope  $m$  of the endurance test: the slope  $b$  of the step-up test appears to be

$$b = n \cdot m.$$

The scatter in the results of step-up tests is consequently far smaller than with endurance tests as the life line slope  $n$  tends to be large, in the order of 10 to 20.

A relationship with the time constant of the endurance test can also be made. If the steps of the step-up test were of duration  $T$ , this corresponds to an endurance test at constant voltage  $U_0$  with a time constant  $t_0 = T$ . Moreover, endurance tests at other voltages can be derived from the one at  $u_0$  by applying the  $n^{\text{th}}$  power rule.

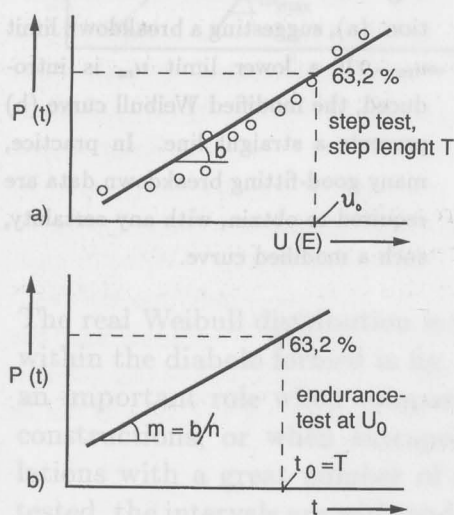


**Fig. 6.3.** Figure a illustrates the use of a Weibull distribution for a step-up test: the voltage (or stress) is increased every  $T$  minutes. The breakdown voltages/stresses are recorded.  $U_0$  is the resulting scale parameter,  $b$  the shape parameter. Figure b represents the Weibull curve of an endurance test for an identical set of samples: a step test with steps of duration  $T$  corresponds to an endurance test at  $U_0$  with a scale parameter  $T$  and a shape parameter  $b = n \cdot m$ .

## 6.4 Weibull distribution with lower limit

Sometimes, a Weibull distribution is used with a lower limit  $u_m$

$$P = 1 - \exp\left[-\left(\frac{u - u_m}{u_0}\right)^b\right],$$

which expresses the assumption that below a certain voltage  $u_m$  (or  $E_m$  if field strength is used) no breakdown can take place. The normal Weibull distribution is then curved, as shown in fig. 6.4a, and is represented as a straight line if  $u - u_m$  is entered at the horizontal scale, as shown in fig. 6.4b.

Two remarks have to be made here:

1. A large number of statistical results is needed to ascertain that the Weibull distribution is curved and to find out, by trial-and-error, which value for  $u_m$  yields a straight line as in fig. 6.4b. At least a hundred or more results are required to recognize this lower level distribution.
2. In practical cases, such low values for  $u_m$  are found so that little difference between the low-probability branches in fig. 6.4a and b results.

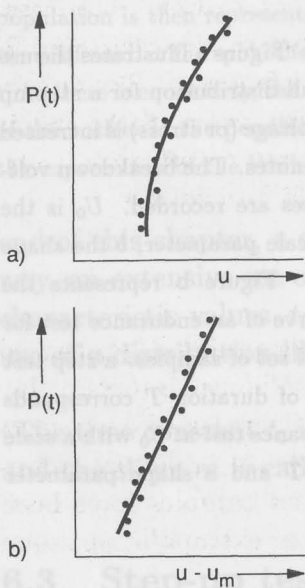


**Fig. 6.4.** Curved Weibull distribution (a), suggesting a breakdown limit  $u_m$ . If a lower limit  $u_m$  is introduced, the modified Weibull curve (b) presents a straight line. In practice, many good-fitting breakdown data are required to obtain, with any certainty, such a modified curve.

## 6.5 Confidence intervals

Breakdown tests at industrial components are so laborious and so expensive, that only limited numbers of samples can be tested; at

the utmost, 20 to 30 samples of medium voltage level, or 5 samples of high voltage level can be afforded.

The Weibull curves derived from these numbers contain much uncertainty. For this reason, confidence intervals are introduced, which express the fact that, with 95 % probability, the real  $t_0$  (of an infinite number of samples) may be found between  $t_{min}$  and  $t_{max}$ , as shown in fig. 6.5.

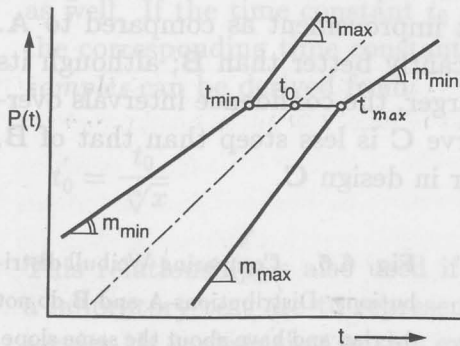


**Fig. 6.5.** Confidence limits. The time constant  $t_0$  lies with 95 % probability between  $t_{min}$  and  $t_{max}$ . Starting from  $t_{max}$  lines are drawn with maximum en minimum slopes. These lines represent the upper confidence limits (with 97.5 % probability). In a similar way the lower confidence limits (2.5 %) are derived from  $t_{min}$ . The diabolo-shaped figure represents the area in which the real Weibull curve is situated with 95 % probability.

The real Weibull distribution is then with great probability situated within the diabolo formed in fig. 6.5. These confidence intervals play an important role when comparing Weibull diagrams of competing constructions, or when extrapolating test results to actual populations with a great number of samples. If few samples have been tested, the intervals are wide and comparisons or extrapolations soon lose their value.

Several techniques exist to determine these intervals, with slightly different results, but no generally adopted calculation technique is available. For this reason, reference to a calculation procedure is given in the annex of this book. This procedure is used in the H.V. laboratory of Delft University. It is not claimed that this procedure is the best one available.

## 6.6 Applications

### Comparison between tests

#### *Tests at the same voltage level*

The most frequent application of the Weibull distribution is the comparison of sets of different design samples, especially when checking improvements in design.

Breakdown tests are performed for different sets of various designs, and the Weibull curves are compared, as shown in the example in fig. 6.6. Confidence intervals play an important role here. In fig. 6.6, design **B** constitutes a significant improvement as compared to **A**. Design **C**, however, is not significantly better than **B**; although its time constant  $t_0$  is significantly larger, the confidence intervals overlap. Even worse, the slope of curve **C** is less steep than that of **B**, representing an increase of scatter in design **C**.

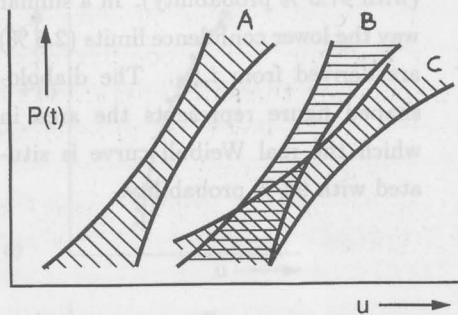


Fig. 6.6. Comparing Weibull distributions. Distributions **A** and **B** do not overlap and have about the same slope, so that **B** is definitely better than **A**. Population **C** has a 63 % breakdown voltage that is higher than that of **B**, and would for that reason have been regarded as "better". Weibull's analysis, however, reveals that the confidence intervals overlap and that the slope of **C** is less steep so that no physical improvement of **C** over **B** can be concluded.

#### *Tests at different voltage levels*

If endurance tests have been performed at different voltage levels (or different field strengths), the results are not directly comparable. However, the effect of field strength is incorporated in the assumptions made by Weibull, see section 6.2. It can readily be shown that the time constant  $t_0$ , found on a test at field strength  $E$ , is equivalent to the time constant  $t'_0$  obtained at another field strength  $E'$ , if

$$t'_0 = \left(\frac{E}{E'}\right)^n t_0,$$

where  $n$  is the slope of the well-known life line  $L = \frac{c}{E^n}$ .

Tests at different levels can be transformed to one voltage (or field strength) level and can then be compared, as in fig. 6.6. A warning should be added here: Do not stretch this extrapolation too far as the life line parameter  $n$  is generally not too precisely known.

#### *Effect of the number of samples*

Tests performed with different numbers of samples can be compared as well. If the time constant  $t_0$  of a test of a certain size is known, the corresponding time constant  $t'_0$  for a test with  $x$  times as many samples can be derived from:

$$t'_0 = \frac{t_0}{\sqrt[m]{x}}$$

This relationship is also used if a restricted number of samples in a laboratory test are to represent a large number of components in service. It is clear that in this extrapolation the shape parameter  $m$  plays an important role: a large scatter, i.e. a low value of  $m$ , makes this extrapolation to service conditions unfavourable.

It also entails a warning that extrapolation shall not be carried too far, as the proper value of  $m$  varies between wide limits.

#### *Volume effect*

It can readily be seen that if the volume of the dielectric is increased  $x$  times, the relationship

$$t'_0 = \frac{t_0}{\sqrt[m]{x}}$$

is also valid, as long as the field strengths in the dielectric are maintained at the same level. This is called the *volume effect* of the Weibull distribution.

#### *Test on cables*

Consequently, this relationship is also valid if the lengths of cables under test are increased  $x$  times.

If, however, the insulation thickness of a cable is increased (maintaining the maximum field strength), this relationship *cannot* be used; the distribution of the field is then changed as well. On the other hand, it can be shown that (at least if  $\frac{R}{r} \geq 1.4$  and  $m \geq 1$ ) an  $x$  times larger *cross-section* complies with the relationship above. Cables with different cross-sections can thus be compared, even if they differ in insulation thickness.

(When combining the effect of length and cross section, the remarkable conclusion can be drawn that the life of such a high-voltage cable is statistically related to *the volume of the conductor*, not to that of the insulation.)

### Slope of the life curve

The most ambitious use made of the Weibull distribution is if a series of tests is performed to determine the slope  $n$  of the life curve in the expression  $L = \frac{C}{E^n}$  or  $\frac{C}{U^n}$ . Endurance tests are then performed at different levels and the results are recorded in a diagram as shown in fig. 6.7. The scale parameters  $t_0$  are entered together with their 95 % confidence intervals. A straight line is fitted through these parameters  $t_0$  to represent a life curve and its slope  $n$  is determined.

It is to be realized, however, that this line can, with 95 % probability, be situated anywhere between the boundaries shown in fig. 6.7, which represents an appreciable uncertainty in the value of  $n$ . In order to restrict this uncertainty, the number of tests at each level should be large, at least 15 at each level, but preferably 100. This poses, of course, great problems with respect to the costs of these series of tests.

The number of voltage levels should at least amount to 4 and should be selected such that the tests at high level do not suffer from unwanted effects (flashover at edges, breakdown at terminals, etc.) or from breakdown by other mechanisms (thermal, creepage). The low level tests should be chosen in such a way that breakdown can be expected within a reasonable period, although tests for some years of duration are sometimes accepted.

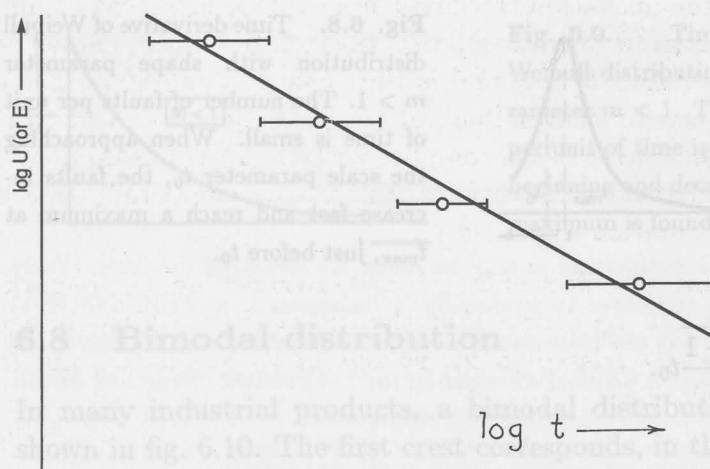


**Fig. 6.7.** Determining the slope of the life curve of a certain design by testing numerous samples (15 to 100) at different voltage levels (at least 4 levels). The results from each test level are summarized in a Weibull distribution. The  $t_0$  and the confidence intervals of these distributions are entered in the figure. An intelligent guess is made of the slope  $n$  of the ensuing life curve.

## 6.7 Differential curve

If the time derivative of the Weibull distribution is calculated, an expression is derived that predicts the number of breakdowns in a period of time:

$$\frac{\Delta P}{\Delta t} = \frac{\text{number of breakdowns in period } \Delta t}{\text{number of samples at the beginning}}$$

The *shape* of this distribution depends on the value of the shape parameter  $m$ .

If  $m > 1$ , this expression has a maximum as shown in fig. 6.8. For a long time practically no breakdowns take place; shortly before  $t_{max}$ , breakdowns start, increase fast in number and reach a maximum. After this, the number of breakdowns per unit of time decrease again, not because the dielectric has improved, but because a decreasing number of samples is available.

The maximum of this curve is found at

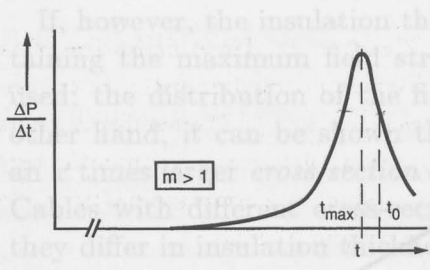


**Fig. 6.8.** Time derivative of Weibull distribution with shape parameter  $m > 1$ . The number of faults per unit of time is small. When approaching the scale parameter  $t_0$ , the faults increase fast and reach a maximum at  $t_{max}$ , just before  $t_0$ .

(When combining no effect of length and cross section, the remarkable conclusion can be drawn that the life of such a high-voltage cable is related to the volume of the conductor, not to its length.)

For instance, if

$$m = 3 \quad t_{max} = 0.87 t_0$$

$$m = 9 \quad t_{max} = 0.99 t_0$$

$$m = \infty \quad t_{max} \rightarrow t_0.$$

The maximum in the differential curve is thus not far from the time constant  $t_0$ .

#### Statistics at operating voltage

Fig. 6.8 is also representative for the life curve of H.V. components or that of cables at operating voltages. Statistically, there is a difference as broken down components are replaced and faulty cables are repaired. But in the first part of the curve, the replacements are few and the distribution remains valid. As soon as many components tend to break down, the population becomes a threat for the service-reliability and the components are integrally replaced, or in the case of a cable circuit, the cable is renewed. Consequently, the first part of the Weibull curve is also valid in operational circumstances.

#### Distribution with a downward slope

If  $m < 1$ , the shape of the differential curve is as shown in fig. 6.9; many breakdowns occur at the very beginning and their number decreases gradually as fewer and fewer samples are left to be broken down. This is a situation that shall be prevented at all costs, as it leads to completely unsatisfactory service-reliability.

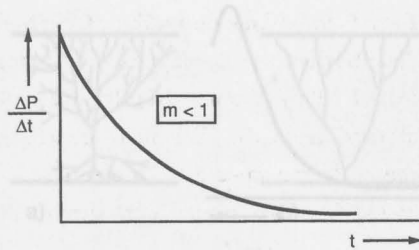


**Fig. 6.9.** Time derivative of a Weibull distribution with a shape parameter  $m < 1$ . The number of faults per unit of time is large from the very beginning and decreases gradually. No maximum is found.

## 6.8 Bimodal distribution

In many industrial products, a bimodal distribution is found, as shown in fig. 6.10. The first crest corresponds, in that case, to samples which have a production fault, for instance an inclusion in the dielectric. After the production faults have been removed by these early breakdowns, the majority of samples contain smaller, natural defects. In a well designed product, these samples live for 30 years or more at  $U_0$  before the breakdown characteristic rises again and the natural life of the product is reached.

This dual distribution is the base for various routine tests: a voltage of 2.5 to 3 times nominal voltage is applied for a relatively short period, 15 to 30 min. to remove the early breakdowns. In this way, production faults are discovered and the healthy samples are left over.

Tests on cross-linked polyethylene cables have, for instance, shown that 99.9 % of the early breakdowns are found in the first half hour at 3 times the nominal voltage. This is an excellent basis for a routine test at  $3U_0$ .

## 6.9 Interpretation of breakdown tracks

After a sample has broken down it still contains information in the form of a breakdown channel. For this reason it is worthwhile to restrict the short-circuit current by fast tripping or by using a resonance transformer (see section 4.1). In this way, as much of the pre-breakdown track is spared as possible. This track is studied, preferably by making a sketch of the track. Photographing may be useful, but only sketching can give a clear picture: the breakdown channel often follows a complicated three-dimensional path, hidden

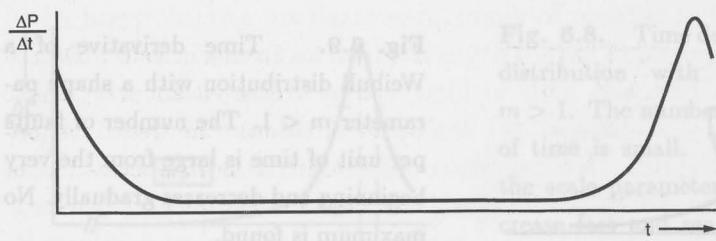


**Fig. 6.10.** Bimodal distribution as may be found for industrial products. Early breakdown which is attributed to production faults appear in a negative ( $m < 1$ ) slope. Thereafter, a very low fault rate occurs until the "natural" voltage life of the product is reached and a nominal distribution ( $m > 1$ ) occurs. Time  $t$  is, in this picture, presented at a very condensed logarithmic scale.

within the insulation material, which can best be reconstructed by drawing projections from different sides.

Studying breakdown tracks is an underdeveloped tool in high-voltage engineering and careful analysis of breakdown channels is a valuable addition to the usual test techniques.

### Treeing in solids

Any defect in a solid dielectric can initiate treeing: a cavity, an inclusion of foreign matter, a protrusion on the electrode, etc. After the first few microns in a solid have broken down, a certain probability exists that further breakdown takes place at a different angle. There is also a probability that the breakdown path forks so that branches appear. The breakdown pattern proceeds in the manner of a fractal, not unlike the tortuous and branching pattern of the lightning stroke and gives a clear indication of the direction of the breakdown.

The direction of the branches reveals the origin of the breakdown. In fig. 6.11a the origin of the breakdown can be found in the dielectric between the two trees, in fig. 6.11b the lower electrode is suspect. If the breakdown path has not been scorched too much, the cause of the breakdown might be found back.

### Branching

The longer a breakdown takes place, the more time is available to form detailed branches. The tree in fig. 6.11a has had a long time to develop; that in fig. 6.11b has been formed in a far shorter time, or probably by impulse voltage.

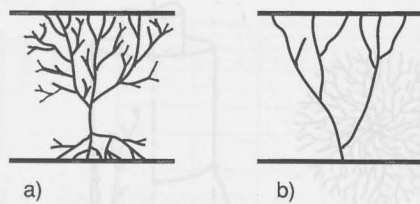


**Fig. 6.11.** Treeing in solids. The origin of the treeing pattern in fig. a is to be found between the trees. The origin of treeing in fig. b is located at, or near the lower electrode.

### Environment

In the vicinity of a breakdown path, details may be found which have been burnt away at the site of the breakdown itself. In fig. 6.12 an example is given of a cause for breakdown that could not be found at the site at breakdown, but the regularly recurring protrusions disclose the cause.

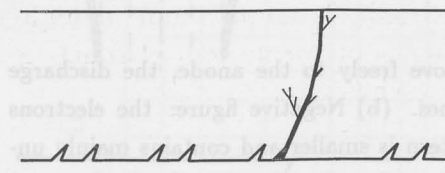


**Fig. 6.12.** Breakdown path initiated at regularly recurring protrusions.

### Surface discharges

The patterns that are formed by surface discharges are based on *Lichtenberg figures*. Lichtenberg figures are formed when a pointed rod is placed at the surface of a dielectric and is given a high voltage against an earthed conductor, as shown in fig. 6.13. A high tangential field strength occurs along the surface and partial breakdown tracks are initiated at the surface.

If the rod is positive, as in fig. 6.13a, avalanches are formed towards the rod and the electrons move freely to the rod. The resulting pattern has an open structure and contains many branches.

If the rod is negative, avalanches start from the rod and the electrons are pushed into the surface and avalanches are less free to develop. The resulting pattern is smaller in diameter, see fig. 6.13b, and is characterized by non-branching and rather straight spokes. In the case of A.C. voltage, the positive pattern prevails. Surface discharges are usually shaped like Lichtenberg figures, their shape tend to reveal the origin of the discharge.

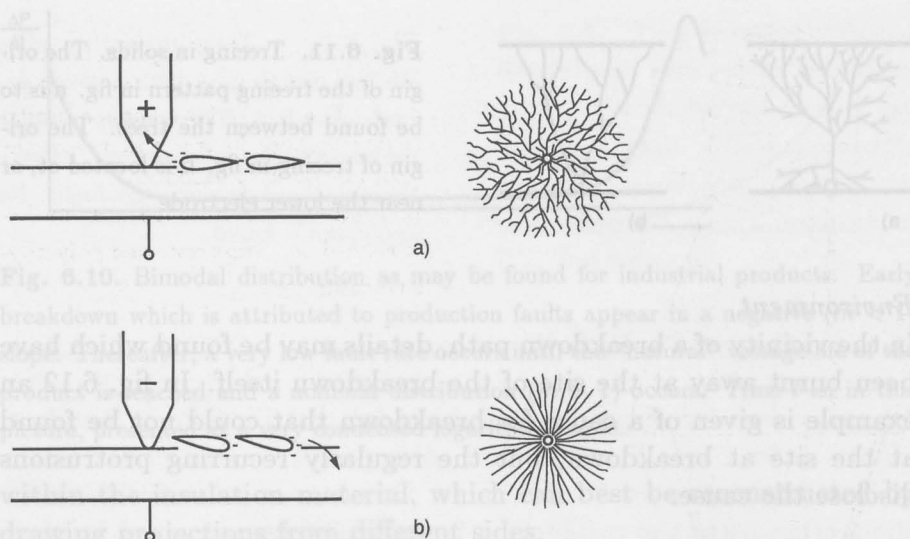


Fig. 6.10. Bimodal distribution as may be found for industrial products. Early breakdown, which is attributed to production faults appear in a *negative* discharge, while later breakdowns appear in a *positive* discharge. The two types of discharges are shown in drawing projections from different sides.

Fig. 6.13. Lichtenberg figures.

(a) Positive figure: electron avalanches move freely to the anode, the discharge pattern is open and contains many branches. (b) Negative figure: the electrons are restrained in their movements, the pattern is smaller and contains mainly unbranched channels. Surface discharges have similar shapes (or parts of the shape) as Lichtenberg figures. At A.C voltages, the shape of the positive figure prevails.

Surface discharges are found, for instance, at the overstressed surface of a cable stress cone, as shown in fig. 6.14. The pattern resembles a positive Lichtenberg figure, and clearly points to a site at the stress cone where the highest tangential stress occurred.

### Interfaces

Two examples of breakdown channels in interfaces are shown as well. Fig. 6.15 shows a breakdown path in polyethylene, that for part of the way runs parallel to the electrodes. This anomaly could be traced back to a junction of two parts, which should be fused by heat and pressure. The junction had not been fused sufficiently.

The example in fig. 6.14b shows the initiation of a breakdown in the interface between a stress-cone and a cable core. The stress cone is made of rubber and stretched over the cable core (see part I, page 147) with the aid of silicon grease. The grease-filled interface is relatively weak as compared to the solid dielectrics of the cable and

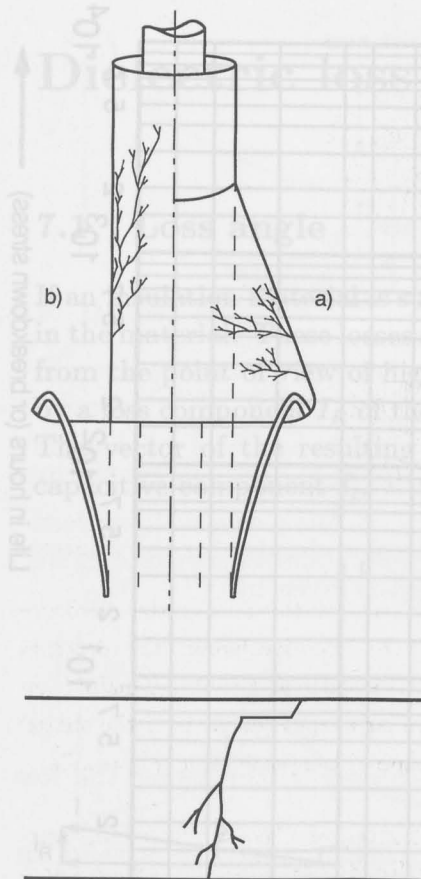


**Fig. 6.14.** a. Discharge tracks at the overstressed surface of a cable stress-cone. The tracks have shapes similar to Lichtenberg figures and reveal the origin of positive flashover.

b. Discharge tracks in the interface between rubber stress cone and polyethylene cable core.

**Fig. 6.15.** Breakdown along semi-fused interface.

stress cone. If the pressure of the rubber on the cable is insufficient, or if the cable surface is not even or not clean, this interface breaks down easily and the direction of the tree-like channels indicate the spot where breakdown was initiated.

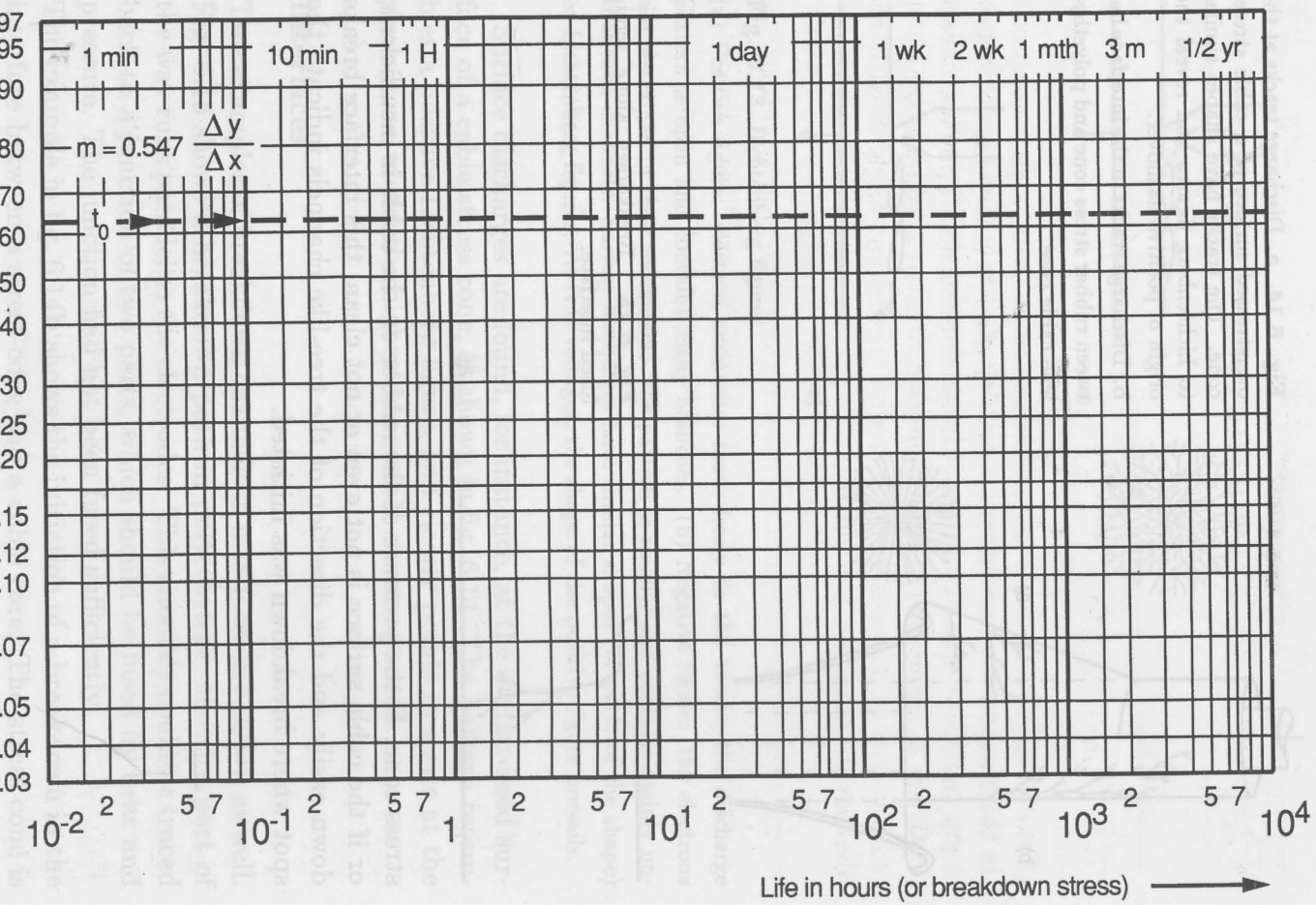
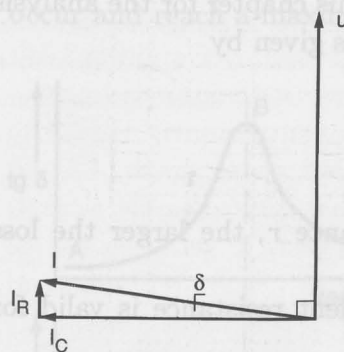


Fig. 6.16. Survival curves of silicon dielectrics. The breakdown resistance is weak as compared to the solid dielectrics of the cable and

## Dielectric loss measurements

### 7.1 Loss angle

If an insulation material is subjected to an A.C. voltage, losses occur in the material. These losses are usually small but they are important from the point of view of high-voltage engineering. They are caused by a loss component  $I_R$  of the dielectric current, as shown in fig. 7.1. The vector of the resulting current  $I$  makes an angle  $\delta$  with the capacitive component  $I_c$ .



**Fig. 7.1.** Dielectric losses are caused by a small loss component  $I_R$ . This component makes an angle  $\delta$  with the purely capacitive current  $I_c$  and equals  $I_R = I_c \cdot \tan \delta$ . The resulting losses are  $W = U^2 \cdot \omega C \cdot \tan \delta$ .

The tangent of this angle is a measure for the dielectric losses  $W$ :

$$W = U \cdot I_c \tan \delta = U^2 \cdot \omega C \cdot \tan \delta,$$

the losses thus being directly proportional to the *loss tangent*  $\tan \delta$ . A lossy capacitor is often represented by one of the equivalent circuits as shown in fig. 7.2. This circuit facilitates the analysis of losses or that of loss measurements in electric circuits.

The *parallel circuit* is more often used. The loss tangent is given by

$$\tan \delta = \frac{I_R}{I_c} = \frac{1}{\omega R C}.$$

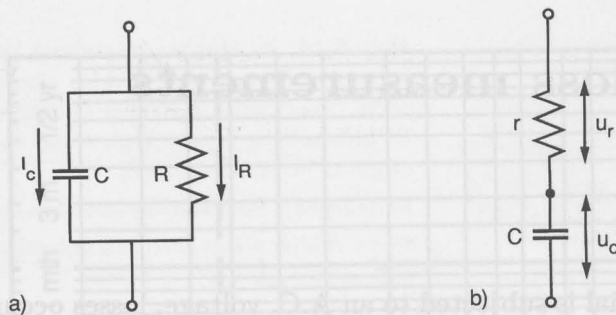


Fig. 7.2. Equivalent circuits for a lossy capacitor.

- Parallel circuit
- Series circuit

The *smaller* the hypothetical parallel resistance  $R$ , the larger the loss tangent.

The *series circuit* will be used later in this chapter for the analysis of the Schering bridge. The loss tangent is given by

$$\tan \delta = \frac{U_r}{U_c} = \omega r C.$$

The *larger* the hypothetical series resistance  $r$ , the larger the loss tangent.

Observe that in both cases the equivalent resistance is valid for *one frequency only*.

## 7.2 Physical origin of losses

Dielectric losses may have various physical origins, some of which are discussed here.

### 1. Conductive losses

If the insulation resistance  $R$  of a dielectric is sufficiently low, the leakage current adds to the dielectric losses. The parallel circuit in fig. 7.2a is now virtually present and the loss tangent is  $\tan \delta = \frac{1}{\omega R C}$ . If the frequency is increased, the  $\tan \delta$  decreases as shown in fig. 7.3.

Varying frequencies are often used when analyzing dielectric losses of materials; conductive losses are readily recognized in this way.

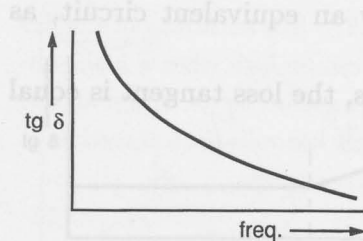


Fig. 7.3. Conductive losses are recognized by a decreasing loss tangent at increasing frequency.

## 2. Dipole losses

Electric dipoles in an insulation material continuously reverse their direction in an A.C. field. At low frequencies the dipoles follow the alternating field well enough, no phase differences occur and no losses are found, see branch A in fig. 7.4. When the frequency increases, friction plays a role and the dipoles lag behind the field vector. Losses occur and reach a maximum in point B of fig. 7.4.

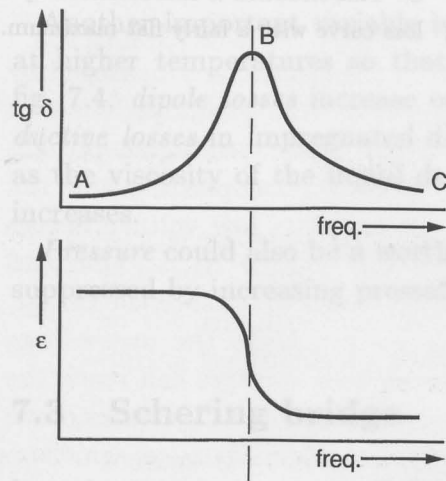


Fig. 7.4. Dipole losses are caused by friction between rotating electric dipoles and the insulation material. At low frequencies, A, this friction is low and  $\tan \delta$  is low. At higher frequency they increase up to a maximum at B. At very high frequencies, C, the dipoles cannot follow the alternating field and losses decrease again.

The dielectric constant  $\epsilon$  is high when dipoles are following the alternating field A, it drops steeply when friction arises B and  $\epsilon$  is low when the dipoles are almost immobile at high frequencies, C.

At frequencies above this maximum, the dipoles can no longer follow the alternating field and the losses decrease: branch C in fig. 7.4. Dipole losses can thus be well recognized by their frequency characteristic.

## 3. Interfaces

Often a perfect dielectric is used in series with a lossy dielectric, for instance a gas in series with a solid material. Such an interface

between materials can be represented by an equivalent circuit, as shown in fig. 7.5.

If the lossy dielectric has conductive losses, the loss tangent is equal to

$$\tan \delta = \frac{\omega R K}{1 + \omega^2 R^2 C (K + C)}.$$

If  $\omega=0$ , the loss tangent  $\tan \delta=0$  and if  $\omega \rightarrow \infty$ , the loss tangent  $\tan \delta \rightarrow 0$ . In between a maximum occurs as shown in fig. 7.5. This maximum is less sharp than in the former case of polarization losses and can thus be distinguished.

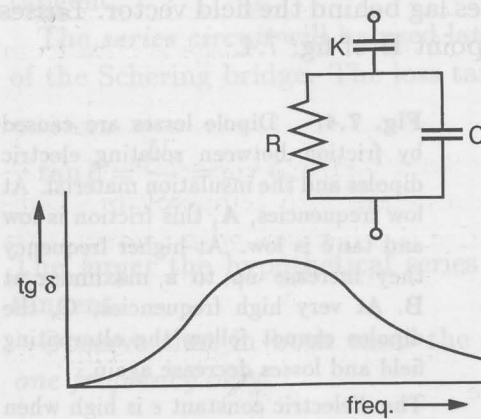
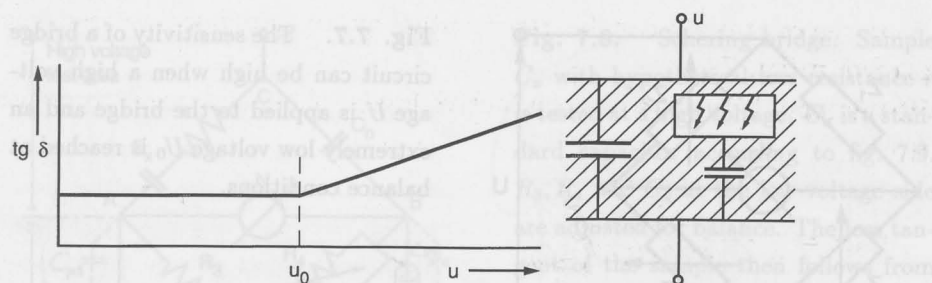


Fig. 7.5. Interface between a loss-free dielectric  $K$  and a lossy dielectric  $C$ . This situation is characterized by a loss curve with a fairly flat maximum.

#### 4. Discharge losses

If partial discharges take place in a dielectric, losses occur which are reflected by an increase in  $\tan \delta$ . From the inception voltage  $U_0$  onwards, the losses grow with increasing voltage as demonstrated in fig. 7.6; this effect is further studied in section 9.7, where it is shown that the rise in  $\tan \delta$  is larger if the number and the magnitude of the discharge is larger.

Below  $U_0$ , the loss tangent is equal to that of the discharge-free material. To recognize this type of loss, the voltage must be varied, in contrast with other cases, where the frequency was varied.



**Fig. 7.6.** Losses caused by internal discharges are recognized by an increasing loss tangent at increasing voltage. The increase starts at the inception voltage  $U_0$ ; the slope of the curve reflects the extent of the discharges.

### Analysis of losses

A complete analysis of dielectric losses comprises the investigation of many variables. The effect of frequency and voltage is clear from the considerations above.

Another important variable is *temperature*; dipoles gain mobility at higher temperatures so that, depending on branch A or C in fig. 7.4, *dipole losses* increase or decrease with temperature. *Conductive losses* in impregnated dielectrics increase with temperature as the viscosity of the liquid decreases and the mobility of charges increases.

*Pressure* could also be a worthwhile variable as discharges may be suppressed by increasing pressure.

### 7.3 Schering bridge

In order to measure a small factor like  $\tan \delta$ , a bridge circuit is required. A high voltage is applied to one diagonal of the bridge and a sensitive null detector is connected to the other diagonal as shown in fig. 7.7. The impedances are adjusted in such a way that the null detector indicates zero voltage. This occurs if  $Z_1 : Z_3 = Z_2 : Z_4$ . The unknown  $Z_1$  may then be derived from a calibrated  $Z_2, Z_3$  and  $Z_4$ .

The large ratio between the applied voltage  $U$  (kilovolts) and the smallest observable voltage  $\Delta U_0$  at the null detector (millivolts or less) makes this measurement very sensitive and accurate measurements can be obtained; the sensitivity is given by

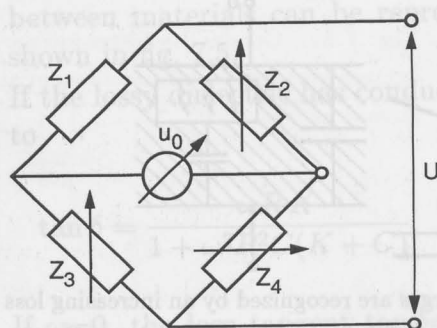


Fig. 7.7. The sensitivity of a bridge circuit can be high when a high voltage  $U$  is applied to the bridge and an extremely low voltage  $U_0$  is reached at balance conditions.

$$\Delta Z_1 = C \frac{\Delta U_0}{U},$$

where  $\Delta Z_1$  is the smallest deviation in  $Z_1$  that can just be observed by the detector and  $C$  is a constant. Ratios  $\frac{\Delta U_0}{U}$  of  $10^{-6}$  to  $10^{-8}$  can readily be obtained.

The capacitance and the loss tangent of a dielectric are measured by means of a *Schering bridge*, according to fig. 7.8. The impedances in this bridge are chosen so that most of the applied voltage is present at the high-voltage side where the unknown samples  $C_x$  and the standard capacitor  $C_n$  are situated. A harmless low voltage occurs at the low-voltage side, where a standard resistor  $R_3$  is found and calibrated impedances  $R_4$  and  $C_4$  can be varied to balance the bridge. If the values chosen for  $R_3$  and  $R_4$  are too high, the overvoltage protectors  $O$  react so that no dangerous high voltages can reach the operator of the bridge. The same applies if sample  $C_x$  breaks down if flashover occurs.

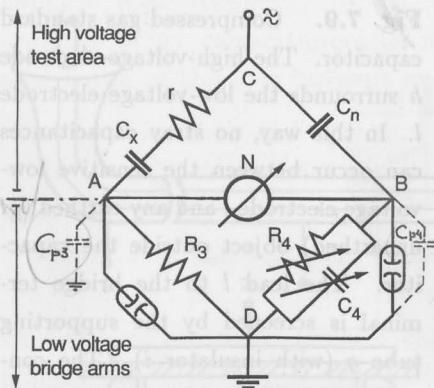
If the bridge is in balance, then

$$\bar{Z}_1 = \frac{\bar{Z}_2 \bar{Z}_3}{\bar{Z}_4}.$$

from which it can be calculated that

$$C_x = \frac{R_4}{R_3} C_n,$$

and



$$\tan \delta = \omega R_4 C_4,$$

so that both  $C_x$  and  $\tan \delta$  can simply be determined by reading the impedance banks  $R_4$  and  $C_4$ .

The null detector  $N$  usually comprises the following components:

- A shielded input transformer to receive the differential signal  $v_{AB}$ . It has a high ratio between the sensitivity for the wanted signal  $v_{AB}$  and the common mode voltage  $v_{AD}$ .
- A variable gain amplifier, often with a negative feedback so that the sensitivity of the amplifier is automatically matched to the amplitude of the signal when the signal is decreasing during the balancing procedure.
- A narrow band filter tuned to the basic frequency of the voltage source: the bridge is in balance for one frequency only and higher harmonics from the voltage source must not affect the balance conditions.

The accuracy of the calibrated components  $Z_2$  to  $Z_4$  is chosen to match the sensitivity  $\Delta Z$  so that the overall accuracy is maximal. This is obtained by using precision banks for the variable impedances at the low-voltage side.

The standard capacitor  $C_n$  at the high-voltage side is constructed along the lines of fig. 7.9. The high-voltage electrode  $h$  surrounds the low-voltage one  $l$  completely. The low-voltage electrode is supported

**Fig. 7.8.** Schering bridge. Sample  $C_x$  with hypothetical loss resistance  $r$  is tested at a high voltage.  $C_n$  is a standard capacitor according to fig. 7.9.  $R_3$ ,  $R_4$  and  $C_4$  at the low-voltage side are adjusted for balance. The loss tangent of the sample then follows from  $\tan \delta = \omega R_4 C_4$  and its capacitance from  $C_x = \frac{R_4}{\omega} C_n$ .

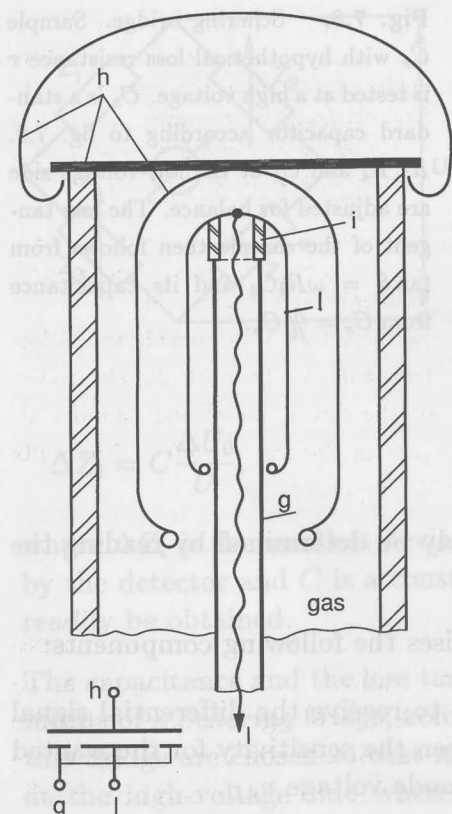


**Fig. 7.9.** Compressed gas standard capacitor. The high-voltage electrode  $h$  surrounds the low-voltage electrode  $l$ . In this way, no stray capacitances can occur between the sensitive low-voltage electrode  $l$  and any earthed (or unearthed) object outside the capacitor. The lead  $l$  to the bridge terminal is screened by the supporting tube  $g$  (with insulator  $i$ ). The construction is filled with compressed gas so that high voltages can be applied to this standard capacitor. The construction results in an equivalent circuit with an accurate capacitance between  $h$  and  $l$  (accuracy for instance 0.2 %,  $\tan \delta \approx 10^{-6}$ ) and a guard  $g$  that is usually connected to earth.

by a steel tube which also acts as a guard  $g$  that screens the low-voltage lead  $l$ . This construction can be electrically represented by the simple equivalent circuit shown in this figure.

In the bridge circuit of fig. 7.8, the guards  $g$  are connected to earth so that their capacitance is not measured.

The same applies to the guards  $g$  in the test sample. These guards can be of different origin. For instance, if a cable is measured the cable terminals are separated and shield  $g$  is earthed as shown in fig. 7.10. Or if a disc of an unknown material is measured, as shown in fig. 7.10, the lower electrode is surrounded by a guard ring  $g$  which is earthed so that edge-effects do not corrupt the results.

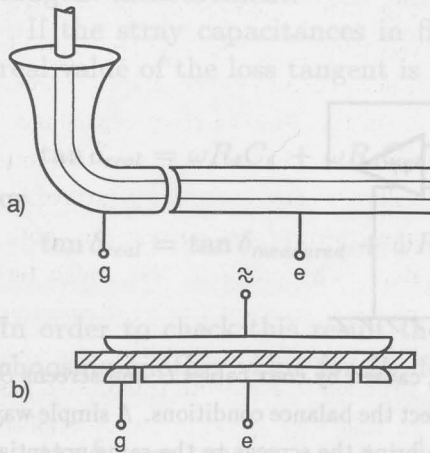


**Fig. 7.10.** Examples of guard electrodes. In figure a the earth shields of cable and terminal are separated. In figure b a slab of insulating material is measured in an electrode system with a guard ring  $g$ . In both cases, the electrodes  $e$  are connected to bridge terminal A in fig. 7.8 and guards  $g$  are connected to earth, so that no edge effects enter the test results.

In the test set of example b, the dielectric shall closely touch the electrodes, or the disc is metallized: minute air gaps in the test set affect the results disproportionately.

## 7.4 Stray capacitances

The accuracy of the results is endangered by the stray capacitances  $C_{p3}$  and  $C_{p4}$ , shown in fig. 7.8. They originate from the long coax cables that connect the capacitors in the high-voltage bay to the bridge terminals, but also by the screen that surrounds the low-voltage arms of the Schering bridge. These capacitances enter the balance conditions and cause an error in the determination of  $\tan \delta$ .

One way to eliminate these capacitances is to bring the coax sheathes and the screen to the same potential as the bridge terminals A and B. This might be done by operating a separate voltage source, but it is more readily accomplished by using an operational amplifier, as shown in fig. 7.11. The high input impedance of the amplifier does not effect the bridge, the amplification factor is exactly 1, so that no capacitive currents can appear between the terminals A or B and the screen.

Another way to eliminate these stray capacitances is to bring the bridge terminals A and B to earth potential by supplying an opposite potential to the lower terminal D. This is accomplished with an active network, as shown in fig. 7.12, which controls both the magnitude and the phase angle of potential D. By connecting one side of the null detector alternately to terminal A or to earth, the voltage at A (and B) is gradually adjusted to earth potential. This way of eliminating stray capacitance errors is called *Wagners earth*.

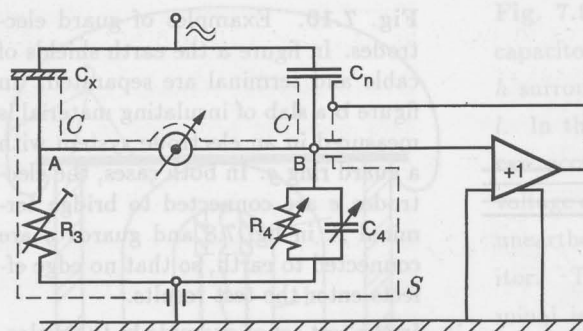


**Fig. 7.11.** Stray capacitances  $C_{p3}$  and  $C_{p4}$ , caused by coax cables  $C$  and screens  $S$ , corrupt the measurement of  $\tan \delta$  as they affect the balance conditions. A simple way of eliminating these stray capacitances is to bring the screens to the same potential as the bridge terminals **A** and **B**. This might be done with an operational amplifier with amplification factor +1.

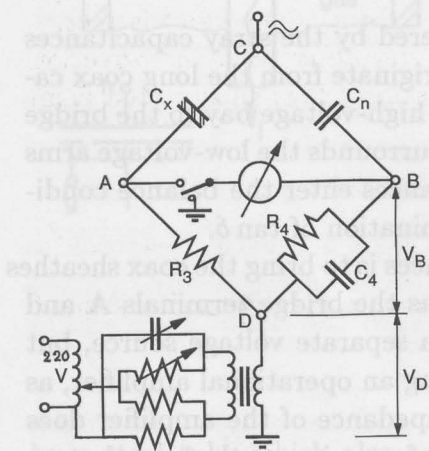


**Fig. 7.12.** Wagners earthing device. The bridge terminals **A** and **B** are brought to earth potential by supplying an opposite voltage to terminal **D**:  $V_D = -V_B$ . Stray capacitances between terminals **A** or **B** and earth are eliminated and errors in estimating  $\tan \delta$  are prevented.

## 7.5 The dual-balance method

In order to check whether all stray capacitances have been eliminated, a dual-balance method has been developed. Simultaneously, this method enables us to calculate the true value of  $\tan \delta$  if the measured value has been corrupted by stray capacitance. Although this method has gained little attention in literature, it has proven to be a valuable aid to check and, if required, to correct errors in a loss

tangent measurement.

If the stray capacitances in fig. 7.11 are taken into account, the real value of the loss tangent is

$$\tan \delta_{real} = \omega R_4 C_4 + \omega R_4 C_{p4} - \omega R_3 C_{p3},$$

or

$$\tan \delta_{real} = \tan \delta_{measured} + \omega R_4 C_{p4} - \omega R_3 C_{p3}.$$

In order to check this result the bridge is balanced a second time, choosing another value for  $R_3$ , for instance  $\frac{1}{2}R_3$ . Then:

$$\tan \delta_{real} = \tan \delta'_{measured} + \omega \frac{1}{2}R_4 C_{p4} - \omega \frac{1}{2}R_3 C_{p3},$$

where  $\tan \delta'_{measured}$  is the new result for the loss tangent.

If this second test yields *the same value* for  $\tan \delta$  as the first one, the parasites are inactive and *the measured value* for  $\tan \delta$  is *true*.

However, if the second test yields a deviating result a correction factor can be derived as follows: Equation (2) is subtracted from (1)

$$0 = \Delta \tan \delta + \frac{1}{2}\omega R_4 C_{p4} - \frac{1}{2}\omega R_3 C_{p3},$$

where  $\Delta \tan \delta$  is the *difference in measured values*. Inserting  $\Delta \tan \delta$  in (1) yields:

$$\tan \delta_{real} = \tan \delta_{measured} - 2\Delta \tan \delta.$$

The effect of stray capacitances can readily be eliminated in this way. The dual-balance method is of great value when testing large test objects like power transformers or full reels of cable. It proves to be very difficult in those cases to avoid stray capacitances. Also inductive couplings or coupling by common current paths may cause errors. In all these cases a check by the dual-balance method is indispensable.

A further advantage of the method is that the correction factor,  $2\Delta \tan \delta$ , is constant for any particular test set up. If, for instance, the loss tangent of a sample shall be tested at different voltages or

temperatures, or as a function of time, the correction factor needs to be determined only once and can be used throughout the full series of tests.

### Characteristics

Schering bridges are in use in all kinds of shapes and sizes. Capacitances from a few pC to many hundreds of  $\mu\text{F}$  can be measured; often with a bridge device provided with accessories. The accuracy depends on the sensitivity of the null detector, on the accuracy of the applied resistors and capacitors and on the control of the stray capacitances. Accuracies in measuring  $C_x$  of 0.1 % reflect normal practice.

The measuring range for  $\tan \delta$  is usually between  $1 \cdot 10^{-4}$  and several thousands times  $10^{-4}$  ( $10^{-4}$  is the customary unit for  $\tan \delta$ ). The accuracy is usually also equal to  $10^{-4}$ , however, far better accuracies, for instance  $10^{-5}$  or even  $10^{-6}$ , can be reached if required.

## 7.6 Permanently earthed objects

The low-voltage electrode of a sample cannot in some cases be disconnected from earth. This is generally the case for components in service, such as buried cables, installed G.I.S. or transformer banks. In those cases, a variation on the Schering bridge is used where one side of the test sample  $C_x$  can be earthed.

The most widely used circuit is the *inverted Schering bridge*, according to fig. 7.13. The variable components of the bridge are located in a cage of Faraday at high potential. The bridge is operated either by remote control, or the Faraday cage is large enough to accommodate an operator.

The standard capacitor is either used without the advantage of separate guards, as shown in the figure, or it is mounted on insulators as well, and guards are "earthed" at the Faraday cage.

The usual considerations about stray capacitance apply here as well. Wagners earth can be used and the dual-balance method is useful again for correcting errors caused by stray capacitance.

The inverted Schering bridge is often found in mobile installations designed to test installed H.V.-equipment at site. A large test transformer (up to 1 MVA reactive power) is installed on a truck, together

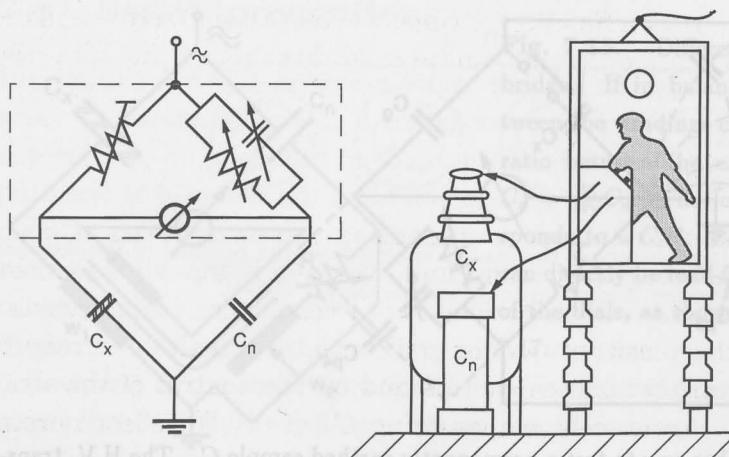


**Fig. 7.13.** In the inverted Schering bridge, the variable components are located in a cage of Faraday at high potential. The bridge is either operated by remote control or the operator is situated in the Faraday cage. This circuit is used for the  $\tan \delta$ -measurement of permanently earthed samples  $C_x$ .

with a 50/60 Hz generator, a standard capacitor and a Faraday cage with Schering bridge.

Another possibility is to disconnect the H.V. transformer from earth and to earth one bridge terminal instead, see fig. 7.14. A complication is introduced by the capacitance  $C_g$  between the windings of the transformer and earth.

The effect of this capacitance is eliminated by measuring twice. The first time  $C_x$  is disconnected and  $C_g$  and  $\tan \delta_g$  are measured. The second time  $C_x$  is connected to high voltage and  $C_x + C_g$  is measured. The corresponding loss tangent is equal to

$$\frac{C_x \tan \delta_x + C_g \tan \delta_g}{C_x + C_g},$$

from which  $\tan \delta_x$  can be calculated.

Stray capacitances play a role here as well, especially  $C_{p3}$ , as can be seen from fig. 7.14. Compensation by screening, or a Wagner earth, are not possible, therefore the dual-balance method must be applied. Combined with the two test positions, this leads to quadruple balancing.

This circuit is less reliable than the former one.  $C_g$  is not quite

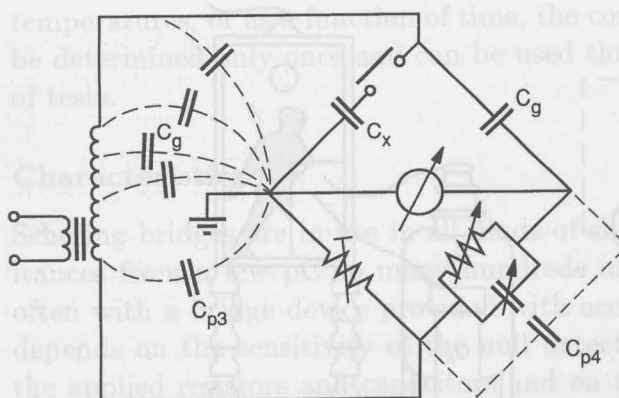


**Fig. 7.14.** Another way to test a permanently earthed sample  $C_x$ . The H.V. transformer is disconnected from earth and connected to the lower terminal of the bridge. The effect of the stray capacitances in the transformer is eliminated by measuring twice: with and without sample  $C_x$ .

stable and disconnecting the sample effects  $C_g$ . Moreover, if a low-loss sample is measured, the parasitic  $\tan \delta_g$  may be far larger than the  $\tan \delta$  to be measured, which impairs the accuracy.

## 7.7 Differential transformer bridge

For routine tests by unskilled operators, a deviating type of bridge has been developed which makes use of a differential transformer. The circuit is shown in fig. 7.15. The capacitors  $C_x$  and  $C_n$  are placed in the usual way, but the low-voltage arms have been replaced by the windings  $W_1$  and  $W_2$  of this transformer. The third winding of the transformer is connected to the null detector.

The bridge is in balance if

$$C_x = \frac{W_1}{W_2} C_n.$$

The number of turns  $W_1$  can be switched to four fixed positions so that a ratio 0.1, 1, 10 or 100 can be chosen. The winding position  $W_2$  is continuously variable, the winding ratios are chosen so that, for  $C_n = 100 \text{ pF}$ , the position of the dials shows directly the capacitance of the test object  $C_x$ . In fig. 7.16 an example is shown.

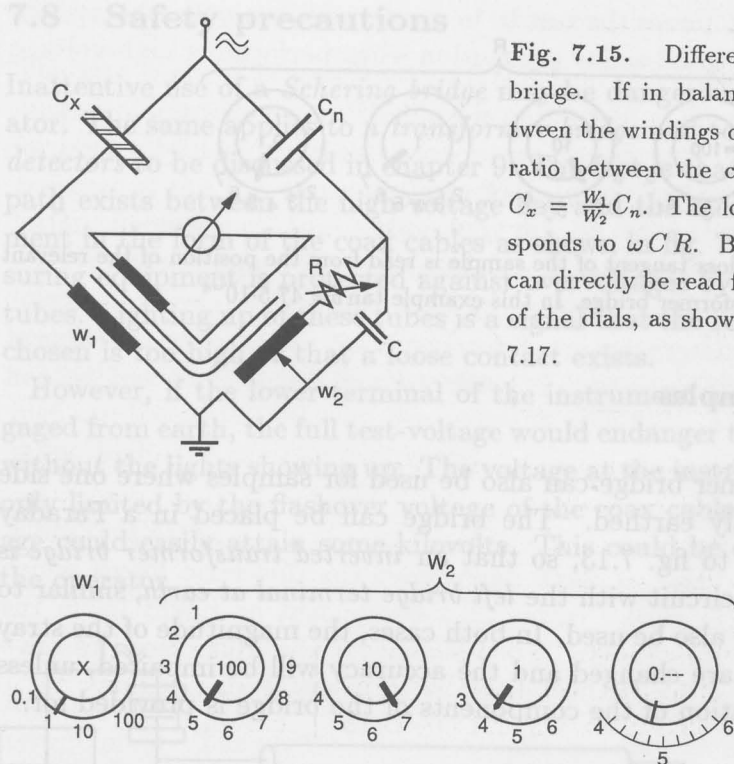


**Fig. 7.15.** Differential transformer bridge. If in balance, the ratio between the windings corresponds to the ratio between the capacitors so that  $C_x = \frac{w_1}{w_2} C_n$ . The loss tangent corresponds to  $\omega C R$ . Both  $C_x$  and  $\tan \delta$  can directly be read from the positions of the dials, as shown in fig. 7.16 and 7.17.

However, if one terminal of the instrument is left unengaged from earth, the full test-voltage would endanger the equipment without the safety device showing up. The voltage at the terminals is then only limited by the flashover voltage of the bridge. But the insulation of the windings could easily attain some high voltage. This is the reason of taking care of the insulation of the bridge.

**Fig. 7.16.** If the transformer ratio bridge is in balance, the capacitance of the sample is read from the position of the dials. In this example  $C_x$  proves to be 574.45 pF.

In order to determine  $\tan \delta$ , a variable resistor and a variable capacitor have been added to this bridge, as shown in fig. 7.15. The loss tangent proves to be

$$\tan \delta = \omega C R.$$

This does not seem to differ from the Schering bridge. However, the readings of  $C$  and  $R$  are here independent of  $C_x$ , which makes it possible for  $\tan \delta$  be read directly from the positions of the dials too. Capacitor  $C$  can be switched to three positions in such a manner that (at 50 or 60 Hz)  $\omega C = 0.1$  or 1 or 10. Resistor  $R$  is adjustable in small steps. Fig. 7.17 gives an example of a reading of  $\tan \delta$ .

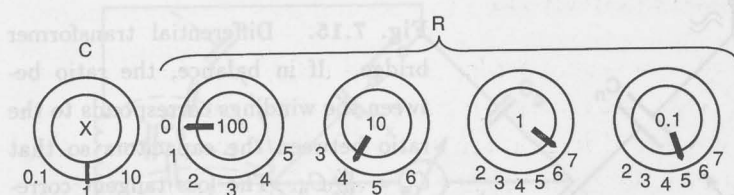


Fig. 7.17. The loss tangent of the sample is read from the position of the relevant dials of the transformer bridge. In this example  $\tan \delta = 47.5 \cdot 10^{-4}$ .

### Earthing samples

The transformer bridge can also be used for samples where one side is permanently earthed. The bridge can be placed in a Faraday cage, similar to fig. 7.13, so that an *inverted transformer bridge* is formed. The circuit with the *left bridge terminal at earth*, similar to fig. 7.14, may also be used. In both cases, the magnitude of the stray capacitances are changed and the accuracy will be impaired, unless a new calibration of the components of the bridge is provided for.

### Accuracy and reliability

The accuracy of the measured capacitance is estimated at 0.1 %, that of the loss tangent at  $2 \cdot 10^{-5}$ . This is valid, however, for the standard circuit which includes the standard length of coax cable that is supplied with the bridge. No other cable (and no extension) is allowed if the situation in the high-voltage bay would so require it.

The greatest disadvantage of this bridge, however, is that no dual-balance test can be made, so that no check on errors or a possible correction of errors can be made. This decreases the reliability of this bridge. The application should therefore be restricted to routine tests on series of products. The results shall regularly be checked with a conventional Schering bridge.

Sophisticated laboratory tests, however, must be made with a Schering bridge, using all available means for preventing errors.

## 7.8 Safety precautions

Inattentive use of a *Schering bridge* may be dangerous for the operator. The same applies to a *transformer bridge* and to the *discharge detectors* to be discussed in chapter 9. The fact is that a conducting path exists between the high-voltage bay and the measuring equipment in the form of the coax cables as shown in fig. 7.18. The measuring equipment is protected against overvoltages by gas discharge tubes. Lighting up of these tubes is a signal that the resistance value chosen is too high or that a loose contact exists.

However, if the lower terminal of the instrument would be disengaged from earth, the full test-voltage would endanger the equipment without the lights showing up. The voltage at the instrument is then only limited by the flashover voltage of the coax cables, which voltage could easily attain some kilovolts. This could be dangerous for the operator.

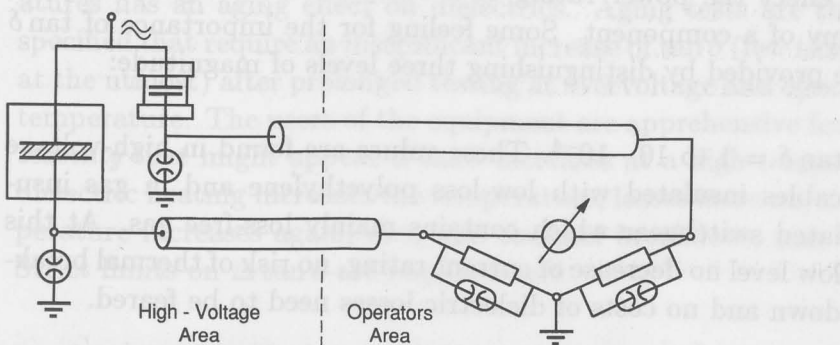


Fig. 7.18. The measuring leads might bring high voltages out if earthing conditions are not optimal. This could be dangerous for the operator. Double safety with overvoltage protectors inside and outside the test bay is preferred.

A solution is to place an overvoltage protection at the entrance of the coax cable as well and to earth them separately; in that way a double safety measure is achieved.

The same safety problems apply to the inverted Schering bridge. Extra safety by gas discharge tubes in the high-voltage test area is difficult to achieve here, so that double-checking of the connection bridge-to-cage is indispensable.

Another safety measure is to lock the door of the Faraday cage from outside, therefore the operator can never leave the cage when voltage

is on. This also forces the test to be made with two operators, which is in any case a good safety precaution when performing high-voltage tests.

### 7.9 Industrial value of $\tan \delta$

Measuring  $\tan \delta$  provides a test whether H.V. equipment or H.V. insulation material will perform well in operational circumstances.

Several characteristics are of interest, such as the *absolute value* of  $\tan \delta$  and the *increase* of  $\tan \delta$  with *voltage*, *temperature* and *time of exposure*.

#### Absolute value

The absolute value of  $\tan \delta$  determines the dielectric losses which might effect the power rating of a component or might harm the economy of a component. Some feeling for the importance of  $\tan \delta$  can be provided by distinguishing three levels of magnitude:

- $\tan \delta = 1$  to  $10 \cdot 10^{-4}$ . These values are found in high-voltage cables insulated with low-loss polyethylene and in gas insulated switchgear which contains mainly loss-free gas. At this low level no decrease of current rating, no risk of thermal breakdown and no costs of dielectric losses need to be feared.
- $\tan \delta = 20$  to  $50 \cdot 10^{-4}$ . This level is found in paper-oil insulation of transformers and cables, in rubber insulated cables, in cable accessories, in bushings, etc. Current rating effects and cost effects occur at the highest voltage ranges (400 to 700 kV) only. Risk of thermal breakdown is not present, but if aging effects raise the losses above this value, thermal breakdown might become a threat.
- $\tan \delta \geq 100 \cdot 10^{-4}$ . This level is regarded to be too high for high-voltage insulation. It occurs in PVC insulation which may be used upto 6 kV at the utmost. At higher voltages than 6 kV, the current rating is offset, thermal breakdown might occur at full load and dielectric losses are unacceptable.

### Effect of voltage

The loss tangent is measured as a function of voltage to check the quality of impregnation. This test is performed at oil insulated transformers, oil-filled cables and capacitors. An important measure is the *increase* of the loss tangent  $\Delta \tan \delta$ . In oil-impregnated paper insulation, for instance, the  $\Delta \tan \delta$  may not be more than  $5 \cdot 10^{-4}$  if the test-voltage is raised from  $\frac{1}{2}U_0$  to  $2U_0$ . If  $\Delta \tan \delta$  is higher than this level, the insulation is considered to contain gas or impurities and is rejected.

Machine insulation, mass-impregnated cable and resin bonded bushings are tested for *internal discharges* in this way. Again, if  $\Delta \tan \delta$  is too high, the product is rejected.

### Effect of time

Prolonged exposure to high voltages combined with high temperatures has an aging effect on dielectrics. Aging tests are therefore specified that require an insignificant increase of  $\tan \delta$  (few times  $10^{-4}$  at the utmost) after prolonged testing at overvoltage and operational temperature. The users of the equipment are apprehensive for an *instability* that might appear if  $\tan \delta$  increases at a high temperature: dielectric heating increases the temperature, losses increase, the temperature increases again, etc., and thermal breakdown may follow. Strict limits on  $\Delta \tan \delta$  are required here.

dielectric in which discharges take place, see fig. 8.1 d. Discharges in interfaces perpendicular to the field, see c, or with a substantial tangential field, as in e, belong to this category as well. The field strength at which discharges occur can be calculated in the case of well defined cavities, as indicated in fig. 8.1 a to e. Other examples have been shown in part I, fig. 9.2. In all these cases, the field strength in the cavity can either be calculated or be determined by field plotting.

It is known from experiments that the dielectric strength of the gas in such cavities is reasonably well represented by the Paschen curve. This curve is shown in fig. 8.2 for air. A modification of the curve was introduced in part I, fig. 8.3, in order to indicate the *ignition field strength* in KV/mm² rms.

is on. This also forces the test to be made with two generators. It is in any case a good safety precaution when performing high-voltage tests.

Several characteristics are of interest, such as the absolute value of  $\tan \delta$  and the effect of temperature on  $\tan \delta$ .

### Absolute value

The absolute value of  $\tan \delta$  determines the dielectric losses which must affect the power factor of a component. In general, the effect of the power factor of a component is proportional to the square of  $\tan \delta$ . A low value of  $\tan \delta$  is therefore desirable. Some testing for the loss tangent of  $\tan \delta$  can be provided by distinguishing three levels of insulation quality:

- $\tan \delta = 20$  to  $50 \cdot 10^{-3}$ . This level is found in paper oil insulation of transformers and cables, in rubber insulated cables, in cable accessories, in bushings, etc. Current rating effects and cost effects occur at the highest voltage ranges (600 to 700 kV) only. Risk of thermal breakdown is not present, but if aging effects raise the losses above this value, thermal breakdown might become a threat.

- $\tan \delta \geq 100 \cdot 10^{-3}$ . This level is regarded to be too high for high-voltage insulation. It occurs in  $\text{B/C}$  insulation which may be used up to 6 kV at the moment. At higher voltages than 6 kV, the current rating is offset; thermal breakdown might occur at full load and dielectric losses are unacceptable.

# Chapter 8

## Partial discharges

### 8.1 Types of discharges

Partial discharges are breakdown phenomena that do not completely bridge the distance between electrodes. They can be harmful for a dielectric and have therefore been mentioned before in part I, section 9.4, on solid dielectrics. Generally three types of partial discharges can be distinguished:

- Internal discharges, including those in electrical treeing.
- Surface discharges.
- Corona discharges.

#### Internal discharges

Internal discharges occur in cavities in a solid dielectric, which are usually gas-filled. A number of examples are shown in fig. 8.1 **a**, **b** and **c**. Furthermore, electrical treeing will create cavities in a dielectric in which discharges take place, see fig. 8.1 **d**. Discharges in interfaces perpendicular to the field, see **c**, or with a substantial tangential field, as in **e**, belong to this category as well.

The field strength at which discharges occur can be calculated in the case of well defined cavities, as indicated in fig. 8.1 **a** to **c**. Other examples have been shown in part I, fig. 9.2. In all these cases, the field strength in the cavity can either be calculated or be determined by field plotting.

It is known from experiments that the dielectric strength of the gas in such cavities is reasonably well represented by the Paschen curve. This curve is shown in fig. 8.2 for air. A modification of the curve was introduced in part I, fig. 9.3., in order to indicate the *ignition field strength* in kV/mm r.m.s.

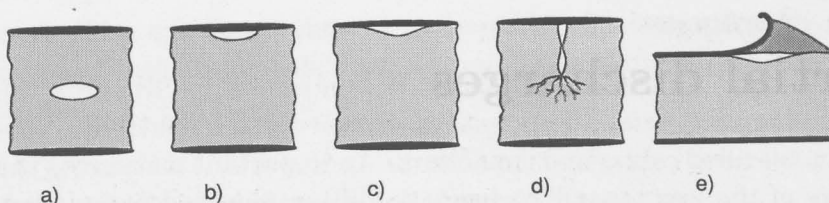


**Fig. 8.1.** Internal discharges.

- (a) completely surrounded by the dielectric.
- (b) electrode bounded cavity.
- (c) non-adhering electrode.
- (d) initiated by treeing.
- (e) in an interface with a longitudinal field.

The highest field strength in the cavity (and thus the lowest inception stress in the dielectric) occurs if the cavity is flat, for instance as in fig. 8.1 c. The inception field strength  $E_i$  is then approximately

$$E_i = \epsilon E_d = \epsilon \frac{U_b}{d},$$

where  $U_b$  can be found in fig. 8.2.

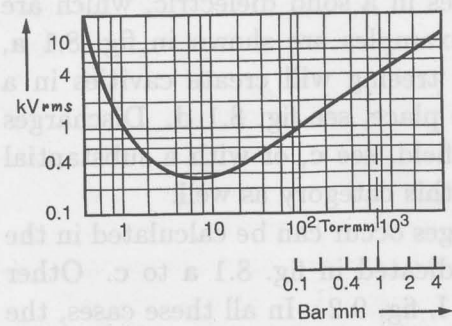


**Fig. 8.2.** Paschen curve.

$U_d$  is the breakdown voltage of an air-filled cavity. See also part I, fig 9.3.

Take, for example, a flat cavity of 0.1 mm height in polyethylene, with  $\epsilon=2.2$ . It may be assumed that the air pressure in the cavity is 1 Bar, as such a cavity will, in the long run, adopt atmospheric pressure because of *diffusion*. The inception stress appears to be as low as 3.2 kV/mm. This illustrates how readily discharges may occur in solid dielectrics, which are used in practice from 3 to 10 kV/mm.

### Surface discharges

Surface discharges occur along dielectric interfaces where a substantial tangential field strength is present. The interface is either gas- or liquid-bounded. Examples are shown in fig. 8.3.

The inception stress, i.e. the field strength *in* the dielectric where discharges occur at the surface, is fairly low. In fig. 8.3 the inception voltage is shown for discharges at the edges of metallic foils. Such foils are, for instance, used in condenser bushings, as described in part I, section 11.4. It can be seen from these values that relatively thin layers are needed to prevent surface discharges.

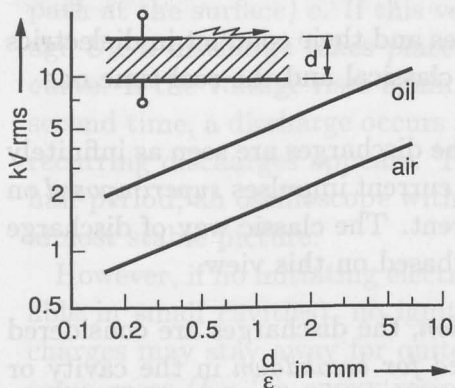


Fig. 8.3. Surface discharges at the edge of a metallic foil under oil and in air. The inception voltage is shown as a function of  $\frac{d}{\epsilon}$ .

### Corona discharges

Corona discharges occur at sharp metallic points in an electric field. They may be found at the high-voltage electrode, but it should be kept in mind that they can also occur at the earthed side or half-way between electrodes. The inception voltages, as found in small gaps, are shown in fig. 8.4.

Corona is also a source of interference when making discharge tests. The test area must therefore be free of sharp edges, pointed wire ends, thin connection wires, etc., to prevent corona, not only at the high-voltage side, but also at the floor of the test area.

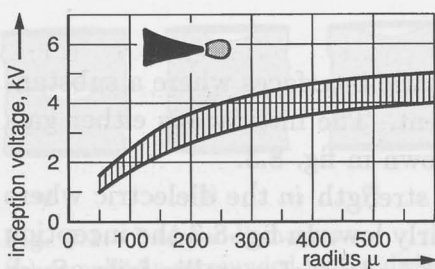


Fig. 8.4. The inception of corona is determined by the absolute voltage, not by the average field strength between electrodes. The inception voltage of negative corona is shown here in kV. Corona at positive points starts later.

## 8.2 Appearance (classic description)

The appearance of partial discharges and their conduct in dielectrics can be described in two ways: the classical and the real-time one.

1. In the *classical description*, the discharges are seen as infinitely short phenomena; they cause current impulses *superimposed* on the 50 (60) Hz dielectric current. The classic way of discharge detection (see section 9.2) is based on this view.
2. In the *time-resolved description*, the discharges are considered during the *short time required for breakdown* in the cavity or in the discharge gap. Wide band detection and travelling wave location (see section 9.4) are based on this view.

In the following section, the classical description will be followed; see also part I, section 9.4.

### Internal and surface discharges

The behaviour of voltages and currents in a sample with an internal or a surface discharge can be described with the aid of the well-known abc-circuit of fig. 8.5. This equivalent circuit is a too simplified representation of the actual behaviour of the electrical fields in a dielectric, however, for industrial purposes it has proved to be an adequate model. The part of the configuration that breaks down is represented by capacitance  $c$ ; the dielectric in series with  $c$  is called  $b$ . The unaffected part of the dielectric is represented by capacitance  $a$ , which in most cases is practically equal to the sample capacitance.

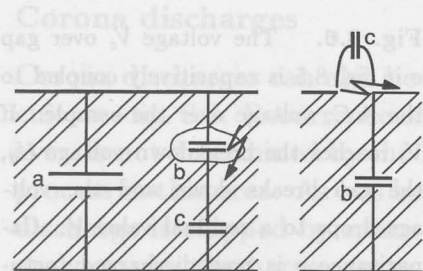


**Fig. 8.5.** The equivalent circuit for internal and surface discharges: a represents the sound part of the configuration; b represents the dielectric in series with the (gaseous) capacitance c; c represents a cavity or part of the surface that flashes over.

If an A.C. voltage is applied to this dielectric, a recurrent discharge phenomenon appears in the way shown in fig. 8.6. The A.C. voltage over the sample causes a voltage  $V_c$  over the cavity (or discharging path at the surface) c. If this voltage surpasses the breakdown voltage  $U_d$ , a discharge takes place where  $U_d$  follows from the Paschen curve. If the voltage rises again, the breakdown voltage is reached a second time, a discharge occurs again, and so on, so that a pattern of recurring discharges appears. This pattern is repeated during every half-period; an oscilloscope with a 50 (60) Hz time base will show an almost stable picture.

However, if no initiating electrons are present (which is quite probable in small cavities), no ignition takes place and the partial discharges may stay away for quite a while. This is the reason that in some cases (e.g. in epoxy resin) a sample is subjected to X-ray to create initiating electrons.

In actual cases the resulting discharge pattern is less stable than suggested by this model. This follows, among other things, from  $U_d$  (and  $V$ ) not being equal at the positive and negative halves of the period. Moreover, several discharge channels can be present in one cavity or at one surface; also leakage currents play a role, both in the dielectric and along the walls of the cavity or the discharge surface. The discharges then wander along the sine-wave, are of unequal size, disappear and return, etc., which may result in a rather turbulent picture.

It can also be derived from this model that a discharge pattern, once ignited, can persist far below the inception voltage. This is shown in fig. 8.7. The voltage  $V_c$  over the cavity is too low for breakdown. Now ignition is forced, for instance by a short overvoltage: the sine wave of  $V_c$  is shifted, breakdown occurs at the negative side, the sine

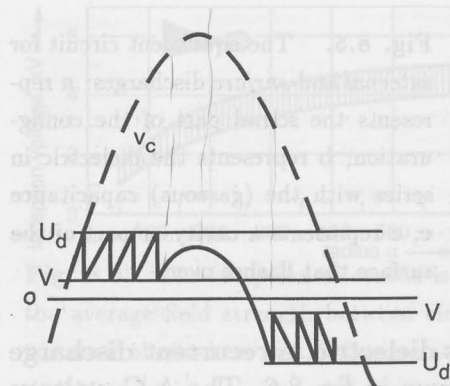


**Fig. 8.6.** The voltage  $V_c$  over gap  $c$  in fig. 8.5 is capacitively coupled to the A.C. voltage over the sample. If  $V_c$  reaches the breakdown voltage  $U_d$ , the gap breaks down and the voltage drops to a residual value  $V$ . Capacitance  $c$  is now discharged (actually surface charges are deposited at the gap-surfaces which counteract the main field). The resultant voltage rises again until  $U_d$  is reached and breakdown occurs again. In this way, several discharges take place until the voltage reverses and a series of discharges occurs at the negative half of the period. A recurrent discharge pattern results.

wave of  $V_c$  is shifted again, the discharge recurs, etc.

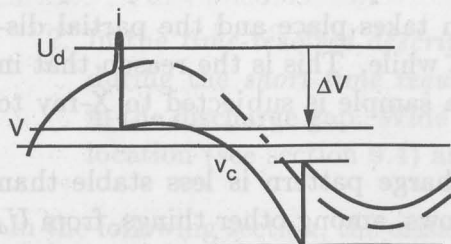


**Fig. 8.7.** Partial discharges can persist below the inception voltage. Once ignition has taken place ( $i$ ), the sine wave  $V_c$  is shifted over a distance  $\Delta V$ . Breakdown recurs at the negative half. Voltage  $V_c$  is shifted again, and so on. This may take place at a voltage as low as half the inception voltage.

This phenomenon may occur in practice when H.V. equipment is tested for discharges. If discharges are found at a certain voltage and the voltage is decreased, the discharges may persist: the *extinction voltage* is lower than the inception voltage. In theory, this could go on to 50 % below the inception level, in practice this is often not more than 10 to 35 % below inception voltage.

All preceding phenomena occur at A.C. voltage. At D.C. voltage no discharges occur, or they occur very infrequently caused by leakage currents in the dielectric. This is one of the reasons why D.C. voltage is far less harmful to dielectrics than A.C. voltage.

### Corona discharges

Corona discharges can also be described with the abc-equivalent circuit, see fig. 8.8. Recurrence of the breakdown in capacitance  $c$ , however, is not determined by the H.V. wave-shape but by the ionization process in this area. As has been described in part I, section 6.5, the discharge is stopped by space charges, the space charges then move away, a new discharge starts, etc., so that a train of discharges is formed. Corona discharges also occur thus at *D.C. voltage*. At *A.C. voltage* they appear first at the negative top of the sine wave, see fig. 8.8. When raising the voltage, the number of discharges increases rapidly, their magnitude remains about the same. At higher A.C. voltage, discharges appear also at the positive top. Consequently, corona discharges appear in a characteristic pattern that is well distinguishable from other partial discharges.

At sharp edges under *oil*, similar phenomena occur but the discharge patterns are less stable and less reproducible.

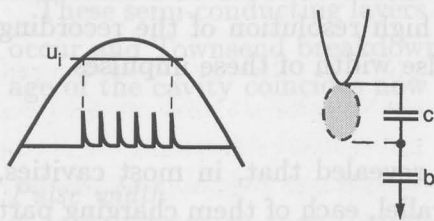


**Fig. 8.8.** Negative corona at A.C. voltage. Corona discharges occur at the negative period as long as the voltage at point  $U$  exceeds the inception voltage  $-U_i$ . The recurrence of the corona impulses is determined by the physical process near the point and is independent of the type of voltage. At far higher voltages, discharges appear at the positive side as well. Corona discharges can by their appearance be well distinguished from other types of partial discharges.

At D.C. voltage, a continuous train of discharges appears, similar to the impulses shown here.

### 8.3 Appearance (time resolved)

The second way of describing the behaviour of discharges does not consider the discharge as infinitely short, but describes the physical phenomenon at its proper time scale. This time scale stretches from a few nanoseconds to part of a microsecond.

### Virgin cavity

In an unaged cavity within a dielectric no cathode is available, so that no secondary electrons are provided by the  $\gamma$ -mechanism and a Townsend discharge (see part I, section 5.3) cannot be formed. A starting avalanche does not develop into a breakdown of the gap. The voltage has to be increased until the condition for a *streamer breakdown* (part I, section 6.1) is reached. Then breakdown in the gas occurs independently of the dielectric walls. The overvoltage required to start a streamer is usually 5 % higher than the voltage corresponding to the Paschen curve.

### Pulse width

The formation of a streamer is very fast. It is determined by the drift velocity of the electrons which, in these circumstances, is in the order of 100 mm/ $\mu$ s. (The velocity of the photons that provide the propagation of the streamer also plays a role, but their speed of 300 m/ $\mu$ s may be regarded here as infinite.) The *time-to-breakdown* is consequently very short: cavities with a thickness of 0.1 to 1 mm break down in 1 to 10 ns. An extremely high resolution of the recording devices is required to record the pulse width of these impulses.

### Pulse height and number

Observation with fast cameras has revealed that, in most cavities, several small streamers occur in parallel, each of them charging part of the dielectric surface, see fig. 8.9. Only in small-diameter cavities (with a diameter height ratio  $\leq 1$ ) a large part of the surface is (dis)charged by one streamer.

It appears from oscillograms that these partial discharges occur rapidly in succession: the photons from one streamer ignite streamers at other sites. The intervals are sometimes so small that they are hardly dissolved by the recording equipment and are therefore often recorded as one large discharge. Each streamer impinges on the dielectric surface and produces a tiny Lichtenberg figure at that point, as shown in fig. 8.9

### Aged cavity

When testing a dielectric cavity for some time, a transition takes place after which a completely different discharge phenomenon oc-

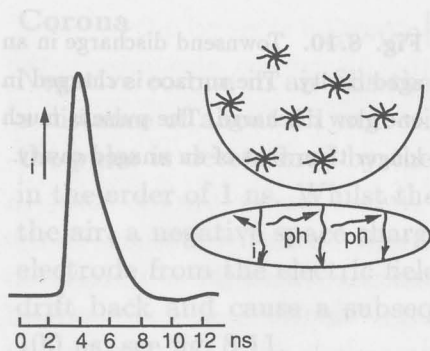


**Fig. 8.9.** Streamer discharge in an unaged cavity. If the cavity has a diameter height ratio larger than 1, several of these discharges occur almost simultaneously, ignited by photons  $ph$  of the first discharges. When the streamers strike at the walls of the cavities, small Lichtenberg figures are formed and occupy the surface of the cavity.

curs. After some time, varying from 5 to 60 minutes, the surface resistivity of the cavity walls decreases appreciably. This is caused by chemical changes at the surface, such as the formation of organic acids. Together with moisture in the air, these acids form layers which are at the borderline between an isolating and a conducting layer. Typical values for this transition are a conductivity of  $10^{16}\Omega$  square for virgin material and  $10^{11}\Omega$  square after aging.

These semi-conducting layers act as a cathode,  $\gamma$ -feedback can now occur and Townsend breakdown can take place. The inception voltage of the cavity coincides now with the Paschen curve.

#### Pulse width

The breakdown time is determined by the velocity of the forming avalanches. Avalanches are formed and initiate feedback again until sufficient avalanches have been formed to provide for the required charge displacement representing a breakdown. The transit time is far longer than in the former case: for cavity depths from 0.1 to 1 mm the *time-to-breakdown* is found to be 80 ns to 0.8  $\mu$ s.

Pulsed discharges injure the surface of the dielectric. Several mechanisms notwithstanding, the damage is due to the presence of the

#### Pulse height

A large part of the surface of the cavity is now charged in one single glow discharge. This is confirmed by optical observation where a diffuse discharge is observed which is characteristic for Townsend breakdown. The total charge displacement is about equal to that in the former case of streamer discharges. As the pulse is longer than in the former case, the height of the pulse will be lower, see fig. 8.10.

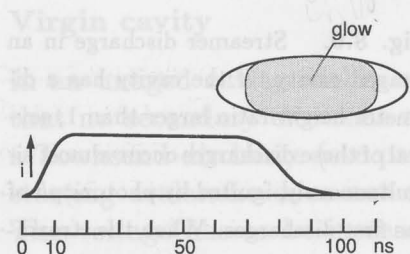


**Fig. 8.10.** Townsend discharge in an aged cavity. The surface is charged in one glow discharge. The pulse is much longer than that of an unaged cavity.

### Transition

The transition from streamer discharges to Townsend discharges takes a time that is dependent of the dielectric material. In glass this transition time is about 5 minutes; in polyethylene and PMMA about an hour. During the transition time both types of breakdown occur; sometimes combined shapes are found.

In time resolved-observation the differences are clear: at first, short streamer-like discharges are found, after the transition long Townsend discharges occur. With *classical* detection (as described in the following chapter) *no difference in impulses* can be seen, only the *inception voltage* changes, which may lead to temporary extinction of the discharges.

After a far longer period, a third mechanism may appear. Heavy discharges start from the edge of the cavity in a spacious and intermittent way. These discharges seem to be related to the initiation of breakdown in the dielectric that often takes place from the edge of a cavity. This third mechanism is a symptom of progressive ageing.

### Surface discharges

If surface discharges are observed just about their inception voltage, no difference with internal discharges is found initially: a short impulse as in fig. 8.9 is seen, caused by small discharges at the edge of the electrode.

However, if the test voltage is increased, streamers are formed at the surface and far longer pulses are observed, about ten times the length of those of fig. 8.9. A surface discharge can clearly be recognized in this way.

### Corona

Negative corona in air fills the space around a sharp electrode over a distance of about 0.1 mm with a glow discharge. The rise-time of the pulse is determined by the drift velocity of the electrons and is in the order of 1 ns. Whilst the fast moving electrons are trapped in the air, a negative space charge is formed which shields the pointed electrode from the electric field. The discharge stops, the slow ions drift back and cause a subsequent current, which decays in 50 to 100 ns, see fig. 8.11.

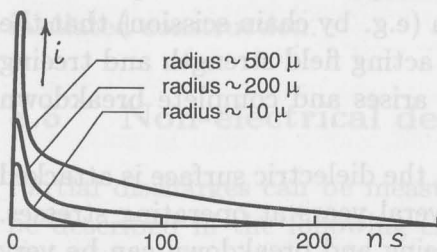


**Fig. 8.11.** The typical shape of negative corona. The front is less than 1 ns, the time constant of the first part of the tail is in the order of 10 to 20 ns, corresponding to a streamer discharge. The second part of the tail reflects the displacement of the space charge. The tail is longer when the radius of the point is larger.

It follows from this figure that the shape of a corona pulse can be well distinguished from other types of discharges. An additional information that is revealed by the wave shape is the radius of the point: the larger the radius, the longer the impulse. Positive corona (not shown here) corresponds to a Townsend-like discharge with a larger front and a relatively long plateau before decay sets in.

## 8.4 Deterioration

Partial discharges injure the surface of the dielectric. Several mechanisms are responsible for this effect.

*Heating* the surface of the dielectric causes chemical aging of the material; *oxidation* plays an important role as may be derived from the fact that adding anti-oxidants to plastics often improves their resistance against discharges.

*Chain scission* of polymer molecules is caused both by oxidation and by the direct impact of electrons at the insulation material and makes it more brittle. Stress cracking can occur: tiny crazes appear

at the surface of the material.

*Ultra-violet* light transmitted by the discharges also injures the dielectric: it is a well-known fact that ultra-violet light promotes stress-cracking.

The deterioration in *cavities* follows several stages, see fig. 8.12. In the first stage, the erosion takes place over the entire surface. In the second stage, preferential areas are formed where the deterioration is far more severe than at other places. In the last stage, one of these preferential areas develops into a deep pit. The discharges are then concentrated at that pit. The pit further develops and the dielectric material degrades so much (e.g. by chain scission) that the breakdown strength falls below the acting field strength and treeing is initiated. An unstable situation arises and complete breakdown soon follows.

The initiating phase during which the dielectric surface is attacked takes a long time; this can take several years at operating stresses. The finite stage, which includes treeing and breakdown can be very short: minutes to some hours.

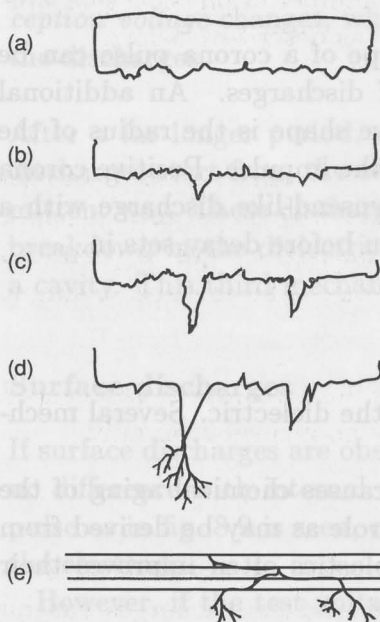


**Fig. 8.12.** Successive stages of deterioration by internal discharges:

- (a) erosion
- (b) preferential erosion
- (c) pit forming
- (d) treeing.
- (e) Deterioration of composite dielectrics follows more complicated routes.

The mechanism is more complicated in dielectrics that are built up of several layers. After one layer has been penetrated, the interface

between the layers is followed, after which further penetrations occur at other places, see fig. 8.12.

Deterioration by *surface discharges* follows the same lines as in cavities, but because of the larger surface available the effect tends to be less severe and larger discharge magnitudes are allowable.

Deterioration by *corona discharges* follows completely other lines. Corona is, by its very character, located adjacent to a metal electrode and not to a dielectric, so that little or no harm is done. There is one exception: corona in SF<sub>6</sub>-gas creates aggressive by-products, which attack both the metal conductors and the insulating bodies of a gas insulated construction.

## 8.5 Non-electrical detection

Partial discharges can be measured with electrical methods as will be described in the following chapter. Their presence can also be detected by *non-electrical* methods which, however, do not permit quantitative measurements.

Non-electrical detection is based on a number of physical phenomena which accompany partial discharges as described below..

### Gas and heat

The simplest detection method consists of the measurement of *gas-pressure*. This is applied to transformers with impregnated paper insulation. If discharges occur in the insulation, gas is produced which is detected with the Buchholtz relay. The method is simple but at the same time insensitive.

Another simple but insensitive method is the detection of *heat* caused by discharges. This applies to extremely poor insulation only.

### Noise detection

The detection of acoustical or ultra-sonic noise is more effective. *External* discharges, such as corona and surface discharges can be detected by ultra-sonic detectors which are commercially available for this purpose. These detectors function usually at a frequency of about 30 kHz. This frequency has proven to be optimal: at higher

frequencies the effect of environmental noise is less, but the attenuation of the noise in air becomes too large. The detected noise signal is concentrated by a parabolic mirror as shown in fig. 8.13a.

Such detectors can also be connected to a plastic rod to pin-point a discharge source, see fig. 8.13b.

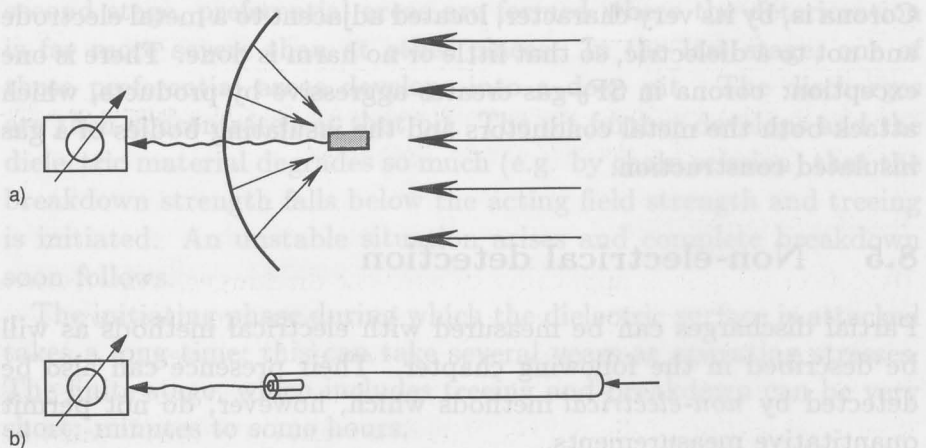
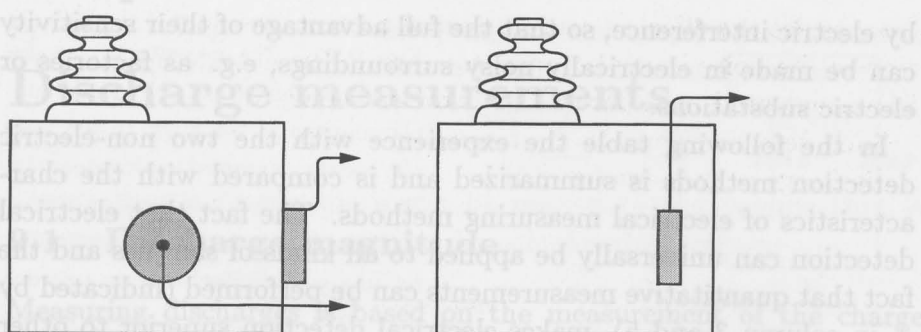


Fig. 8.13. Noise detection in air.

*Internal* discharges can sometimes be detected with the aid of sensors placed at the surface of the sample, such as GIS, transformers or cable accessories. An alternative way is to immerse hydrophones in the insulating oil of, for instance, a transformer, see fig. 8.14. The noise signals are amplified and reproduced at a 50 (60) Hz time-base on an oscilloscope. This has the great advantage that signals originating from electrical discharges are synchronized and can be represented as stable pictures, whereas disturbing signals from arbitrary sources are moving over the time-base. There are, however, also sources of disturbances which synchronize with the power frequency. This emerges, for instance, from magnetostrictive noise in the core of transformers, from dynamical forces in windings of transformers and machines and from piezo-electric forces in capacitor-foils. The best way to suppress these disturbances is to measure the acoustic noise signal at a fairly high frequency, say 100 kHz, with a bandwidth of some tens of kHz.



**Fig. 8.14.** Noise detection: sensors are placed at the tank of a sample or a hydrophone is immersed in the oil of a power transformer

### Light detection

Detection of light is applicable to external discharges. An effective method is photography. By choosing long exposure times and sensitive films, high sensitivities can be reached. Moreover, the site of the discharges is well determined; no other method yields such an accurate location of discharges. The disadvantage is that it must be possible to shield the H.V. test area completely from ambient light.

The sensitivity can be further increased by using image intensifiers. In these cases sensitivities can be reached which surpass those of electric detection techniques.

### Survey

Non-electric observations are restricted to the *detection* of the presence of discharges and no quantitative results can be obtained. They form, however, a welcome addition to electric measurements. In certain cases the high sensitivity is attractive or location of the discharge sites can be performed.

*Noise detection* is not particularly sensitive. Discharges in air can be detected at a sensitivity of several picocoulombs. Internal discharges are reported to be detected at a level of 10 pC, but in many cases the sensitivity is not better than 100 pC.

*Light detection* can be very sensitive. Long exposures with a camera enable detection of discharges as low as 1 pC, accessories like image intensifiers may increase the sensitivity to 0.01 pC or less. An additional advantage is that non-electric methods are not affected

by electric interference, so that the full advantage of their sensitivity can be made in electrically noisy surroundings, e.g. as factories or electric substations.

In the following table the experience with the two non-electric detection methods is summarized and is compared with the characteristics of electrical measuring methods. The fact that electrical detection can universally be applied to all kinds of samples and the fact that quantitative measurements can be performed (indicated by + in column 3 and 5), makes electrical detection superior to other methods.

	sensitivity	resistant to electrical disturbances	universal method	location of discharges	quantitative measurements
Noise detection					
· in air	+	+	—	+	—
· internal	□	+	—	+	—
Light detection					
· photo camera	+	+	—	++	—
· image intensifier	++	+	—	++	—
Electric detection					
· small samples	++	□	+	□	+
· large samples	+	□	+	□	+

+ few  $pC$

++ down to 0.01  $pC$

□ order of 100  $pC$

+ within cm's

++ within mm's

□ dm's to m's

# Chapter 9

## Discharge measurements

### 9.1 Discharge magnitude

Measuring discharges is based on the measurement of the charge displacement in the leads to a sample. This is actually performed by placing an impedance  $Z$  in the lead, see fig. 9.1. In this way we measure a quantity that is related to the discharge but does not represent the discharge itself; what we measure is the external charge displacement

$$q = b\Delta V.$$

The displacement of charge at the site of the discharge (cavity, surface or corona) is

$$\boxed{q_1 = c\Delta V.}$$

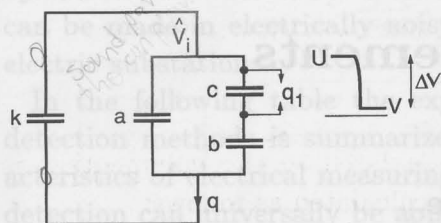
Capacitance  $b$  is usually far smaller than  $c$  so that

- the magnitude which is measured is far smaller than that of the actual discharge, and
- this magnitude has an unknown relation to the actual discharge.

One can thus wonder whether measuring  $q$  is the correct approach. Much has been written on this subject and many proposals have been made, but H.V. engineers have always returned to the charge displacement  $q$  as the preferred definition of *discharge magnitude*. There are two reasons for this, which will be discussed below.

#### Energy dissipation

The energy  $p$  that is dissipated in a discharge can be related to the discharge magnitude  $q$  as follows:



a, b and c as in figure 8.5

**Fig. 9.1.** The magnitude of a discharge is defined as the charge displacement  $q$  in the leads to the sample, usually expressed in picocoulombs. This magnitude is not equal to the actual charge displacement in a cavity (or in a surface discharge or a corona discharge), but is nevertheless a good representation of the intensity of the discharge as it is directly related to (1) the energy dissipated in a discharge (2) the dimensions of the discharge site.

$$\begin{aligned} p &= \frac{1}{2}c(U^2 - V^2) \\ &= \frac{1}{2}c(U - V)(U + V) = \frac{1}{2}c\Delta V(U + V). \end{aligned}$$

Now  $U + V$  is replaced by  $U$ , making an error in the order of 10%.  
And

$$U = \frac{b}{b+c} \hat{V}_i \approx \frac{b}{c} \hat{V}_i,$$

where  $\hat{V}_i$  is the inception voltage over the sample and  $b+c$  is replaced by  $c$ , making an error in the same magnitude order, but in the other direction. It then follows that

$$p \approx \frac{1}{2}b\Delta V \hat{V}_i = \boxed{\frac{1}{2}q\hat{V}_i},$$

or if the inception voltage  $V_i$  is expressed in the usual r.m.s.-value:

$$p \approx 0.7qV_i.$$

Thus the discharge magnitude  $q$  gives a *reasonable representation of the energy* that is dissipated in the partial discharge. For samples of

the same voltage class the inception voltage is usually of the same level and discharge magnitudes are thus directly comparable.

### Physical size

The discharge magnitude  $q$  can be related to the volume that is occupied by a discharge and can be calculated as follows:

$$q = b\Delta V$$

where  $\Delta V$  is the breakdown voltage of the discharge gap and

$$b \approx \epsilon_0 \epsilon_r \frac{S}{d}, \quad \text{see fig. 9.2.}$$

Thus

$$q \approx \epsilon_0 \epsilon_r S \Delta V \frac{1}{d}$$

and as  $\Delta V$  increases with increasing length of the discharge gap,  $q$  increases with  $S\Delta V$ , that is with the volume of the discharge. Some examples for a cavity in a dielectric with  $\epsilon = 2$  and insulation thickness  $d=10$  mm:

- an air-filled cube of 0.3 mm gives about  $\frac{1}{4}$  pC,
- an air filled cube of 0.5 mm gives about 1 pC.

In consequence of the calculation above, the adopted discharge magnitude  $q$  is representative for both the *energy* and the *volume* of a discharge and is therefore a good measure for partial discharges.

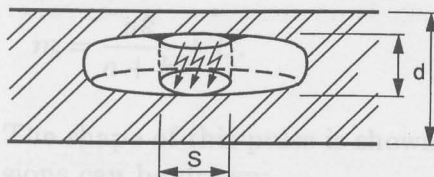


Fig. 9.2. The volume occupied by a partial discharge is directly related to the discharge magnitude  $q$ .

### Classification of methods

Two basic methods exist for measuring discharges; in addition there are some deviating techniques. These methods will be described in the following section. A brief survey is given here as an introduction:

- *Classic detection*; the discharge impulses are amplified with a bandwidth of about 100 to 500kHz. The discharges are displayed as short impulses at a 50(60) Hz time-base, as shown in fig. 9.3.
- *Time resolved detection*; the discharge impulses are amplified with a bandwidth of about 100 to 500 MHz. The true shape of the discharge impulses is shown on a triggered time-base, as viewed in fig. 9.3

Then two deviating techniques follow that can be used in a few cases only:

- *Schering bridge test*; a deviating technique is the schering bridge measurement, where all the pulses of the 50(60)Hz time-base are integrated.
- *E.M. field detection*; this technique is applicable if the screen is absent or imperfect so that electromagnetic waves are radiated.

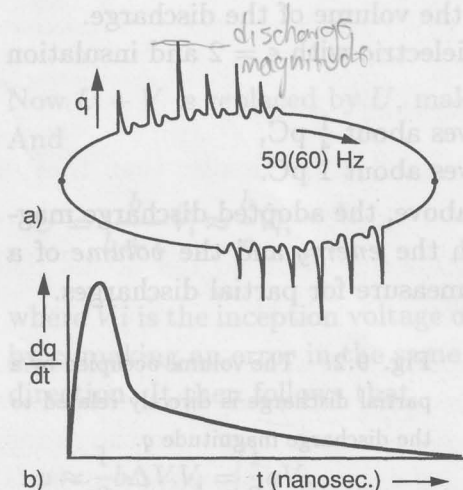


**Fig. 9.3.** Display of discharges.  
 (a) Classic detection. The discharges are displayed as discharge patterns, superimposed on a 50(60) Hz. time-base.  
 (b) Time resolved detection. The actual discharge process is shown at a triggered time-base in the nanosecond region.

## 9.2 Classic detection

### Basic circuit; pulse height

Any circuit for the measurement of discharges can be reduced to the basic circuit shown in fig. 9.4.

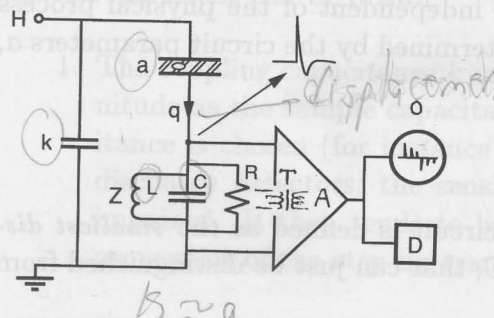


**Fig. 9.4.** Basic circuit for discharge measurements.

$H = H.V.$  source, preferably free of discharges.

$k$  = coupling capacitor, providing a closed circuit for the discharge displacement  $q$ . The coupling capacitance  $k$  shall be of the same order of magnitude as that of the sample  $a$ .

$Z$  = at this impedance, voltage pulses are formed which are stepped up (T) and amplified (A), displayed on an oscilloscope (O) and analyzed with a discharge analyzer (D).

The discharge impulses are formed by a detection impedance  $Z$  that usually consists of a heavily attenuated LCR circuit. The resulting impulse is equal to

$$v = \frac{q}{a + C(1 + a/k)} \cos \omega t \exp - \frac{t}{2Rm},$$

where

$$\omega = \sqrt{\frac{1}{Lm} - \frac{1}{4R^2m^2}}$$

and

$$m = \frac{ak}{a + k} + C.$$

The shape of this pulse is shown in fig. 9.4. Some important conclusions can be drawn:

1. For larger samples, the amplitude  $\hat{v}$  of the pulse tends to be  $\hat{v} = \frac{q}{a}$ , thus inversely proportional to the sample capacitance.
2. The coupling capacitance  $k$  is indispensable. If  $k \rightarrow 0$ , the pulse amplitude  $\hat{v} \rightarrow 0$ .

3. The *shape of the pulse* is independent of the physical process of the discharge and is determined by the circuit parameters  $a$ ,  $k$ ,  $L$  and  $C$  only.

### Sensitivity

The sensitivity of a detection circuit is defined as the *smallest discharge impulse*, measured in pC, that can just be distinguished from background noise.

We have seen above that the impulse height decreases proportionally with the sample capacity. At a fixed noise level, for instance that of the amplifier, the smallest detectable discharge thus increases proportionally with the sample capacitance. If a given amplifier yields a sensitivity of 1 pC at a sample of 10 nF, the sensitivity will decline to 100 pC at a sample of 1  $\mu$ F.

This situation is not acceptable and measures have been devised to improve the sensitivity. This is accomplished by introducing a step-up transformer as indicated by  $T$  in the basic circuit of fig. 9.4. This transformer amplifies both the signal and the circuit noise (which is lower than the amplifier noise) to slightly over the amplifier noise. The sensitivity is now determined by the circuit noise and it appears that this noise decreases with the square root of the circuit capacitance  $m$ :

$$v_c \approx \frac{1}{\sqrt{m}},$$

where

$$m = C + \frac{ak}{a+k}$$

and  $m$  tends to equal the sample capacitance  $a$  for larger samples ( $C$ ,  $a$ , and  $k$  as indicated in fig. 9.4 and  $a \approx k$ ).

It now follows that the smallest detectable discharge increases proportionally with the *square root* of the sample capacity, a considerable improvement indeed. It can be calculated as

$$q_{min} \approx \sqrt{\frac{a}{k} + 1} \sqrt{a + (1 + \frac{a}{k})C}$$

Two conclusions can be drawn:

1. The coupling capacitance  $k$  must be of the same order of magnitude as the sample capacitance  $a$ . If a fixed coupling capacitance is chosen (for instance 1000 pF), as is done with some discharge detectors, the sensitivity for large samples will be impaired. It then tends to be proportional to  $a$  and the improvement of the step-up transformer is lost.
2. If  $k$  is sufficiently large, the smallest detectable discharge increases with  $\sqrt{a}$ .

The ratio of the step-up transformer must be increased with increasing sample capacitances, most discharge detectors provide this ratio in a number of fixed steps. Examples of sensitivities with and without a step-up transformer are:

Sample capacitance	Sensitivity without step-up trafo	Required step-up ratio	Sensitivity with step-up trafo
2 nF	0.1 pC	2	0.05 pC
50 nF	2 pC	10	0.2 pC
1 $\mu$ F	50 pC	50	1 pC

## Resolution

A discharge detector generates a number of pulses which form a characteristic pattern as shown in fig. 9.5.

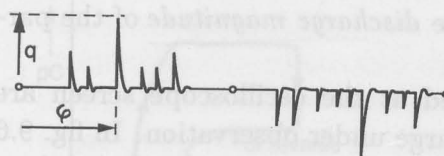


Fig. 9.5. Discharge pattern generated by a classic discharge detector. The pattern is characteristic for the type of discharge under observation. Consequently the phase angle and the pulse height  $q$  of each discharge impulse must be maintained at further processing. This requires sufficient resolution of detector and amplifier.

This pattern is repeated every 20(16.7) ms. The information assembled in this discharge pattern shall be maintained during processing. For this reason two characteristics shall be kept unaltered:

- the relative height  $q$  of the impulses;
- the phase angle  $\varphi$  of the impulses.

The shape of the impulses, however, need not to be maintained.

The lower band of the amplifier is chosen so that the power frequency and its higher harmonics do not reach the oscilloscope. The bandwidth of the amplifier is in the order of 100 to 400 kHz. The parameters of the detector impedance are chosen in such a way that the pulse width is in the order of 2 to 10  $\mu$ s and two pulses at that distance are separated. The *resolution* of the detector can be checked:

1. By observing a corona discharge as shown in fig. 8.8. The number of impulses is increased by increasing the voltage until the picture is blurred. The distance between pulses that occur just before blurring is the *resolution* of the detector.
2. The same can be performed by applying a commercially available calibrator where the time lag between two discharge pulses can be varied and the smallest time lag that can be resolved, is determined.

### Recognition by oscilloscope

The discharges are displayed on an oscilloscope screen as shown in fig. 9.3a. In addition, a crest voltage meter is provided which measures the highest impulse that is present in pC. This highest discharge impulse is usually referred to as the *discharge magnitude* of the partial discharge under observation.

The discharge patterns displayed at the oscilloscope screen are characteristic for the type of discharge under observation. In fig. 9.6 several examples of these patterns are shown.

These observations are backed up by recording the discharge magnitude as a function of voltage. It is strongly recommended to record such kV-pC-diagrams both for improving recognition and for documenting the results of discharge measurements as shown in fig. 9.7.

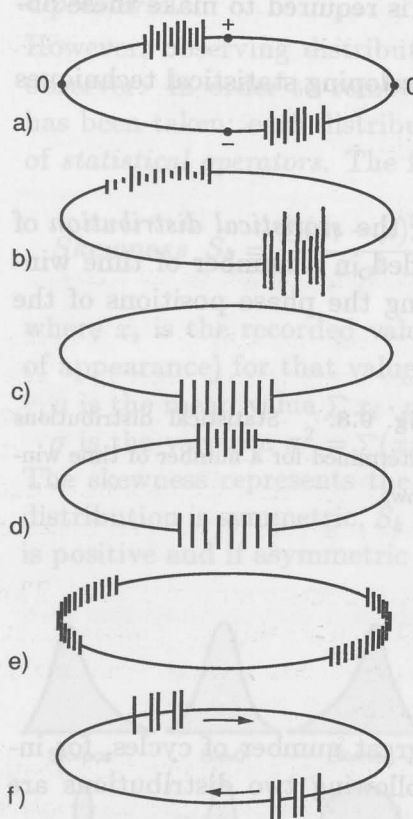


**Fig. 9.6.** Characteristic discharge patterns.

- (a) Cavity completely surrounded by a dielectric: the discharges at both polarities are equal or do not differ more than a factor 3.
- (b) Cavity or surface discharge, at one side bounded by an electrode: the discharges at both polarities differ more than a factor 3.
- (c) Negative corona in gas: discharges are of equal magnitude and occur at one polarity only. At higher voltages positive corona may appear at the other side of the ellipse.
- (d) Corona in oil: typical corona pattern at one side, indistinct corona pattern at the other side of the ellipse.
- (e) Contact noise: indistinct noise pattern at the zero-points where the capacitive current is maximal.
- (f) Floating part: imperfect contact of an electrode floating in the electric field causes regularly repeating discharge groups, sometimes rotating along the ellipse.

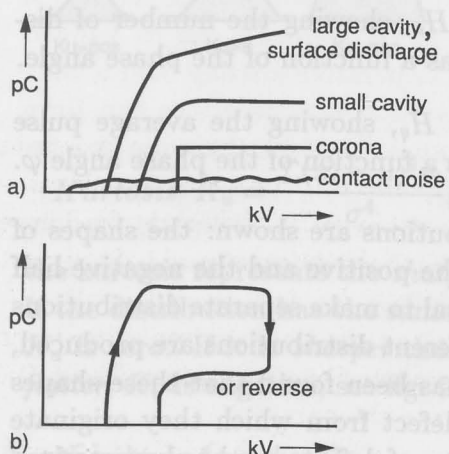


**Fig. 9.7.** Discharge diagrams: records of discharge magnitude in pC versus applied voltage in kV.

- a. The shape of these diagrams may add to the recognition of discharges by oscilloscopic observation.
- b. The diagrams may change at prolonged voltage exposure. The inception voltage often increases because of the formation of semi-conducting layers in cavity or surface. But the extinction voltage may also be lower than the inception voltage, because of the effect shown in fig. 8.7.

### Recognition by statistical analysis

The recognition of discharges by oscillographic observation show some disadvantages: it covers only a limited number of discharge

types and a well experienced operator is required to make these observations.

Much progress has been made by developing statistical techniques for the analysis of discharge patterns.

### Statistical distributions

Each analysis starts with determining the *statistical distribution* of the discharges. The time base is divided in a number of time windows, as shown in fig. 9.8, representing the phase positions of the discharges.

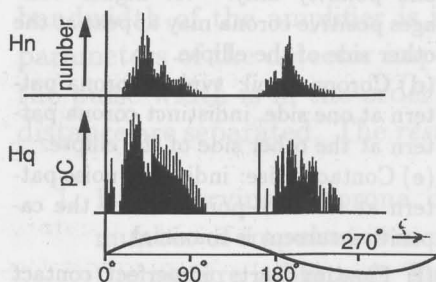


Fig. 9.8. Statistical distributions determined for a number of time windows.

Each time window is observed for a great number of cycles, for instance during some minutes. The following two distributions are determined:

1. The *pulse count* distribution  $H_n$ , showing the number of discharges in each time window as a function of the phase angle.
2. The *pulse height* distribution  $H_q$ , showing the average pulse height in each time window as a function of the phase angle  $\varphi$ .

In fig. 9.8, examples of both distributions are shown: the shapes of the distributions differ greatly for the positive and the negative half of the voltage cycle. It appears logical to make separate distributions for each halv-cycle, so that four different distributions are produced, each with its particular shape. It has been found that these shapes are characteristic for the type of defect from which they originate and it has been found that more types of defects can be characterized with these distributions than with the conventional oscillosograms.

### Operators

However, observing distributions again requires a well experienced observer. In order to remove this disadvantage, the following step has been taken: each distribution is analyzed by means of a number of *statistical operators*. The following operators are used:

$$\text{Skewness } S_k = \frac{\sum(x_i - \mu)^3 \cdot p_i}{\sigma^3},$$

where  $x_i$  is the recorded value and  $p_i$  the probability (= frequency of appearance) for that value  $x_i$  in time window  $i$ ,

$\mu$  is the mean value  $\sum x_i \cdot p_i$  and

$\sigma$  is the variance  $\sigma^2 = \sum(x_i - \mu)^2 p_i$ .

The skewness represents the *asymmetry* of the distribution. If the distribution is symmetric,  $S_k$  is zero, if it is asymmetric *to the left*,  $S_k$  is positive and if asymmetric *to the right*,  $S_k$  is negative, see fig. 9.9.

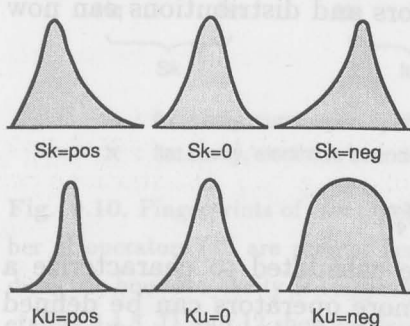


**Fig. 9.9.** The shape of a distribution can be characterized by operators, like skewness  $S_k$  which describes the asymmetry of a distribution and kurtosis  $K_u$  which describes the sharpness of a distribution.

$$\text{Kurtosis } K_u = \frac{\sum(x_i - \mu)^4 p_i}{\sigma^4},$$

the kurtosis represents the *sharpness* of the distribution, see fig. 9.9. If the distribution has the same sharpness as a normal distribution,  $K_u$  is zero. If it is *sharper* than normal,  $K_u$  is positive, and if it is *flatter*,  $K_u$  is negative, see fig. 9.9.

*Number of peaks Pe,*

which is defined by the *number of local tops* in the distribution, where a local top is defined as

$$\frac{dy_i - 1}{dx_i - 1} > 0 \quad \text{and} \quad \frac{dy_i + 1}{dx_i + 1} > 0.$$

In actual cases one to eight peaks have been distinguished.

$$\text{Crosscorrelation factor } cc = \frac{\sum x_i u_i - \sum x_i \sum y_i / n}{\sqrt{[\sum x_i^2 - (\sum x_i)^2 / n][\sum y_i^2 - (\sum y_i)^2 / n]}},$$

where  $x_i$  is the mean discharge magnitude in window  $i$  of the positive half-cycle, and  $y_i$  the mean discharge magnitude in the *corresponding* window in the negative half-cycle.

The cross-correlation factor indicates the *difference in shape* of the distributions in the positive and negative *half-cycle*. If the shapes are the same (but not necessarily of equal height),  $cc$  is 1, if they differ completely,  $cc = 0$ .

### Fingerprints

The following combinations of operators and distributions can now be made:

Skewness of  $H_n^+ H_n^- H_q^+ H_q^-$

Kurtosis of  $H_n^+ H_n^- H_q^+ H_q^-$

Peaks of  $H_n^+ H_n^- H_q^+ H_q^-$

Cross-correlation between  $H_q^+$  and  $H_q^-$ ,

so that 13 different operators can be calculated to characterize a particular discharge pattern. Many more operators can be defined (and are actually in use), but these 13 operators already offer a wide scope. It can be estimated that the 13 operators above can form about 3000 combinations, many of which could be characteristic for a particular source of discharges.

A number of artificial defects, incorporated in dielectric models, have been studied. The discharges in these defects have been analyzed with the above mentioned distributions and operators. Each defect shows a typical combination of operators, forming a "fingerprint" of that particular defect. Defects that can be characterized in this way are:

*Cavities; electrode or dielectric bounded flat, square or sharp*

*Surface discharge:* in air, in SF<sub>6</sub>, or oil

*Corona:* in air or oil

*Treeing:* at a cavity or at a sharp point

Examples of such fingerprints are shown in fig. 9.10.

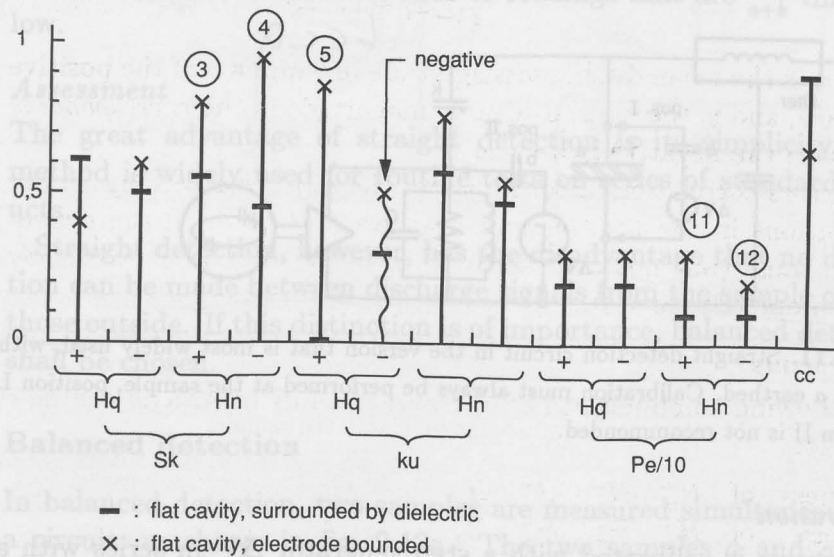


**Fig. 9.10.** Fingerprints of two types of cavities, each fingerprint consists of a number of operators (13 are present here, but many more can actually be used). A dielectric-bounded cavity is compared here with an electrode-bounded cavity. Operators 3,4,5, 11 and 12 show distinct differences.

If now an unknown discharge pattern is analyzed and compared with these existing fingerprints, a simple algorithm can tell us whether the discharge pattern can be attributed with some probability to a certain defect.

Moreover, the variation in some operators, when the sample is aged under voltage, is also characteristic for certain types of defects.

The observation of discharges with a statistical analyzer is thus an effective means for recognizing discharge sources.

### 9.3 Implementation of classic detection

In practice, two basic methods exist for performing classical discharge detection: straight detection, introduced by Dr. Mole in 1954,

and balanced detection, introduced by the author in 1958.

### Straight detection

Straight detection uses either the circuit as shown previously in fig. 9.4, or that shown here, in fig. 9.11, where the sample is earthed.

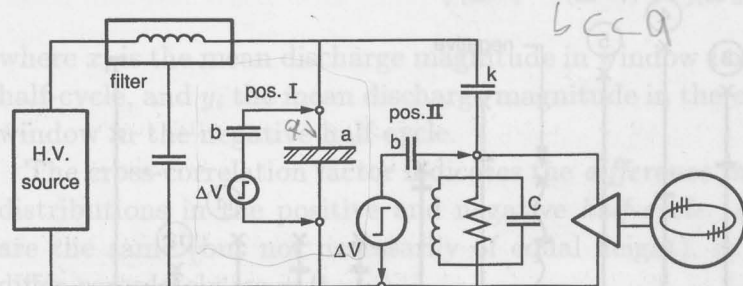


Fig. 9.11. Straight detection circuit in the version that is most widely used, with sample  $a$  earthed. Calibration must always be performed at the sample, position I. Position II is not recommended.

### Calibration

The circuit is calibrated with a step generator  $\Delta V$  in series with a small capacitor  $b$ . With this generator a discharge

$$q_{cal} = b \Delta V$$

is injected into the sample  $a$  ( $b$  must then be far smaller than  $a$ ). Usually a discharge of fixed magnitude is injected, for instance 50 pC and the recording instruments, such as oscilloscope and discharge magnitude meter, are calibrated.

The calibrating discharge *must always be injected in the sample*, notwithstanding the disadvantages: the calibrator must be removed before high voltage can be applied and no calibration can be made during the test. Some discharge detectors have a built-in calibrator which injects calibrating pulses into the detection impedance (see fig. 9.11), which can be operated during the test, however the response to this pulse is

$$\hat{v} = \frac{q_{cal}}{C + \frac{a \cdot k}{a+k}} = \frac{a+k}{aC+kC+ak} q,$$

whereas the correct response when injecting the sample is

$$\hat{v} = \frac{q}{a + C(1 + \frac{a}{k})} = \frac{k}{aC + kC + ak} q,$$

The built-in calibrator leads thus to readings that are  $\frac{k}{a+k}$  times too low.

#### *Assessment*

The great advantage of straight detection is its simplicity. The method is widely used for routine tests on series of standard products.

Straight detection, however, has the disadvantage that no distinction can be made between discharge signals from the sample or from those outside. If this distinction is of importance, balanced detection shall be chosen.

#### **Balanced detection**

In balanced detection, two samples are measured simultaneously in a circuit, as shown in fig. 9.12a. The two samples  $a$  and  $a'$  have preferably the same insulation material, so that their loss factors are equal over a broad frequency spectre. Capacitance  $a$  does not need to be equal to  $a'$ . However, samples of equal capacitance yield optimal results.

Discharges in the samples  $a$  and  $a'$  are detected, but discharge signals from outside, such as from  $k$  or from the H.V. source, can be suppressed. For this purpose the bridge is balanced by injecting a large discharge between H.V. and earth, and adjusting the variable impedances  $R$  and  $C$  to minimal response. The conditions for balance are

$$\frac{R}{R'} = \frac{a'}{a}, \quad \frac{C}{C'} = \frac{a}{a'}$$

and  $\tan \delta = \tan \delta'$  over the full bandwidth of the detector.

The quality of the balance is described by the rejection ratio  $m$ :

$$m = \frac{\text{response to a discharge } q \text{ injected into } a}{\text{response for the same discharge injected into } k}$$

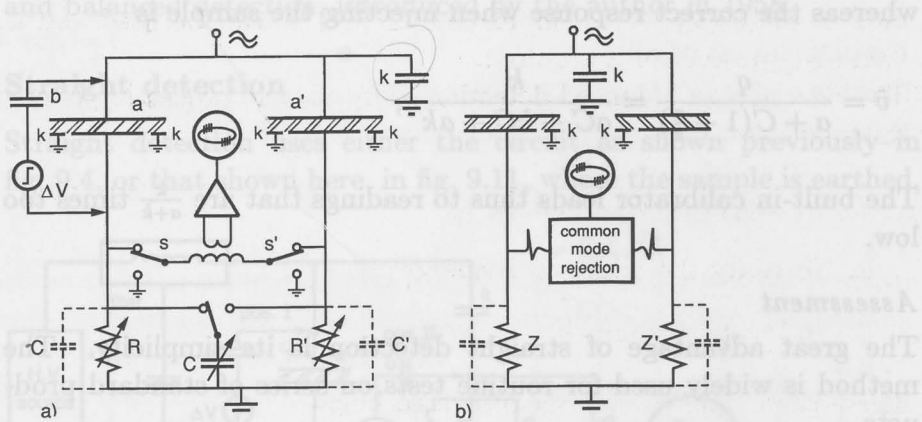


Fig. 9.12.

Balanced detection.

(a) Bridge detection: by adjusting  $R$ ,  $R'$  and  $C$ , the bridge is balanced so that discharge signals from outside (capacitance  $k$  or H.V. source) are rejected. The origin of a discharge signal is determined by switching: if switch  $S$  is opened, *internal* discharges (in  $a$ ) disappear, *external* discharges (in  $k$ ) increase. Calibration is performed by injecting a known discharge  $b\Delta V$  into the sample.

(b) Pulse discriminator: common-mode signals are rejected so that discharges of *external* origin (in  $k$ ) are suppressed, and *internal* discharges (in  $a$ ) are displayed. By pushing the common-mode button, these discharges are distinguished.

The following rejection ratios have been obtained in actual cases:

Two identical samples  $m = 1000$  to  $5000$

Two unequal samples, with  
the same insulation material  $m = 100$  to  $500$

Two unequal samples  $m = 3$  to  $30$

#### *Electronic processing*

In fig. 9.12b, an interesting variant of balanced detection is shown. The pulses from the left-hand and the right-hand side of the bridge are processed in a pulse discriminator. Pulses which arrive at the same time and which are of the same polarity originate from sources *outside* the bridge circuit. When the processor is activated, these pulses are rejected and disturbances from outside are suppressed. Pulses of opposite polarity are accepted. The rejection ratio  $m$  is smaller than in a balanced detector, but the method has the advan-

tage of simplicity: fixed impedances  $Z$  and  $Z'$  can be used and no balancing procedure is required.

The rejection by balanced detection or by electric processing is used in three ways:

1. To suppress disturbances
2. To verify the origin of discharges
3. To locate discharges

These three applications are discussed below.

#### *Suppression of disturbances*

An obvious application is the measurement of discharges in the presence of an outer disturbance. If the samples are well screened, and if they are reasonably equal, the full sensitivity of a discharge detector can be reached in the presence of heavy disturbances. The use of a cage of Faraday for suppressing interference is then not required. Discharges as low as 0.03 pC have been measured in this way.

#### *Verification*

The greatest advantage of balanced detection is the possibility of verifying whether a discharge signal results from the sample or from outside, such as from the H.V. circuit, the coupling capacitor, or other sources. There are two ways to do this:

1. By slightly varying the balance conditions. External discharges will then show great variations in response, whereas discharges from the sample do not vary at all.
2. By switching the switches  $S$  and  $S'$ , indicated in fig. 9.12a. The response to *external* discharges increases manifold but internal discharges in sample  $a$  disappear if switch  $S$  is opened, and remain the same when switch  $S'$  is activated. A similar effect is obtained when activating an electronic pulse discriminator.

This verification removes the uncertainty that is found with straight detection. It functions also at small rejection ratios, so that an asymmetric bridge ( $m = 3$  to 30) or an electronic pulse-discriminator (e.g.  $m$  is 20) can be used.

*Location*

Balanced detection is successfully used to locate the site of discharges in complicated samples. For this purpose, the earth screen is interrupted at several places, as shown, for instance, in the cable connector of fig. 9.13.

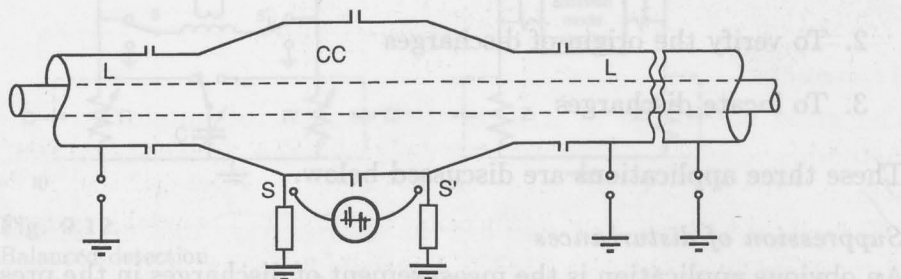


**Fig. 9.13.** Location by subdivision of the electrodes. In this example, the cable connector CC is divided in two halves and is further separated from the adjoining cable lengths  $L$ . The cable connector is measured for discharges in a balanced detector. Manipulating the balance reveals the origin of a discharge: left-hand or right-hand side of CC, or in lengths  $L$ . By further subdividing either CC or  $L$ , the discharge site can precisely be located.

At first the two halves of the cable connection CC are measured in a balanced circuit; the cable lengths  $L$  are earthed. With the switches  $S$  and  $S'$  it is established whether the discharges originate from the right-hand or from the left-hand side of the cable joint. The joint can be further subdivided and measured until the site of the discharge has been located within a few centimetres.

If it is found that the discharge is located in one of the adjoining cable lengths, that particular cable length can be subdivided and further subdivided until the discharge is located with great precision. This method is not non-destructive (interruptions are made to the sheath) but it is very effective.

The interruptions can be made according to fig. 9.14a, where the earth electrodes are made to overlap. This method, however, is sensitive to errors. If the insulation  $O$  in the overlap is not perfect, unwanted discharges will occur in this region. The interruption shown in fig. 9.14b is therefore preferred. A semi-conductive layer  $L$  is applied (or was already present) and the interruption is made by removing part of the metallic sheath  $M$ . In this way an impedance

is formed that is sufficiently high in order to separate the electrodes, but sufficiently low not to interfere with the electric field in the insulation, so that no additional discharges can occur.

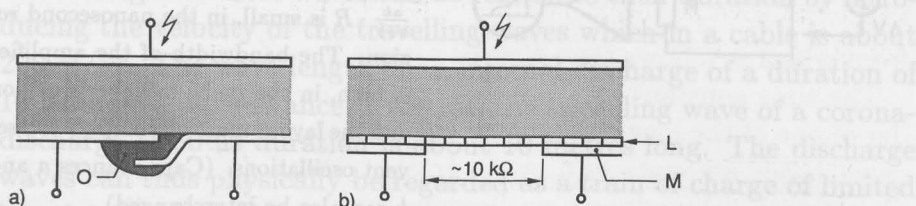


**Fig. 9.14.** Interruptions in earth screen. In (a) the metal electrodes are made to overlap. Extra insulation  $O$  is inserted in the overlap to prevent discharges in this region. In (b) a semiconduc layer  $L$  terminates the dielectric. The metallic electrodes  $M$  are sufficiently separated to create a longitudinal resistance of some  $k\Omega$ 's.

In another example, a bushing is used to enter H.V. equipment as shown in fig. 9.15. Straight detection does not discriminate between discharges in the actual sample  $a$  or those in the bushing  $C_B$ , a parasite capacitance  $C_p$  or the coupling capacitor  $C_k$ . By using a balanced detector, the terminals  $C_k$  to  $a$  can alternately be measured or earthed. Distinction can then be made between discharges in different parts.

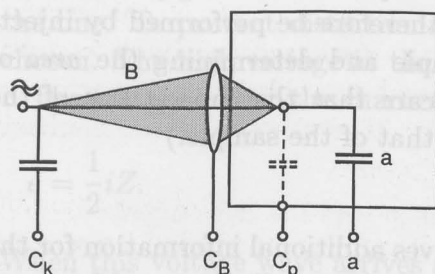


**Fig. 9.15.** Location: by alternately connecting  $C_k$ ,  $C_B$ ,  $C_p$  and  $a$  to a balanced circuit, it can be verified whether a discharge is located in the sample or in one of the other parts.

## 9.4 Time resolved detection

Time resolved detection may give useful information by observing partial discharges in the nanosecond region. The basic circuit is the same as in classic detection, see fig. 9.16, but the time constants are far smaller and the layout is far more compact for keeping self-induction low and preventing unwanted oscillations.

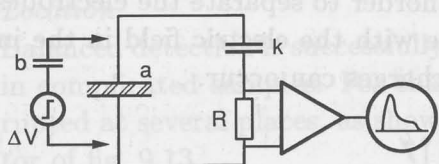


**Fig. 9.16.** Time resolved detection. Discharges are measured in a straight detection circuit. The time constant  $\frac{ak}{a+k} \cdot R$  is small, in the nanosecond region. The bandwidth of the amplifier is high, in the multi-megahertz region and the layout must be compact to prevent oscillations. (Capacitances  $a$  and  $k$  can also be interchanged).

The pulses at the detection impedance are amplified with a bandwidth of 500 to 1000 MHz for research purposes and of 50 to 100 MHz for industrial tests. The pulses are displayed at a triggered time-base; the oscillograms represent the current in the discharge gap as a function of time. When doing research on the behaviour of discharges in small spaces, the shape of the impulse is accurately displayed, including the front of the pulse which may be shorter than 1 ns. For industrial purposes recognition of the tail of the impulse may be sufficient and a time constant of about 10 ns may be adequate.

#### *Calibration*

The magnitude of the discharges is represented here by the area of the oscillogram. Calibration shall therefore be performed by injecting a known discharge in the sample and determining the *area* of the matching oscillogram. (Take care that the capacitance of the calibrator is small as compared to that of the sample.)

#### *Recognition*

The shape of the discharge pulse gives additional information for the distinction between internal, surface or corona discharges. Moreover, thickness and width of a detected cavity can be estimated and a guess can be made to the extend of deterioration, as shown in section 8.3 and figures 8.9 and 8.10. In a similar way, the radius of a source of corona can be estimated, see fig. 8.11.

#### **Location by travelling waves**

Location by travelling waves was introduced by the author in 1960: time resolved detection is applied to samples where travelling waves

may occur, such as in high-voltage cables and large GIS-stations. If a partial discharge takes place in a long line, as shown in fig. 9.17, two travelling waves result: one to the left and one to the right.

The length of these waves can be related to their duration by introducing the velocity of the travelling waves which in a cable is about 200 m/ $\mu$ s. The wave length of an internal discharge of a duration of 10 ns is then, for instance, 2 metres; the travelling wave of a corona-discharge of 50 ns duration is about 10 metres long. The discharge waves can thus physically be regarded as a train of charge of limited length which travels along the length of the line at a speed that is almost the velocity of light.

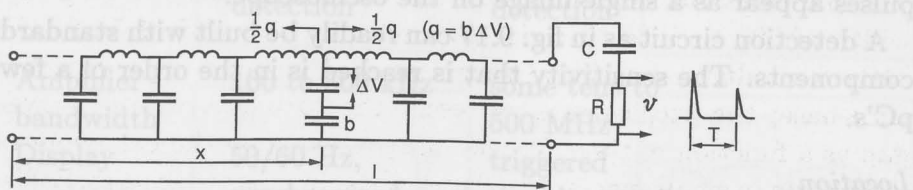


**Fig. 9.17.** Location by travelling waves. Two travelling waves with velocity  $v$  start at the site of the discharge. The time lag  $T$  between direct wave and reflection is a measure for the distance  $x$  between far end and discharge site,  $x = \frac{T \cdot v}{2}$ . The amplitude of the wave is  $e = \frac{i}{2}Z$ , where  $i$  is the current at the discharge site.

The travelling waves are detected with an impedance at the end of the line. To prevent distortion of the pulses, a pure resistance  $R$  is chosen. The high voltage at the line is blocked by a capacitor  $C$ .

The voltage  $e$  over the characteristic impedance  $Z$  in the line is

$$e = \frac{1}{2}iZ.$$

When this voltage wave arrives at the end of the line, the voltage  $v$  over the detection resistor is

$$v = \frac{2R}{Z + R}e.$$

The thermal noise from this resistor  $R$  is proportional to  $\sqrt{R}$ . For an optimal signal-noise ratio the expression

$$\frac{v}{V_{noise}} = C_0 \frac{2R}{(2 + R)\sqrt{R}} \quad (C_0 \text{ is a constant})$$

shall reach a maximum, which is found at

$$\frac{d}{dR} \frac{\sqrt{R}}{Z+R} = 0,$$

from which it follows that  $R$  shall satisfy  $R = Z$ .

The time constant  $\tau$  of the  $RC$  network is chosen to be in the order of one of the longer discharge pulses, 250 ns, so that the blocking capacitance amounts to  $C \approx \frac{\tau}{R}$ , or about 5 nF. The pulses are observed with a broadband oscilloscope with a time constant of some ns. The time-base is triggered by the discharge pulses, so that the pulses appear as a single image on the oscilloscope.

A detection circuit as in fig. 9.17 can readily be built with standard components. The sensitivity that is reached is in the order of a few pC's.

#### *Location*

The location of a discharge can now be determined by measuring the time lag of the reflections. One of the two travelling waves reaches the detector and triggers the time-base, the opposite wave reflects at the other end and arrives  $T$  microseconds later, see fig. 9.17. The time to arrival of the first wave is

$$\frac{l-x}{v},$$

and that of the second wave is

$$\frac{l+x}{v},$$

the time lag is then

$$T = \frac{2x}{v},$$

where  $x$  is the distance of the discharge site from the far end and  $v$  is the velocity of the travelling wave, which in high-voltage cables is of the order of 200 m/ $\mu$ s. The position of the discharge is located in this way with an accuracy of 5 to 10 metres in cable lengths of 1 to 2 km. (With very high bandwidth detection, an accuracy of part of

a metre can be reached in GIS switchgear.)

In fig. 9.18, a series of oscillograms is shown with increasing distance between discharge and detector. The attenuation of the discharge impulses can clearly be seen, as well as redoubling of the reflection when the discharge approaches the far end.

### Comparison

The characteristics of classic and time resolved detection can be compared in the following way:

	Classic detection	Time resolved detection
Amplifier bandwidth	100 to 500 kHz	some tens to 500 MHz
Display	50/60 Hz, synchronized	triggered time-base < 1 $\mu$ s
Characteristic information	discharge pattern $q = f(\varphi)$ , see fig. 9.3a	pulse shape $i = f(t)$ , see fig. 9.3b

## 9.5 Evaluation of discharges

After a discharge has been detected and its magnitude has been measured, the question must be answered whether this discharge is detrimental to the voltage life of the insulation.

1. To begin with, the *type of discharge* shall be determined. Corona discharges, for instance, are harmless unless their breakdown products, such as ozon or derivates of SF<sub>6</sub>, endanger the construction. Corona of several hundreds of pC's might be acceptable in air-insulated constructions, whereas corona in SF<sub>6</sub>-insulations must be less than 1 pC.

Surface discharges are less dangerous than internal discharges as they are less concentrated.

Treeing discharges, however, are very dangerous. If a discharge is recognized as resulting from treeing, any discharge magnitude is unacceptable.

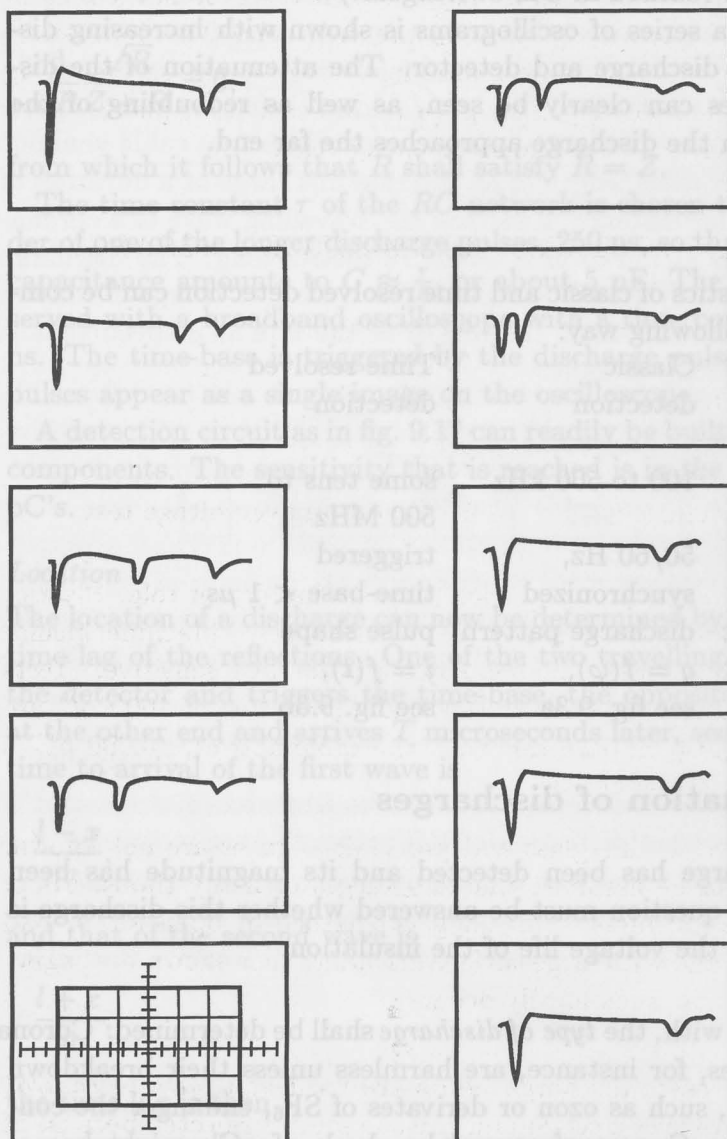


Fig. 9.18. Travelling waves in high-voltage cables. In the oscilloscopes 1 to 9 the discharge site moves away from the detector, or  $x$  in fig. 9.17 decreases.

2. The *order of magnitude* of discharges is of importance: in the order of 1-3-10-30-100 pC, not their exact value.

3. An important variable, more important than discharge magnitude, is the *operating stress* in the dielectric. The permissible discharge magnitude decreases fast with increasing operating stress. The following table gives an indication for plastics such as polyethylene, elastomers or epoxy-resin.

OPERATING STRESS	PERMISSIBLE DISCHARGE
$\leq 1.5 \text{ kV/mm}$	no test required
2 kV/mm	100 pC
2.5 kV/mm	30 pC
3 kV/mm	5 pC
3.5 kV/mm	1 pC
$\geq 4 \text{ kV/mm}$	1 pC and an overvoltage test

4. The *insulation material* itself plays an important role. Plastics are generally quite sensitive to discharges. Machine insulation with a large amount of mica is far less sensitive. Tests on machine bars have shown that discharges of 1000 pC are acceptable (compare this with the table above), 10.000 pC is regarded as dangerous.

For materials like glass and porcelain, figures are not known, but it can be assumed that discharges of many thousands of pC's are harmless. The long experience in open air in bad climates and with large surface discharges has shown that aging of these materials hardly occurs.

5. In many cases discharge limits are used as a *quality control*. Discharges over a certain magnitude are not rejected because of their effect on the voltage life, but as a check on the production quality.

## 9.6 Deviating detection techniques

In this section, two deviating techniques for discharge detection are described, both of them having a limited field of application.

### Schering bridge

If many discharge sites are present at a time, Schering bridge measurements may be useful. The discharges add to the dielectric losses and a sudden increase of the loss angle, shown as  $\Delta \tan \delta$  in fig. 9.19, reveals the ignition of a great number of discharges at voltage  $U_i$ .

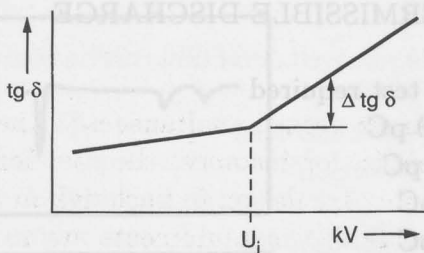


**Fig. 9.19.** From the inception voltage  $U_i$  on, partial discharges contribute to the losses. The increase in loss tangent, caused by the discharges, is represented by  $\Delta \tan \delta$ .

In order to determine the sensitivity of a Schering bridge for discharges, the energy-balance in a sample is calculated. The dielectric losses  $W_1$  which are measured in a sample with capacitance  $a$  are

$$W_1 = \omega a \tan \delta U^2.$$

The energy  $p$  in one discharge is according to section 9.1 equal to

$$p = \frac{1}{\sqrt{2}} q U_i.$$

If  $n$  discharges per half-cycle are present, the dissipated power  $W_2$  is

$$W_2 = \frac{1}{\sqrt{2}} q U_i 2 f n.$$

Now  $W_1$  shall be equal to  $W_2$  and at the inception voltage  $U = U_i$ . We are further interested in the smallest detectable discharge  $q_{min}$  which corresponds to the smallest increase in losses  $\Delta \tan \delta_{min}$  that can be determined by the Schering bridge. From this it follows that the sensitivity of a Schering bridge test for  $n$  discharges per half-cycle is equal to

$$q_{min} = \sqrt{2\pi} a U \Delta \tan \delta_{min} \cdot \frac{1}{n}.$$

Take, for example, one discharge in a machine bar of  $1 \text{ nF}$ , measured at  $10 \text{ kV}$  where an increase  $\Delta \tan \delta$  of  $1 \cdot 10^{-4}$  just can be measured:

$$q_{min} \approx 5000 \text{ pC},$$

which is several thousand times worse than a conventional discharge detector. However, if  $n = 50,000$ , the sensitivity is

$$q_{min} = 0.1 \text{ pC},$$

so that if many thousands of discharges occur simultaneously, the method becomes very sensitive. This is, for instance, the case for mica insulation in machine bars or paper insulation in bushings and cables. For these products, Schering bridge measurements are required and severe demands are made for the magnitude of  $\Delta \tan \delta$  as a function of voltage as mentioned before in section 7.9.

### Detection of stray E.M.-fields

In samples without earthscreens, electromagnetic radiation is transmitted by the fast charge displacements of partial discharges. Examples are

- insulators in air
- epoxy-resin insulated transformers and open switchgear
- the upper part of cable terminals.

The E.M. radiation can be picked up by wideband probes, see fig. 9.20, which can be either capacitive or inductive. By moving these probes along the sample, location of discharges can be performed. Great care should be taken, however, not to ignite partial discharges by the probe and to prevent dangerous situations for the operator. Detection of E.M. radiation is regarded as an auxiliary method; calibration, and thus determining the discharge magnitude, is difficult to perform. Non-electric detection might be a useful alternative.

The calculation of confidence intervals is found in

bedroom, living and similar areas in which there are many discharge sites. If many discharge sites are present at a time, Schering bridge measurements may be useful. The discharges add to the dielectric losses and a sudden increase of the loss angle, shown as  $\Delta$  in fig. 9.18, indicates a possible discharge site.

The wideband probe of fig. 9.20 can be used to pick up electromagnetic radiation from open insulation constructions such as cable terminals or epoxy-resin insulated components. The probe  $P$  is moved along the sample for locating the discharge site. The probes can either be capacitive or inductive.

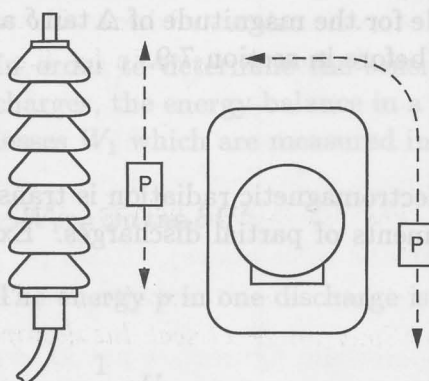


**Fig. 9.20.** A wideband probe can be used to pick up electromagnetic radiation from open insulation constructions, such as a cable terminal or an epoxy-resin insulated component. The probe  $P$  is moved along the sample for locating the discharge site. The probes can either be capacitive or inductive.

$$I = \frac{dV}{dt} = \frac{dQ}{dt} \quad \text{or} \quad Q = I t$$

If a discharge per half-cycle generates sides, the total number of discharges  $N$  is

The E.M. radiation can be picked up by wideband probes, see fig. 9.20. The E.M. radiation can be picked up by wideband probes, see fig. 9.20. Wideband probes can be either capacitive or inductive. By moving wideband probes along the sample, position of discharge can be determined. Care should be taken to avoid damage to the insulation during the measurement. We consider a discharge current  $I$  which starts at time  $t = 0$  and ends at  $t = T$ . The discharge current is zero for  $t < 0$  and  $t > T$ . The total charge  $Q$  is given by

$$Q_{\text{max}} = \sqrt{2\pi} n U / \Delta \tan \theta_{\text{min}} = \frac{\pi}{n} U^2 \Delta \tan \theta_{\text{min}}$$

## Annex

Determining a Weibull distribution from a number of breakdown tests entails two different operations:

- **Parameter estimation:** finding the best fit of the Weibull curve to the data available. This includes the processing of data of samples that failed to breakdown during the test.
- **Determining confidence intervals:** the parameters  $\alpha$  and  $\beta$  (see the expression below) are determined with some uncertainty. The real values of  $\alpha$  and  $\beta$  are found with 95 % probability within the confidence intervals calculated here. These intervals are entered in the Weibull plot, as shown in fig. 6.5.

### Parameter estimation

A calculation procedure and a flow chart for estimating the parameters of a Weibull distribution is given in

*G.C. Stone and R.G. van Heeswijk; "Parameter estimation for the Weibull distribution", IEEE transactions on Electrical Insulation, vol. EI-12. no 4, August 1977.*

In this paper an algorithm is given for the estimation of  $\alpha$  and  $\beta$  with the maximum likelihood-method in the expression

$$F(t) = 1 - \exp\left[-\left(\frac{t}{\alpha}\right)^\beta\right],$$

if a limited number of observations is available. It also takes into account a number of samples that have *not* broken down at the end of the test.

### Confidence intervals

The calculation of confidence intervals is found in

*N.R. Mann, R.E. Schafer, N.D. Singpurwalla; "Methods for statistical analysis of reliability and life data", Wiley, New York, 1974. pp. 191-233.* (for a limited number of samples)

*B.R. Billman, C.E. Antle, L.J. Bain; "Statistical inference from censored Weibull samples", Technometrics vol. 14, November 1972, pp. 831-840.* (for a larger number of samples)

These papers include tables of variables generated with the Monte Carlo method.

See also: *R.E. Schafer and T.S. Scheffield; "On procedures for comparing two Weibull populations", Technometrics vol. 18, no 2, May 1976.*

See also: *R.E. Schafer and T.S. Scheffield; "On procedures for comparing two Weibull populations", Technometrics vol. 18, no 2, May 1976.* This paper describes a method for comparing two Weibull populations. The method can be used to pick up electromagnetic radiation from lightning strikes, such as a radio receiver or an ionosphere detector, for example. It also includes a discussion of the best way to estimate the parameters of the Weibull distribution. The method is based on maximum likelihood estimation, and it is shown that the estimated parameters are unbiased and consistent. The method is also compared with other methods, such as the maximum likelihood method and the method of moments.

In this paper an algorithm for the estimation of the parameters of the Weibull distribution is given. The algorithm is based on the maximum likelihood principle, and it is shown that the estimated parameters are unbiased and consistent. The algorithm is also compared with other methods, such as the maximum likelihood method and the method of moments.

$$\left[ \frac{1}{\lambda} \left( \frac{1}{\lambda} - e^{-\lambda t} \right) - 1 = \left( \frac{1}{\lambda} \right)^2 \right]$$

If a limit is imposed on the number of observations in a sample, it is also possible to use the method of moments to estimate the parameters of the Weibull distribution.

Secondly, a number of samples that have not been drawn from the same population are used to estimate the parameters of the Weibull distribution.

Thirdly, a number of samples that have been drawn from the same population are used to estimate the parameters of the Weibull distribution.

Fourthly, a number of samples that have been drawn from the same population are used to estimate the parameters of the Weibull distribution.

Fifthly, a number of samples that have been drawn from the same population are used to estimate the parameters of the Weibull distribution.

# Some further reading

Abs-circuit, 120-122, 133-135  
A.C.

- sources, 38-41  
- measuring (see 59)

**INSULATION COORDINATION:** M.S. Naidu & V. Kamaraju  
After-installation test, 11, 12, 18-19  
Bilateral coordination, 127-135

**HIGH VOLTAGE TESTING:**

Basic circuit, 137  
Basic insulation level (see BIL)  
Balanced detection, 146, 147-151  
BIL, 13, 14, 15, 26-28  
Bimodal distribution, 91, 92  
Breakdown  
characteristic, 23

**WEIBULL STATISTICS:**

- cracks, 91, 95  
Bridge, 101, 143  
Bushing, 13, 114

**DISCHARGE DETECTION:**

Calibration, 60, 146, 148, 152  
Capacitive divider, 67-69  
Cavity, 118, 124-125, 134  
Cascade

**DISCHARGE RECOGNITION:**

- Transformer, 36, 37  
Chopped wave, 53, 54  
Classic detection, 120-123, 136-151  
Cockcroft, 46  
Conductive losses, 98  
Confidence intervals, 84-86, 89, 161  
Common mode, 148  
Contact noise, 141  
Corona, 119, 120, 123, 127  
Cross correlation, 141  
Current-carrying capacity, 8  
Current measuring, 71-77  
Current wave, 54

**D.C.**

- link, cable, 9, 17

- sources, 43-48  
- measuring, 59  
- discharges, 122, 123  
Dissipation, 127-135

**A.D. Schwab**  
High Voltage Measurements techniques  
M.I.T. Press, Cambridge, USA

**N. Hylten-Cavallius**  
High voltage laboratory planning  
ASEA-Haefely, Basel

**T. Tanaka & A. Greenwood**  
Advanced Power Cable Technology,  
Volume 1, Concepts & Testing, chapter 2  
CRC Press, Florida

**F.H. Kreuger**  
Partial discharge detection in  
High-voltage equipment  
Butterworth, London

**E. Gulski**  
Computer aided recognition of  
partial discharges  
Delft University Press, Delft

Electrodynamic voltmeter, 59-60  
Endurance test, 15, 16, 83  
Extinction, 23, 122  
Extrapolation, 85

Failure risk, 21, 22, 30  
Fault clearing, 3  
Firing impulse generator, 52  
Floating part, 141  
Front resistor, 49

**Greinscher, 46**  
**Guards, 104, 105, 148**

N.R. Mann, R.E. Schafer, N.D. Singpurwalla; "Methods for statistical analysis of reliability and life data", Wiley, New York, 1974, pp. 191-233. (for a limited number of samples)

B.R. Billman, C.E. Antle, L.L. Bain; "Statistical inference from censored Weibull samples", *Technometrics* vol. 14, November 1972, pp. 831-840.

These papers include tables of variables generated with the Monte Carlo method.

See also: R. Hinkin-Cox, J. Gart, "On procedures for comparing two Weibull populations", *Technometrics* vol. 18, no 2, May 1976.

A.O. Spawls, A.D. Spawls, "High voltage insulation breakdown

ASCE-High-voltage Breakdown Test, Part I, 1971.

T.J. Sauer, R.A. Grossman, "A comparison of various power tests

Vadavane, Power Comparison of Tests, chapter 5

CGC Power, Power

E.H. Kandil, "A note on the power of the lognormal distribution

Parikh, Lognormal distribution in reliability engineering

Hill, Voltage distribution

Hannan, Probability distributions

E.G. Saiti, "A note on the power of the lognormal distribution

Compton, Normal distribution, vol. 10, 1970

Burkhardt, Distribution

Dale, Distribution Power, Deltaplano, 1970

Shewhart, Statistical methods for quality control, 1931

Montgomery, Statistical quality control, 1974

Montgomery, Design and analysis of experiments, 1976

Montgomery, Quality improvement methodology, 1982

Montgomery, Quality engineering handbook, 1985

Montgomery, Quality improvement methodology, 1988

Montgomery, Quality engineering handbook, 1991

Montgomery, Quality improvement methodology, 1994

Montgomery, Quality engineering handbook, 1995

Montgomery, Quality improvement methodology, 1996

Montgomery, Quality engineering handbook, 1997

Montgomery, Quality improvement methodology, 1998

Montgomery, Quality engineering handbook, 1999

Montgomery, Quality improvement methodology, 2000

Montgomery, Quality engineering handbook, 2001

Montgomery, Quality improvement methodology, 2002

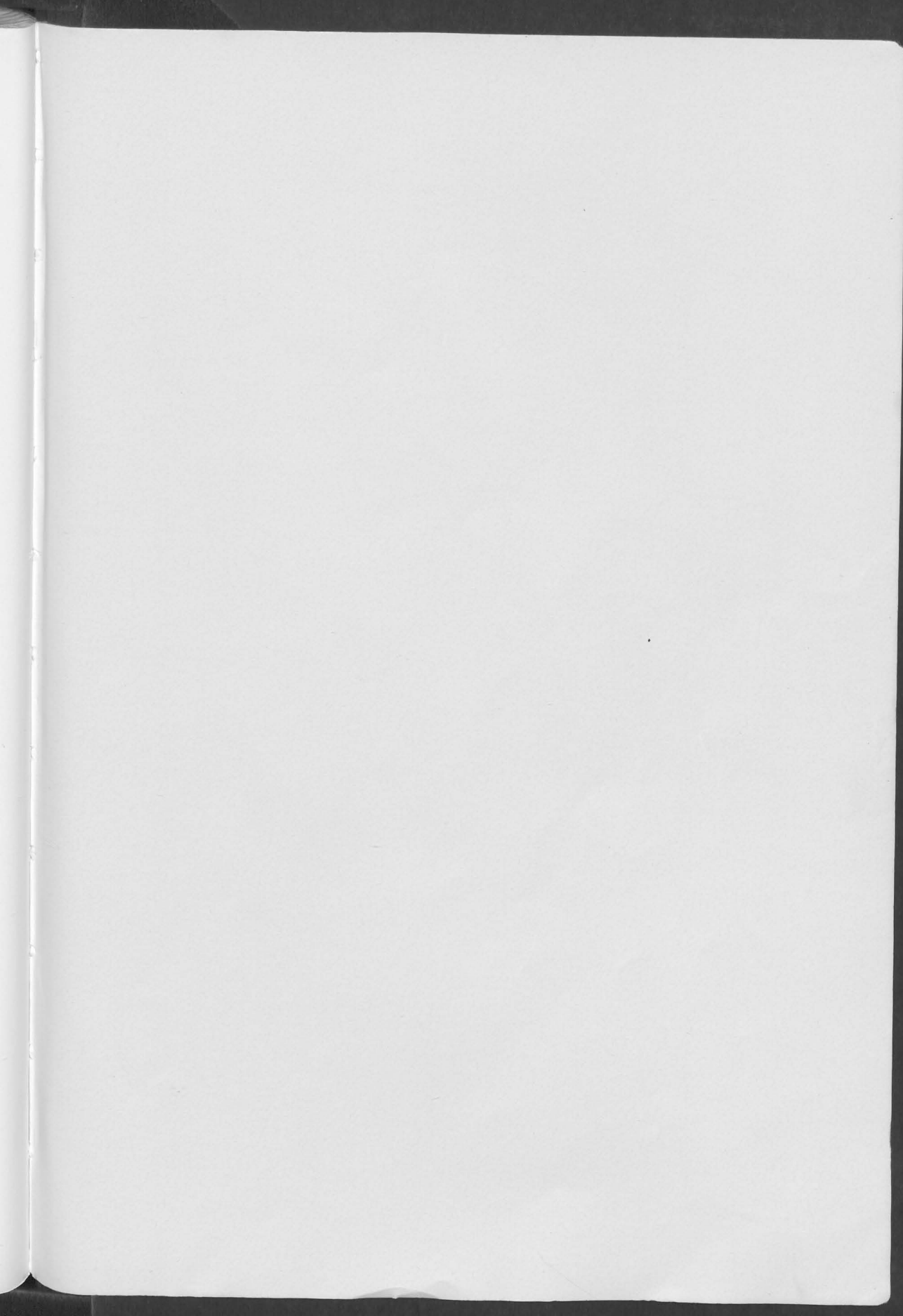
# Index

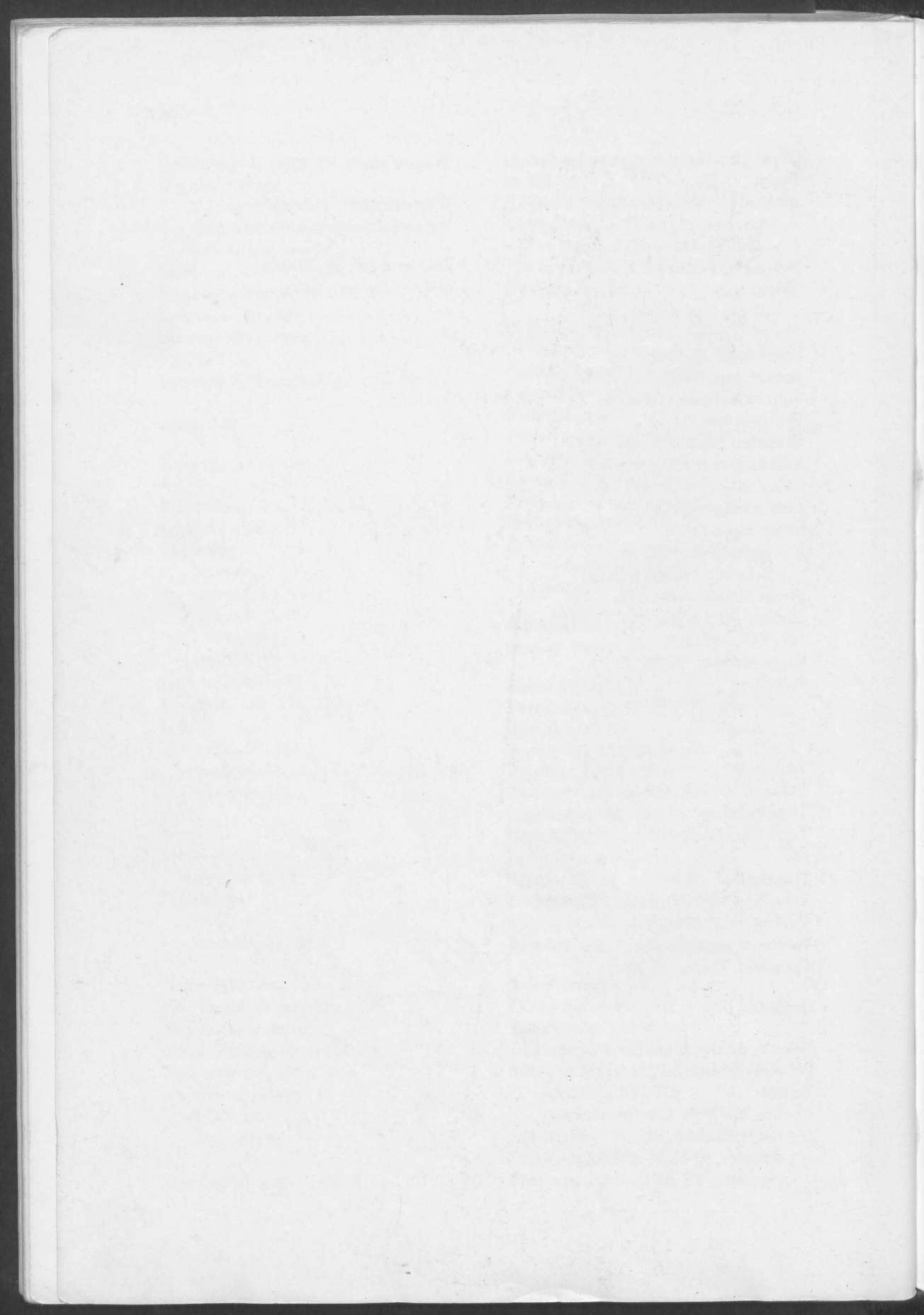
- Abc-circuit, 120-122, 133-135  
A.C.
  - sources, 35-41
  - measuring: see 59
  - overvoltage, 7Aeroplane (testing), 57, 58  
After-installation test, 11, 12, 15, 17, 19  
Arcing horn, 23  
  
Basic circuit, 137  
Basic insulation level (see: BIL)  
Balanced detection, 146, 147-151  
BIL, 13, 14, 15, 26-28  
Bimodal distribution, 91, 92  
Breakdown
  - characteristic, 23
  - test, 79
  - tracks, 91, 95Bridge, 101, 148  
Bushing, 13, 114  
  
Cable, (see: power cable)  
Calibration, 60, 146, 148, 152  
Capacitive divider, 67-69  
Cavity, 118, 124-126, 134  
Cascade
  - rectifier, 46
  - transformer, 36, 37Chopped wave, 53, 54  
Classic detection, 120-123, 136-151  
Cockcroft, 46  
Conductive losses, 98  
Confidence intervals, 84-86, 89, 161  
Common mode, 148  
Contact noise, 141  
Corona, 119, 120, 123, 127  
Cross correlation, 144  
Current-carrying capacity, 8  
Current measuring, 71-77  
Current wave, 54  
  
D.C.
  - link, cable, 9, 17
- Deterioration, 127, 155  
Dielectric losses, 8  
Differential Weibull curve, 89  
Differential transformer bridge, 110, 111, 113  
Digital recording, 69-71  
Dipole losses, 99  
Discharge
  - stray fields, 159
  - evaluation, 155-157
  - detectors, 145-151
  - magnitude, 133, 140, 152
  - measurement (test), 16, 113, 133-160
  - losses, 100, 115, 134, 158
  - pattern, 121, 141Disconnecting
  - trafo, 4
  - cable or line, 4, 5Disturbance, 119, 147-149  
Dual balance, 106-108  
Duration test, 79  
  
Earth impedance, 2  
Earthered samples, 108-110, 112, 146, 152  
Efficiency, impulse generator, 50  
Electrostatic voltmeter, 59-60  
Endurance test, 15, 16, 83  
Extinction, 23, 122  
Extrapolation, 85  
  
Failure risk, 21, 22, 30  
Fault clearing, 3  
Firing impulse generator, 52  
Floating part, 141  
Front resistor, 49  
  
Greinacher, 46  
Guards, 104, 105, 148

- Ignition, 117, 122  
 Impulse voltage  
   - standard shape, 2, 7, 48  
   - generator, 48-53  
   - measuring, see 59  
 Inception, 118, 122, 134  
 Insulation coordination, 1  
 Interfaces, 94, 99  
 Internal discharges, 117, 118, 120-122, 130, 132  
 Inverted Schering bridge, 108, 109  
 Joint, 150  
 Kurtosis, 143  
 Lichtenberg figures, 93, 94, 124  
 Light detection, 131, 132  
 Lightning  
   - arrester, 21-30  
   - current, 54, 77  
   - impulse, 2, 48  
   - stroke, 2, 57  
   - test, 14  
 Line-to-line voltage, 12  
 Location, 150, 151, 153-156  
 Loss  
   - angle, 97, 158  
   - tangent, 97, 98, 114, 115, 158, 159  
   - analysis, 101  
 Marx, 51  
 Metal oxyde (see: ZnO)  
 1-Minute test, 14  
 Multistage  
   - D.C., 46  
   - impulse, 51, 52  
 Noise detection, 129-132  
 Non-electrical detection, 129  
 Non-linear resistor, 21  
 Non-simultaneous switching, 5  
 Null detector, 103  
 Number of stages  
   - D.C., 47  
   - impulse, 51  
 Open spark gap, 21-23, 27  
 Operating voltage (stress), 12, 14, 15, 19, 90, 157  
 Operator (statistical), 143, 144  
 Oscillations  
   - in impulse generator, 51, 53  
   - in capacitive divider, 67, 68  
 Overvoltage, 1-7  
 Parallel compensation, 38  
 Partial discharges, 9, 117-132, 133-135  
 Paschen curve, 118, 124  
 Polarity reversal, 17  
 Pollution, 30  
 Power (underground) cable, 15, 34, 114, 150, 153  
 Primary compensation, 38  
 Probability for breakdown, 21  
 Probability paper, 82, 96  
 Protective  
   - level, 26, 28, 30, 31  
   - range, 32-34  
 Quality check, 8  
 Quality factor, 40  
 Rated voltage, 12, 14, 15  
 Recognition, 140-145, 152  
 Rectifier, 43-48  
 Re-ignition, circuit breaker, 4, 5  
 Rejection ratio, 148  
 Residual voltage, 25, 26  
 Resistive divider, 63-67  
 Resolution, 139, 140  
 Resonance transformer, 39-42  
 Ripple, 45, 47  
 Rod gap, 21, 22, 30, 53  
 Rogowski coil, 74-77  
 Routine test, 11-16, 19, 91  
 Safety margin, 22  
 Safety measures, 113  
 Sample test, 11, 15, 19  
 Scale parameter, 82, 83  
 Schering bridge, 101-110, 113, 158  
   - inverted, 108, 109  
   - one side earthed, 109, 110  
 Sensitivity, 132, 138, 154, 158  
 Series resonance, 38  
 Shape parameter, 82, 83

- Short circuit, 3
- Shunt, 71-73
- Sic
  - arrester, 21, 24-27
  - disc, 26
- Skewness, 143
- Slope
  - of life line, 88, 89
  - of Weibull curve, 81, 82, 90, 161
- Spark gap, 21, 22-24
- Sphere gap, 60-63
- Square wave generator, 56
- Stability test, 15-19
- Standard capacitor, 103, 104
- Standard operating voltage, 12
- Steep wave, 25, 29, 53, 54
- Step voltage test, 79, 82
- Stray capacitance
  - resistive divider, 64
  - Schering bridge, 105-107
- Stress-distributions, 17
- Surface discharges, 93, 119-122, 126, 141, 145, 152, 155
- Surge arrester, 21-30, 54
- Switching
  - impulse, 3-7, 48, 54
  - current, 55
- Temporary overvoltage (TOV), 29
- Thermal impulse rating, 73
- Time constant, 81, see 161
- Time resolved detection, 123-127, 151-155
- Transformer, 35-37
- Travelling wave detection, 153-156
- Treeing, 9, 92, 128, 145
- Triggered gap, 52, 53
- Type test, 11, 14, 15 19
- Unloaded line, 4, 5
- Velocity of electrons, 124
- Voltage-current test, 73
- Voltage
  - life, 9, 87-91, 155
  - multiplication, 46
  - dividers, 63-69
  - regulator, 43, 44
- Volume effect, 87, 88
- Wagners earth, 105, 106
- Weibull distribution, 80-91
- ZnO arrester, 21, 27-31
- Zinkoxyde (see: ZnO)

- Ignition, 117, 123-88, V8, *zvole směloV*  
 Impulse voltage  
   - standard 084p02, *smělo energieW*  
   - generated 08, *zvole dle výrobyW*  
   - measuring, *zvole 19*
- Inception, 118, 123-25, *zvole OnZ*  
 Insulation coordination, *zvole 25*  
 Interfaces, 94, 99
- Internal discharges, 117, 118, 120-122,  
 130, 132
- Inverted Schering bridge, 108, 109
- Joint, 150
- Kurtosis, 143
- Lichtenberg figures, 93, 94, 124
- Light detection, 131, 132
- Lightning  
   - arrester, 21-30  
   - current, 54, 77  
   - impulse, 2, 48  
   - stroke, 2, 57  
   - test, 14
- Line-to-line voltage, 12
- Location, 150, 151, 153-156
- Loss  
   - angle, 97, 158  
   - tangent, 97, 98, 114, 115, 158, 159  
   - analysis, 101
- Marx, 51
- Metal oxide (see: ZnO)
- I-Minute test, 14
- Multistage  
   - D.C., 46  
   - impulse, 51, 52
- Noise detection, 129-132
- Non-electrical detection, 129
- Non-linear resistor, 21
- Non-simultaneous switching, 5
- Null detector, 103
- Number of stages  
   - D.C., 47  
   - impulse, 51
- Open spark gap, 21-23, 27
- Operating voltage (střídavého Modu),  
 12, 90, 157, 161-171, *zvole 157*  
 Operator (statistical), 143, 144, *zvole*
- Oscillations, 12-42, 12, *zvole 12*  
   - in impulse generator, 55, 56-67  
   - in capacitive dividers, 17, *zvole 17*
- Overvoltage, 1-7  
   - 88, 88, *zvole 88*  
 Parallel supports, *zvole 10*-  
 Partial discharge, 12-22, 12, *zvole 12*  
 Paschen curve, 11, 26-30, *zvole 26*  
 Polarity reversal, 16, *zvole 16*  
 Pollution, 30, 31-32, *zvole 31-32*  
 Power (energetický), *zvole 15*-  
 116, 156, 158, *zvole 156*  
 Primary voltage, *zvole 15*, *zvole 15*  
 Probability *f*, 18, 21, 25, *zvole 21*  
 Probability *p*, 18, 21, *zvole 21*  
 Protective  
   - level, 20, 20, *zvole 20*  
   - range, 22-24, 24, *zvole 22-24*
- Surface discharge, 88, *zvole 88*  
 Quality factor, 10, 581, 581, 841, 841  
 10, 88-12, *zvole 88*  
 Rated voltage, 12, 14, 15, *zvole 15*  
 Recognition, 143-52, 152, *zvole 152*  
 Rectifier, 43-48, 66, *zvole 43*  
 Re-ignition, circuit breaker, 4, 5
- Rejection (VOT), *zvole 157*  
 Residual voltage, *zvole 157*  
 Resistive diode, 48, *zvole 48*, *zvole 48*  
 RIAA, 194-197, 194, *zvole 194*  
 Resonance frequency, 21-42, 22, 22  
 Ripple, 21, 47, 116-122, *zvole 116*  
 Rod 231-231, *zvole 231* ováv Guillotina/T  
 Rogowski coil, 76-17, 821, 82, 8, *zvole 82*  
 Routine test, 11-165, 165, *zvole 165*  
   - 81-81, M, 11, *zvole 81*  
 Safety margin, 21
- Safety measures, 113-5, 5, *zvole 113*
- Sample test, 11, 15, 19
- Scale parameter, *zvole 15*  
 Schering bridge, *zvole 15*  
   - inverted, 108, 109, *zvole 108*  
   - one side earthed, 109, 110, *zvole 109*
- Sensitivity, 132, 133, *zvole 133*
- Series resonance, 38, 98-100, *zvole 98*
- Shape parameter, 24, 161, *zvole 161*







### *The author*

The author was for many years the director of an industrial High Voltage laboratory and simultaneously known as a scientist because of his classic book on discharge detection. He is a professor at the Delft University of Technology.

### *The book*

This book presents both the basic principles of High Voltage science and deals with the practical application of this knowledge. The fusion of basic knowledge and practical usage has prompted the addition of subject headings to those already well-known:

- a chapter on fieldgrading
- a chapter on breakdown statistics
- a section on tracing breakdown
- a method for checking tg  $\delta$ -measurements.

Blending basics and practice has also influenced the treatment of the topics:

- field calculations are critically reviewed
- combinations of dielectrics are studied in a systematic way
- test specifications are related to insulation co-ordination
- discharge tests are critically reviewed

'Industrial High Voltage' is published in two volumes and is systematically divided into six fields:

#### **Volume I**

- *Electric Fields*: behaviour and calculation
- *Dielectrics*: breakdown mechanisms and applications
- *Constructions*: combinations of dielectrics and field grading

#### **Volume II**

- *Co-ordination*: deriving test specifications from insulation co-ordination
- *Testing*: generating and measuring high voltages; statistics
- *Measuring*: C, tg  $\delta$ , partial discharges.

